METAL COMPLEX INTERACTIONS WITH METAL-MODIFIED NUCLEIC ACIDS

DISSERTATION

zur

Erlangung der naturwissenschaftlichen Doktorwürde

(Dr. sc. nat.)

vorgelegt der

Mathematisch-naturwissenschaftlichen Fakultät

der

Universität Zürich

Von

BHAUMIK S. DAVE

aus

Indien

Promotionskomitee

Prof. Dr. Roland K. O. Sigel (Vorsitz, Leitung der Dissertation)
Prof. Dr. Gilles Gasser
Prof. Dr. Per Lincoln

Zürich, 2016

For Mum, Dad, Arth and Lipi

ACKNOWLEDGEMENT

I am deeply indebted to a long list of people, without whom this dissertation would have been incomplete. My foremost acknowledgement goes to my advisor, Professor Roland K. O. Sigel, for accepting me into his group and providing me with a challenging project to work on. His support through my PhD-student lifetime has been enormous.

For being the kindest mentor, I whole-heartedly thank Silke for all the effort, time and company she showered on me. I also would thank her for reading and correcting the thesis and for the German version of the thesis summary.

I would like to thank the thesis committee members, Prof. Dr. Per Lincoln and Prof. Dr. Gilles Gasser for helping shape my project in a constructive way.

Sigel Lab sub-group leaders: Daniela Donghi, Silke Johannsen, Sofia Gallo, Danny Kowerko and Richard Börner.

I appreciate the help of Cristina Mari for time and effort she provided during the separation of metal complex enantiomers.

A big thank you to my laboratory Nachbarin Marianthi Zampakou for her friendship and all the fun times spent together during my PhD life. I also thank her for all the little and big help and the cookies, sweets and chips she fed me or encouraged me to consume. Also, thanks to rest of the NMR sub-group people Magda Rowinska Zyrek, Miriam Skilandat, Maria Pechlaner, Alicia Dominguez, Elena Alberti, Simona Bartova and Kenneth Adea for their friendship, help and good times shared together.

To the other ladies of the SF-Lab, Anastasia Musiari, Erica Fiorini and Helena Guiset Miserachs.

To Pallavi Choudhary for her immense support during the initial days of being in Switzerland, and for her friendship. To former members of SF-Lab Joachim Schnabl, David Egloff, Jens Loebus, Sebastian König and Igor Oleinich for their advice and making my initial days in Switzerland happy. Also thank you to Anita Schmitz and Katsiaryna Tarasava for their help and advice, and to Michelle Schaffer for sharing her experiences.

For administrative help, I thank Nathalie Melunsky-Fichter, Ramona Erni and Chantal Henningsen-Conus. Special thanks to Jae Kyoung Pak for the immense administrative help in the first few months.

Finally, I would thank my parents Sunil Dave and Jayshree Dave, my brother Arth and my wife Lipi for their support and encouragement and for just being what they are.

CONTENTS

ABBREVIATIONS & SYMBOLS

bpy	2,2' -bipyridine
DPPZ	dipyridophenazine
IL	intraligand
MLCT	metal-to-ligand charge transfer
phen	1,10-phenanthroline
bp	base pairs
CT	charge transfer
ctDNA	Calf Thymus DNA
2T	Mismatch DNA
2THg	Hg^{II}-modified DNA
2TN	Natural DNA
2TNHg	Natural DNA + $Hg(NO_3)_2$ in buffer
Ru	Ruthenium metal complex
CD	Circular Dichroism
TCSPC	Time Correlated Single Photon Counting
ITC	Isothermal Calorimetry

1 SUMMARY

Application of nucleic acids in the bottom-up approach takes into consideration their superb self-assembly properties and their well-defined structural features. The possibility to site-specifically functionalize nucleic acids with metal ions might overcome the lack of sufficient conductivity of natural nucleic acids, and would strongly raise their potential as programmable building blocks for the construction of nano-scale molecular wires and devices. The introduction of metal-mediated base pairs is a simple and well-suitable method to achieve a one-dimensional arrangement of metal ions along the helical axis of nucleic acid duplexes.[1,2] Such base pairs can be formed by coordinating metal ions in between opposite nucleobases that can be either natural, or artificial created ones. Recent structural studies of such metal-modified nucleic acids could prove that with the right design consecutive metal-mediated base pairs can be introduced without a substantial distortion of the natural helical conformation.[3,4] However, so far only very few studies have been conducted aiming at investigating the electron transfer properties of such metal-modified nucleic acids.[5] Photo-induced charge transfer experiments using metallo-intercalators as donor-acceptor couples was the first method that was successfully applied to study the electron transfer in natural nucleic acids.[6,7]

Our long-term goal is to use photo-induced charge transfer experiments to investigate the electron transfer properties of metal-functionalized nucleic acids. But to succeed in setting-up such experiments, it is essential to have a profound knowledge on the intercalation properties of the electron donor and acceptor complexes to such metal functionalized nucleic acid structures. The aim of the thesis is a detailed characterization of the intercalative binding of the DNA-light switch complex $[Ru(bpy)_2dppz]^{2+}$, a frequently used electron donor in such experiments, into metal-modified nucleic acid duplexes.

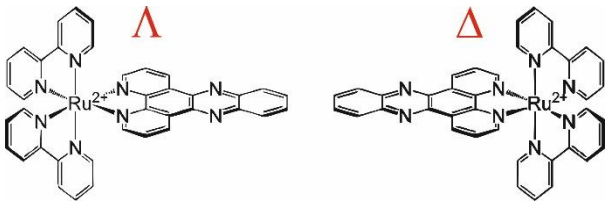

Figure 1.1: The two enantiomers of the DNA-light switch complex $[Ru(bpy)_2(dppz)]^{2+}$.

$[Ru(bpy)_2(dppz)]^{2+}$ is a well-known DNA light-switch complex that exhibits luminescence in aqueous solution only upon intercalation into DNA, as otherwise the emission is quenched by hydrogen-bond formation between water molecules and the phenazine nitrogens of the dppz ligand. Moreover, it was observed that the luminescence properties of $[Ru(bpy)_2(dppz)]^{2+}$ heavily depend on the binding geometry the complex adopts upon intercalation into DNA, which can be either symmetric or canted.[8] This binding geometry is determined by many factors such as the complex isomer (Δ or Λ), the DNA sequence and conformation, as well as salt concentration, temperature and pH conditions.[9,10] The intercalative binding of $[Ru(bpy)_2(dppz)]^{2+}$ has been extensively studied with natural DNA, but no investigation on metal-modified DNA duplexes have been performed so far.

In the first part of the thesis the intercalative binding of $[Ru(bpy)_2(dppz)]^{2+}$ to four different DNA duplexes was spectroscopically characterised using UV-VIS, fluorescence, and circular dichroism spectroscopy. All duplexes were 17 bp in length and differ only in the two central base pairs of the sequence from each other (Figure 1.2).

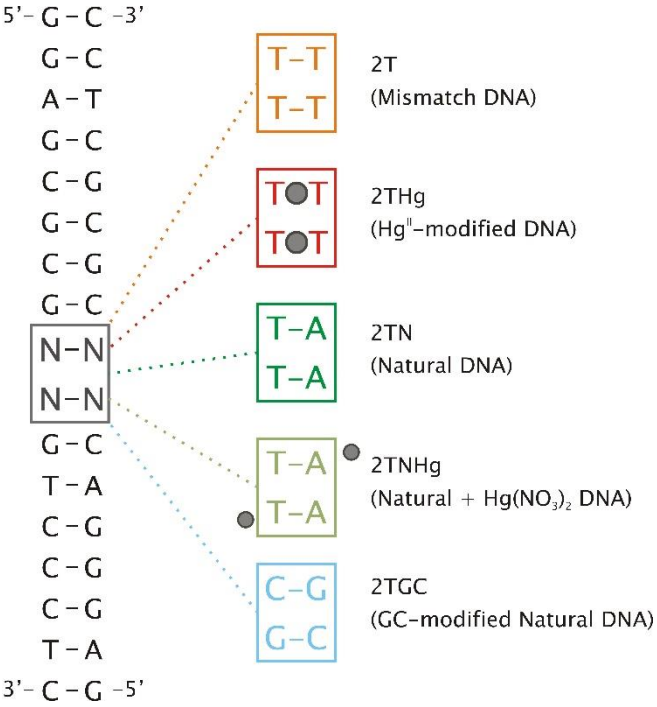

Figure 1.2: The DNA sequences used for the studies. Each of the sequence only differed at the middle.

These DNA constructs contain either two mismatched thymine-thymine base pairs (DNA 2T), two Hg^{II}-mediated T-Hg-T base pairs (DNA 2THg), two natural T-A base pairs (DNA 2TN) or a C-G and a G-C base pair (DNA 2TGC) and are based on a well-studied 12 bp DNA duplex. In addition, some control experiments were carried out with the natural 2TN sequence in the presence of 2 equivalents of Hg^{2+} ions referred to as DNA 2TNHg. In comparison to many intercalation studies of natural DNA in which mainly very long DNA constructs were applied, e.g. Calf thymus DNA or homo polymers like poly(dA)·poly(dT) or poly(dG)·poly(dC), we went for very short and well-defined constructs to directly see the influence of the small sequence variations on the intercalation properties. From simple UV-VIS titrations experiments, keeping the complex concentration constant and adding stepwise the DNA duplexes, it was evident that the metal complex was binding to all sequences in an intercalative manner as in all cases a strong hypochromic effect was observed at the dppz π-π^* transition at around 370 nm. The studies were conducted with both, the separated isomers as well as with the racemic mixture of the ruthenium complex. The hypochromicity was in all cases around 37-40% and is well in line with literature values of similar studies.[11] We also tried to determine the binding constants by fitting our UV-VIS data into the equation developed by Bard et. al. for non-cooperative binding of metallointercalator to DNA of infinite length.[12] However, since the equation is based on the original McGhee-von Hippel model for non-cooperative binding, it does not consider the cooperativity between neighbouring ligands.[13] Thus, the binding constants obtained are only an approximation. Nevertheless the reported values were in the range of 10^5-10^6 M^{-1} which is in accordance with previously reported literature values for similar studies.[11]

We also simultaneously conducted steady-state fluorescence emission titrations as the emission properties are sensitive to the binding geometry assumed by the intercalating metal complex isomer. The results of the fluorescence titrations conducted with the racemic mixture of the metal complex with 2T, 2THg and 2TN reveal on the one hand different curve shapes, and on the other hand different maximum emission intensities. In case of 2T and 2TN the curves show a strong increase in emission until a maximum is reached at a DNA/Ru ratio of 0.3–0.4, followed by a slight decrease up to the final DNA/Ru ration of 1.2, while for 2THg the maximum intensity was reached at a DNA/Ru ratio of 0.4–0.5 and then remained constant. The highest emission was observed when the complex was intercalating into 2T DNA. This finding was not surprising as in a recent study a preferential binding of intercalating metal complexes to thermodynamically weaker mismatched base pairs was observed, and thus resulting in higher emission intensities.[14] Titrations with 2THg DNA and the Ru^{II} complex revealed a maximum emission intensity which was not only two times lower as the one found for 2T but also significantly lower compared to 2TN. This behaviour cannot be explained by differences in the stability of the base pairs, as the thermodynamic stability of a T- Hg^{II}-T base pair is in the same range as the one of Watson-Crick base pairs. To

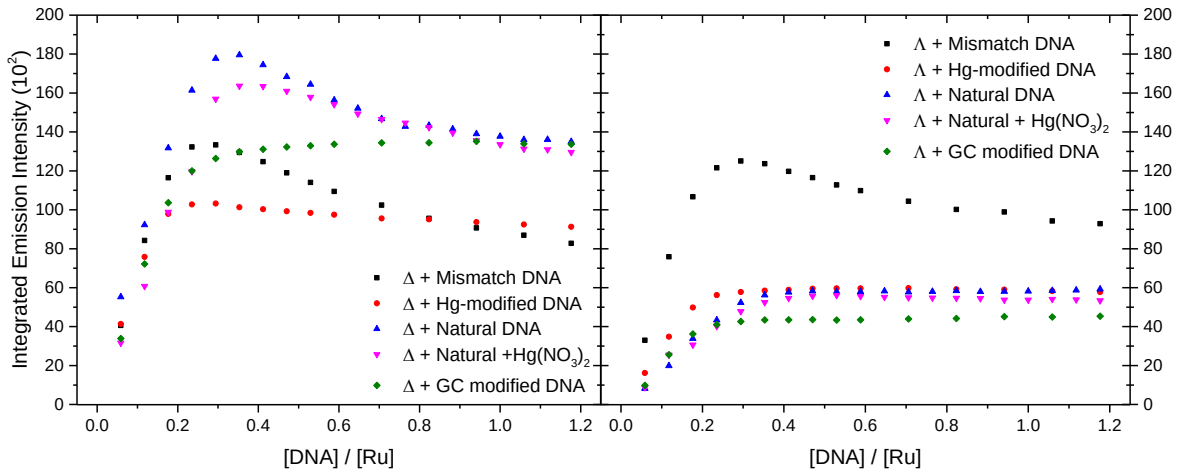

Figure 1.3: Steady-state emission (at 620 nm) of 5 μM Δ (left) and Λ (right) enantiomer of $[Ru(bpy)_2(dppz)]^{2+}$ bound to various DNA duplexes used in the studies. Note how the Λ enantiomer binds similarly to all duplexes except the mismatch DNA.

exclude a quenching of emission upon addition of Hg^{II} ions, additional titrations of 2TN in the presence of 2 eq. Hg^{II} were performed. However, no influence of free Hg^{II} on the emission was found. Already these results demonstrate the complexity of the intercalation process on the one hand, and how sensitive the emission properties respond towards small variations in the sequence on the other. To get even more insights, we performed the titration experiments also with the separated $[Ru(bpy)_2(dppz)]^{2+}$ isomers. As the DNA double

helix itself is chiral, the intercalation geometry of the two enantiomers are different.[8–10] We used also a lower complex concentration (5 µM instead 17 µM) to exclude that inner filter effects are responsible for the subsequent decrease of emission after reaching the maximum intensity, as seen for rac-$[Ru(bpy)_2(dppz)]^{2+}$ with 2T and 2TN. However, no concentration dependency was observed. In addition, another natural DNA sequence, 2TGC, was introduced as recent studies showed noticeably differences of the emission properties of $[Ru(bpy)_2(dppz)]^{2+}$ when intercalating between G-C and A-T base pairs, respectively.

The emission data showed distinct differences among the two enantiomers and the various DNA sequences (Figure 1.3). Therefore, additional job-plots were carried out yielding the exact binding stoichiometry and lifetime measurements at five different DNA/complex ratios were performed. The lifetime data yields not only information on the two geometries the intercalated complex can adopt (canted geometry leads to distinct longer lifetimes as the symmetric geometry) but also on their distribution (pre-exponential factor).

The results of our comprehensive emission study can be concluded as follow:

(I) Both complex enantiomers were emitting equally when bound to the mismatched 2T DNA indicating a binding pocket which can accommodate both isomers in a very similar manner. Additional lifetime measurements and job plot analysis suggest that this flexible binding pocket is the reason for the slightly higher overall emission intensity of the racemic mixture and not a metalloinsertion at the mismatched side as seen for other mismatched oligonucleotides.[15,16]

(II) As the job-plot analysis, steady-state emission and lifetime measurements reveal very similar results for the 2THg and 2TGC sequence it can be suggested that the T-Hg^{II}-T base pairs behaves like a canonical G-C Watson-Crick base pair.

(III) The maximum in the emission curve can be explained with lifetime analysis as the equation

$$I(calc) = \Sigma(\alpha_i \times \tau_i)$$

can be used to obtain calculated emission intensities from the measured lifetime data. The calculated data fits with the measured values and addresses the cause of emission maxima, which is due to adjacently close-bound metal complexes adopting a canted binding geometry.

(IV) In the case of 2THg, the formation of the T-Hg^{II}-T base pairs in the presence of Hg^{II} leads to a restoration of the chiral bias for the right-handed enantiomer as indicated by emission and stoichiometry data.

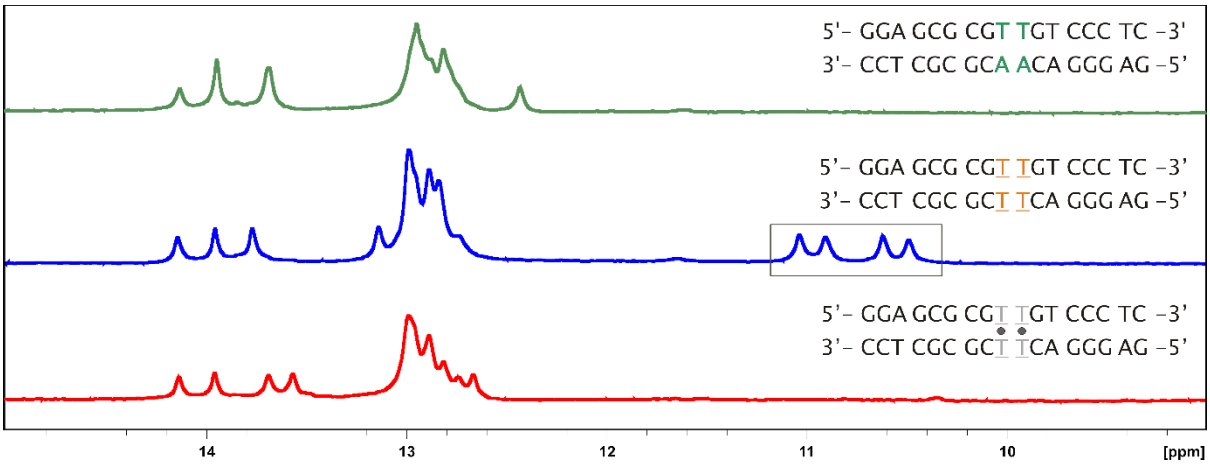

Figure 1.4: 1D-[^{1}H]-NMR stackplot of the exchangeable protons of 2T, 2TN and 2THg in 10 % D_2O, 90 % H_2O. The H3 resonances of the thymines in the T-T wobble base pairs are signified by the black box.

The second chapter of the thesis is an NMR based structural study of the mismatched (2T), the Hg^{II}-modified (2THg) and the natural DNA (2TN) duplexes to directly proof that the observed differences in the emission properties among the various DNA sequences only arise due to subtle structural variations caused by the altered two base pairs. We measured simple 1D [^{1}H] and NMR experiments in D_2O and H_2O to obtain first information on the non-exchangeable and exchangeable protons and to compare the results among the different duplexes. For all three sequences the resonances of the non-exchangeable protons were very sharp and similar distributed indicating three B-helical structures that highly resemble each other. On the other side, the spectral region of the imino resonances (H1 guanine and H3 thymine or uracil in case of RNA) that are only visible in H_2O and give information on the base pair pattern, looks distinct different for each duplex. This behaviour is expected as the number of canonical and non-canonical base pairs differs for each sequence. For the mismatched DNA 2T we observed not only resonances in the chemical shift region of regular Watson-Crick base pairs (12-15 ppm), but also four resonances around 11 ppm, a region in which typically wobble base pairs are found. This is a direct evidence for the formation of two stable T-T base pairs in the 2T DNA duplex. (Figure 1.4).

In addition, we measured 2D homonuclear and heteronuclear NMR experiments that are typically recorded to solve the three-dimensional structure of nucleic acids by NMR. We assigned all aromatic as well as all H1' and H2'/H2" sugar protons from 2D [^{1}H,^{1}H]-NOESY experiments in 100% D_2O, thereby following the sequential walk strategy and cross validating the assignments using [^{1}H,^{1}H]-TOCSY and [^{13}C,^{1}H]-HSQC experiments. Comparison of the non-exchangeable proton chemical shifts of the mismatched 2T and Hg^{II}-modified 2THg duplex with the natural 2TN DNA revealed that the observed differences are only in the region of the altered base pairs or close by.

Even though the structure determination of the three duplexes is still in progress, we can draw some substantial conclusions from our NMR data: (I) The two altered base pairs in the middle of the duplexes lead to only little structural variations. (II) However, these subtle structural differences in the central region are the main reason for the different intercalation patterns amongst the various DNA sequences and enantiomers of $[Ru(bpy)_2(dppz)]^{2+}$ and cause the distinct differences in the emission properties. (III) Two stable T-T wobble base pairs are formed in the 2T DNA sequence. (IV) Due to this stable consecutive arrangement of the mismatched T-T base pair it can be assumed that most likely no metalloinsertion occurs as found for other but less stable non-canonical base pairs like C-A or G-G,[14] but that the planar dppz ligand of $[Ru(bpy)_2(dppz)]^{2+}$ slides in between the base pairs similar to the intercalation between Watson-Crick base pair stacks. (V) However, the presence of the two mismatched T-T base pairs provides a flexible binding pocket to accommodate the enantiomers without chiral bias.

In conclusion, the NMR experiments confirmed our indications from the photophysical studies in which we assigned the obtained differences in emission to different intercalation properties of the complex enantiomers when binding to the altered middle region of the duplexes. In addition, the conducted NMR experiments are the basis for the indented structure determination of the three duplexes, which will give further insights to the structural differences that are responsible for these different binding behaviours. Moreover, they also provide the background for future NMR experiments aiming at identifying the binding sites of $[Ru(bpy)_2(dppz)]^{2+}$ for the individual duplexes. Thereby the complex will be directly titrated to the DNA duplexes and the proton chemical shift changes will be analysed.

In the final part of the thesis we studied the binding of $[Ru(bpy)_2(dppz)]^{2+}$ to RNA duplexes that are structurally analogues of the discussed mismatched DNA 2T and the Hg^{II}-modified DNA 2THg by UV-VIS and fluorescence spectroscopy. Besides DNA, RNA has as well a potential as building block in the bottom-up approach. It possesses the same intrinsic self-assembly properties like DNA and can also serve as scaffold for housing a metal-ion array in pre-defined manner. Moreover, its inherent higher thermal stability might be an additional benefit for the application in nanodevices. The RNA sequences used contain either 2, 3 or 6 consecutive mismatched U-U base pairs, or 2, 3 or 6 consecutive U-Hg^{II}-U base pairs. As starting point, we performed UV melting studies of the mismatched RNA duplexes in the presence and absence of Hg^{II} ions to proof the formation of Hg^{II}-modified RNA oligonucleotides. Our results proof that the destabilisation induced to the mismatched base pairs is completely abolished upon addition of the equivalents of Hg^{II} ions needed to convert all mismatches into U-Hg^{II}-U base pairs. Moreover, we could show that the addition of $Ru(bpy)_2(dppz)]^{2+}$ has no influence on the thermal stability at all. However, UV-VIS and fluorescence emission titrations of RNA 2U, 2UHg, 2UN and 2UNHg (in analogy to 2T, 2THg,

2TN and 2TNHg DNA duplexes) performed in a similar manner as for the DNA sequences reveal no indications for a proper intercalative binding of $[Ru(bpy)_2(dppz)]^{2+}$ to the RNA duplexes. The observed hypochromism at the dppz π-π^* transition band is with around 13-19% almost three times lower as found for the DNA counter parts. Even though the 2U and 2UHg sequences show a slightly higher hypochromicity (19%) no enhanced luminescence properties of the DNA light-switch complex $[Ru(bpy)_2(dppz)]^{2+}$ upon addition of any of the four RNA duplexes was observed. This is most likely due to the structural features of A-form duplexes that does not allow a proper intercalation of the dppz moiety of the complex. Hence the quenching due to hydrogen-bond formation with surrounding water is not prevented and therefore no emission occurs. The reason might be the smaller rise per base pair offered by A-form RNA (2.6 Å instead of 3.4 Å in DNA) along with the groove sizes that highly differ from the ones in B-helical structures. Additional 1D [^{1}H] NMR experiments in water revealed a similar wobble conformation of the U-U mismatches as observed for T-T mismatches in the 2T DNA analogue. Since we do not observe any enhanced luminescence of $[Ru(bpy)_2(dppz)]^{2+}$ also upon binding to the mismatched 2T RNA duplex, we conclude that no metalloinsertion is happening at the mismatch side. This finding indicates that also in the case of RNA stable U-U wobble base pairs are formed that do not cause any noticeable structural distortion of the helix but rather adopt an overall structure which is very similar to the one of the Watson-Crick base pairs.
Even DNA and RNA structures behave in many aspects very similar, the structural differences of the A-and B-helical conformation cannot be neglected and thus, results obtained for DNA structures cannot directly be transferred to RNA structures. Our results reveal the need to develop specific probes that are suitable to intercalate into RNA and which then can be used to set-up charge transfer experiments of metal-modified RNA duplexes.

The results of this thesis describe in detail the influence of subtle changes of nucleic acid structures on the intercalative binding of the "DNA-light switch" $[Ru(bpy)_2(dppz)]^{2+}$, exemplified and amplified by the variation of its fluorescence properties. The findings of this work do not only help to better understand the complex mechanism of intercalation, but is also the required fundament to successfully set up charge transfer experiments which in turn can be used to investigate if metal-modified nucleic acid structures have enhanced conducting properties.

2 ZUSAMMENFASSUNG

Nukleinsäuren werden aufgrund ihrer definierten Struktur und ihrer programmierbaren Selbstorganisation als Bausteine in der "Bottom-up" Methode verwendet. Eine zusätzliche Funktionalisierung mit Metallionen könnte das Problem der zu geringen Leitfähigkeit von natürlichen Nukleinsäuren lösen und so den Einsatz von Nukleinsäuren auch in elektrischen Nanostrukturen, wie molekularen Leitern, ermöglichen. Die Vewendung von Metall-Basenpaaren ist eine einfaches und geeignetes Verfahren, um Metallionen spezifisch entlang der Helixachse von Nukleinsäuren einzubauen.[1,2] Metall-Basenpaare können durch die Koordination von Metallionen zwischen natürlichen oder künstlich hergestellten Basen gebildet werden. Strukturelle Analysen haben gezeigt, dass mit dem richigen Design der Einbau von solchen Metall-Basenpaaren zu keiner wesentlichen Strukturänderung der Dopppelhelix führt.[3,4] Dennoch gibt es bisher nur wenig fundierte Studien, die die Elektronentransfereigenschaften von Metall-modifizierten Nukleinsäuren erforschen.[5] Photoinduzierte Ladungstransferexperimente, mit Hilfe von Metallinterkalatoren als Donor-Akzeptor-Paare, waren die erste Methode mit welcher der Elektronentransport in natürlichen Nukleinsäuren erfolreich untersucht werden konnte.[6,7]

Unser langfristiges Ziel ist es mit photoinduzierten Ladungtransferexperimenten nun auch den Elektronentransport in Metall-funktionalisierten Nukleinsäuren anzuschauen. Um jedoch erfolgreich solche Experimente durchführen zu können, sind tiefgreifende Kenntnisse über die Interkalationsigenschaften der Elektronendonor- und Elektronenakzeptor-Komplexe in diese Metall-modifizierten Nukleinsäurestrukturen erforderlich. Das Ziel dieser Arbeit ist eine detaillierte Charakterisierung, ob und wie der "DNA light-switch" Komplex $[Ru(bpy)_2(dppz)]^{2+}$, ein häufig verwendeter Elektronendonor, in Metall-modifizierte Nucleinsäurestrukturen interkaliert.

$[Ru(bpy)_2(dppz)]^{2+}$ ist ein bekannter "DNA light-switch" Komplex, d.h. dieser Komplex ist in wässriger Lösung nicht fluoreszierend, da Wasser mit den Phenazin-Stickstoffen des dppz-Liganden Wasserstoffbrücken bildet, die eine Emission verhindern. Interkaliert der Komplex jedoch in DNA Strukturen können keine Wassersoffbrücken mehr gebildet werden und der Emissionsübergang existiert wieder. Darüber hinaus wurde festgestellt, dass die beobachteten Lumineszenzeigenschaften von der Bindungsgeometrie, die der Komplex bei der Interkalation in die DNA einnimmt, bestimmt werden. $[Ru(bpy)_2(dppz)]^{2+}$ kann entweder symmetrisch oder schräg interkalieren.[8] Diese Bindungsgeometrie ist von vielen Faktoren abhängig, wie zum Beispiel

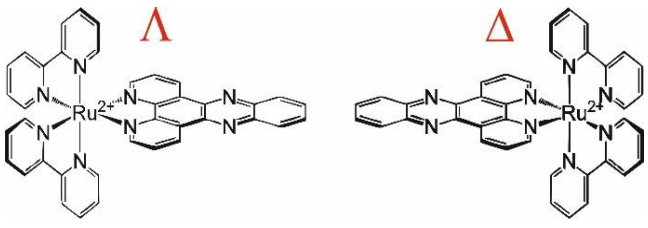

Abbildung 1.1: Die beiden Enantiomere des "DNA light-switch" Komplexes $[Ru(bpy)_2(dppz)]^{2+}$.

vom Komplex Isomer (Δ oder Λ), der DNA Sequenz und Konformation, als auch von der Salzkonzentration, der Temperatur und den pH-Bedingungen.[9,10]

Die Interkalation von $[Ru(bpy)_2(dppz)]^{2+}$ in natürliche DNA wurde intensiv untersucht, aber es wurden bisher keine Studien mit Metall-modifizierte DNA-Duplexe durchgeführt. Im ersten Teil der Arbeit haben wir die Interkalation von $[Ru(bpy)_2(dppz)]^{2+}$ in vier verschiedene DNA Sequenzen spektroskopisch mit UV-VIS, Fluoreszenzspektroskopie und Circulardichroism charakterisiert. Alle DNA Sequenzen sind 17 Basenpaare lang und unterscheiden sich nur um zwei mittlere Basenpaare. (Figur 1.2).

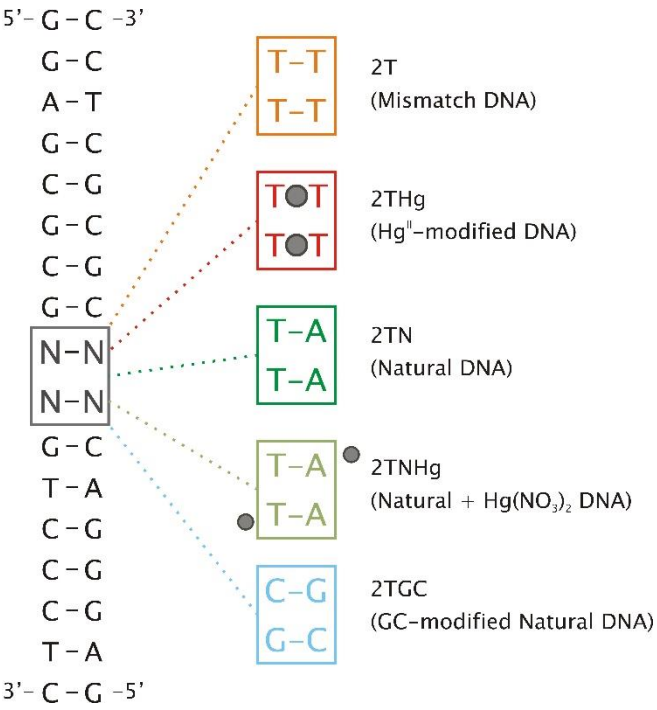

Abbildung 1.2: Die verwendeten DNA-Sequenzen. Die Sequenzen sind bis auf zwei Basenppare in der Mitte identisch.

Die DNA Sequenzen enthielten entweder zwei fehlgepaarte Thymin-Thymin Basenpaare (DNA 2T), zwei Thymin-Hg(II)-Thymin Metallbasenpaare (DNA 2THg), zwei natürliche Thymin-Adenin Basenpaare (DNA 2TN) oder ein Cytosin-Guanin und ein Guanin-Cytosin Basenpaar (DNA 2TGC). Alle Sequenzen basieren auf einer sehr gut charakterisierten, 12 Basenpaar langen DNA Doppelhelix. Zusätzlich wurden einige Kontrollexperimente mit der natürlichen 2TN Sequenz in Gegenwart von 2 Äquivalenten Hg^{2+} Ionen, bezeichnet als DNA 2TNHg, durchgeführt. Im Vergleich zu vielen Studien mit natürlicher DNA, in denen vorwiegend sehr lange DNA-Konstrukte verwendet wurden , zB ct-DNA oder Homo-Polymere wie Poly(dA)·Poly (dT) oder Poly (dG)·Poly(dC), haben wir uns für sehr kurze und gut definierte Konstrukte entschieden. Dadurch können wir den direkten Einfluss der kleinen Sequenzvariationen auf die Interkalationseigenschaften ermitteln. Einfache UV-VIS Titrationen haben gezeigt, dass der Metallkomplex in alle Sequenzen interkaliert. da bei der schrittweisen Zugabe von DNA zu einer konstanten Komplexkonzentration bei 370 nm, dem dppz π-π*-Übergang, ein starker hypochromischer Effekt gefunden wurde. Die Titrationen wurden sowohl mit dem racemischen Gemisch als auch mit den einzelnen Enantiomeren durchgeführt. Die Hypochromie lag in allen Fällen bei 37 bis 40% und stimmt gut mit Literaturwerten von ähnlichen Studien überein.[11] Zusätzlich haben wir versucht, die Bindungskonstanten durch fitten der UV-Daten mit der von Bard et al. entwickelten Gleichung für nicht-kooperative Bindung von Metallointerkalatoren an DNA von unendlicher

Länge, zu ermitteln.[12] Da die Gleichung original auf dem McGhee-von Hippel Modell für einen nicht-kooperative Bindungsmodus basiert, berücksichtigt die Gleichung nicht die Kooperativität zwischen benachbarten Liganden.[13] Die Bindungskonstanten sind deshalb nur Näherungswerte, stimmen jedoch mit Werten im Bereich von 10^5-10^6 M^{-1} sehr gut mit Literaturwerten überein.[11] Da die Emissionseigenschaften von $[Ru(bpy)_2(dppz)]^{2+}$ abhängig von der Bindungsgeometrie sind, die der Metallkomplex einnimmt wenn er interkaliert, haben wir in Analogie zu den UV-VIS Titrationen gleichzeitig auch Fluoreszenzemissionstitrationen durchgeführt. Die Fluoreszenzergebnisse der racemischen Mischung des Metallskomplexes mit 2T, 2THg und 2TN DNA zeigen nicht nur verschiedene Kurvenprofile, sondern auch sehr unterschiedliche Maximumsintensitäten. Im Fall von 2T und 2TN zeigen die Kurven einen starke Anstieg der Emission bis ein Maximum bei einem DNA/Ru-Verhältnis von 0,3-0,4 erreicht wird, gefolgt von einer leichten Abnahme bis zum endgültigen DNA/Ru-Verhältnis von 1,2. Während der Komplex mit 2THg DNA bei einem DNA/Ru-Verhältnis von 0,4-0,5 die maximale Intensität erreicht und danach konstant bleibt. Die höchste Emission wurde beobachtet, wenn der Komplex in 2T DNA interkalierte. Dieses Ergebnis ist nicht überraschend, da in einer aktuellen Studie eine bevorzugte Bindung des Metallkomplexes zu thermodynamisch labileren, fehlgepaarten Basenpaaren beobachtet wurde, die zu einer höheren Emissions führt.[14] Titrationen mit 2THg DNA und dem Ru^{II}-Komplex zeigen eine maximale Emissionsintensität, die nicht nur zwei Mal geringer als die mit 2T ist, sondern auch ebenfalls deutlich niedriger wie mit 2TN. Dieses

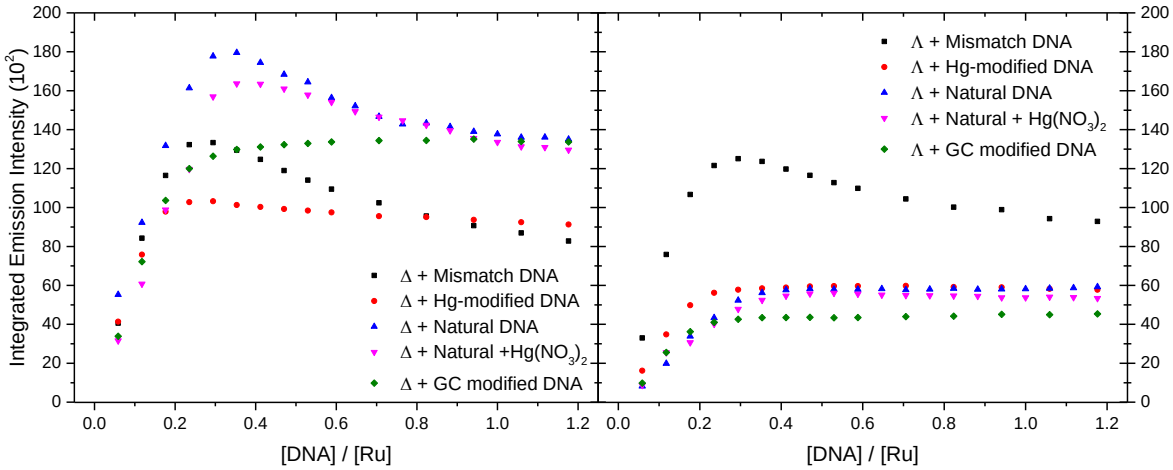

Abbildung 1.3: Steady-State-Emission (bei 620 nm) von 5 uM Δ-(links) und Λ-(rechts) $[Ru(bpy)_2(dppz)]^{2+}$ in Abhängigkeit zunehmender DNA Konzentration.

Verhalten kann nicht durch unterschiedliche Stabilität der Basenpaare erklärt werden, da die thermodynamische Stabilität eines T-Hg^{II}-T Basenpaares in der gleichen Größenordnung wie die von einem Watson-Crick Basenpaar ist. Um einen Einfluss von Hg^{II} Ionen auf die

Emission auszuschließen, haben wir weitere Titrationen von 2TN in Gegenwart von 2 eq. Hg^{II} durchgeführt. Allerdings haben wir keine Korrelation zwischen freien Hg^{II} Ionen und der Emission gefunden. Diese Ergebnisse zeigen bereits die Komplexität des Interkalationvorganges und wie empfindlich die Emissionseigenschaften gegenüber kleinen Variationen in der DNA Sequenz reagieren. Um diesen Vorgang und unsere Daten besser verstehen zu können, haben wir weitere Titrationen mit den isolierten $[Ru(bpy)_2(dppz)]^{2+}$ Isomeren realisiert. Da die DNA-Doppelhelix selbst chiral ist, sind die Interkalations Geometrien der beiden Enantiomere unterschiedlich.[8,9] Um auszuschließen, dass innere Filtereffekte verantwortlich für den Abfall der Emission nach Erreichen des Maximums sind, wie wir es für rac-$[Ru(bpy)_2(dppz)]^{2+}$ mit 2T und 2TN gesehen haben, führten wie zusätzliche Titrationen mit einer geringeren Komplexkonzentration (5 uM statt 17 uM) durch. Wir haben jedoch keine Konzentrationsabhängigkeit beobachten können. Außerdem haben wir eine andere natürliche DNA-Sequenz (2TGC) eingeführt, da jüngste Studien gezeigt haben wie unterschiedlich die Emissionseigenschaften von $[Ru(bpy)_2(dppz)]^{2+}$ interkaliert zwischen GC bzw. AT Basenpaaren sind. Unsere Emissionsdaten zeigte deutliche Unterschiede für die beiden Enantiomeren mit den verschiedenen DNA Sequenzen (Abbildung 1.3). Mit Hilfe der Jobschen Methode haben wir zusätzlich für jede Sequenz und Enantiomer die genaue Bindungsstöchiometrie bestimmt, die teilweise die unterschiedlichen Emissionintensitäten erklären konnten. Zusätzlch haben wir Lebensdauermessungen mit fünf verschiedenen DNA/Komplex-Verhältnissen durchgeführt. Die Lebensdauerdaten liefern nicht nur Informationen über die Geometrie des eingelagerten Komplexes (schräge Geometrie führt zu einer deutlich längeren Lebensdauer als die symmetrische Geometrie), sondern auch über deren Verteilung (Präexponentieller Faktor).

Die Ergebnisse unserer umfassenden Emissionsstudie kann wie folgt zusammengefasst werden:

(I) Die beiden Enantiomere von $[Ru(bpy)_2(dppz)]^{2+}$ zeigen das gleiche Emissionsprofil, wenn sie an die 2T DNA Sequenz binden. Anscheinend formen die zwei T-T Basenpaare eine Bindungstasche, die beide Isomere in einer sehr ähnlichen Weise unterbringen kann. Zusätzliche Lebensdauermessungen und Jobschen Analyse legen nahe, dass diese flexible Bindungstasche der Grund für die etwas stärkere Emission des racemischen Komplexgemisches ist und keine Metalloinsertion an den misgepaarten Basenpaaren stattfindet, wie es für andere Oligonukleotide mit Mispaarungen gefunden wurde.[15,16]

(II) Die Emissionsprofile, die Anzahl bindender Komplexmoleküle, ermittelt durch die Jobsche Methode, sowie die Lebensdauermessungen zeigen sehr ähnlich Ergebnisse für die 2THg und 2TGC Sequenz. Dieses Resultat impliziert, dass sich die T-Hg^{II}-T Basenpaare wie die GC Watson-Crick-Basenpaare verhalten.

(III) Der Verlauf der Emissionskurven kann mit den Daten der Lebensdaueranalyse erklärt bzw mit Hilfe folgender Gleichung berechnet werden.

$$I(calc) = \Sigma(\alpha_i \times \tau_i))$$

Die berechneten Daten stimmen sehr gut mit den Messwerten überein und offenbaren, dass die Ursache für die gefundenen Emissionsmaxima bei 2T und 2TN, benachbarte Metallkomplexe mit schräger Bindungsgeometrie sind.

(IV) Die gebildeten T-Hg^{II}-T Basenpaare in der 2THg DNA bilden keine flexible Bindungstasche, sondern führen zu einer Bevorzugung des rechtshändigen Δ-Enantiomer wie die Emissions- und Stöchiometriedaten zeigen.

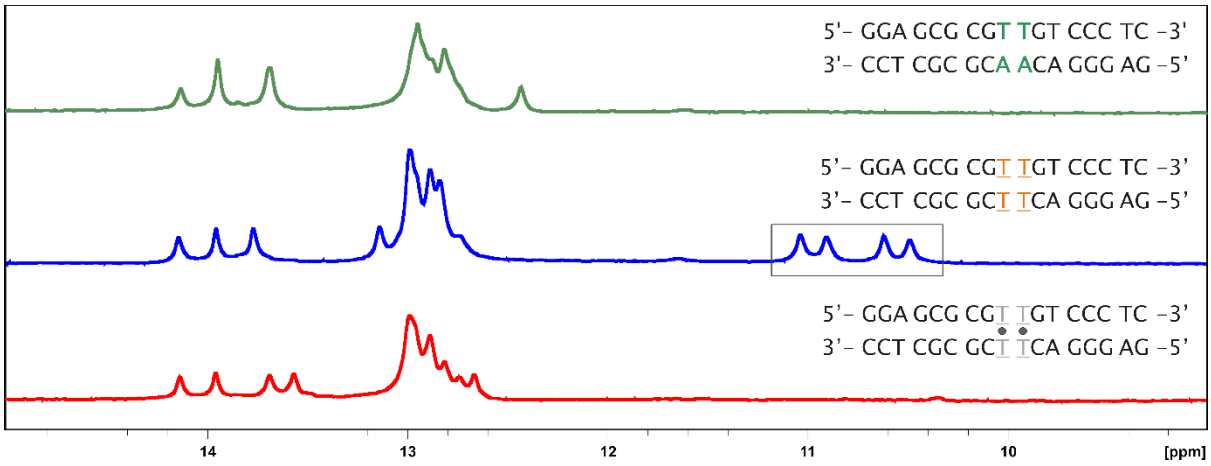

Abbildung 1.4: 1D [^{1}H]-NMR Stackplot der austauschbaren Protonen von 2T, 2TN und 2THg in 10% D_2O, 90% H_2O. Die H3 Resonanzen der Thymine in der T-T Wobble Konformation sind durch ein schwarzes Kästchen markiert.

Das zweite Kapitel der Dissertation ist ein NMR-basierende Strukturanalyse der misgepaarten DNA 2T, der Hg^{II} modifiziertes DNA 2THg und der natürlichen DNA 2TN. Sie sollte verifizieren, dass die beobachtete Unterschiede in den Emissionseigenschaften tatsächlich nur durch geringe Strukturänderungen verursacht wurden, hervorgerufen durch die zwei veränderten Basenpaare in der Mitte der Sequenz. Wir haben 1D [^{1}H]-NMR Experimente in D_2O und H_2O gemessen, um erste Informationen über die nicht-austauschbaren bzw. die austauschbaren Protonen zu erhalten und die Ergebnisse für die verschiedenen Sequenzen zu vergleichen. Alle drei Sequenzen weisen scharfe Signale mit einer sehr ähnlichen Verteilung der nicht-austauschbaren Protonen auf, was auf drei sehr ähnliche B-helikale Strukturen hindeutet. Im Bereich der Iminoresonanzen (H1 Guanin und Thymin oder Uracil H3 im Falle von RNA), die nur in H_2O sichtbar sind und Informationen

über die Basenpaarung geben, sieht man hingegen deutliche Unterschiede. Dieses Verhalten ist nicht überraschend, da die Anzahl der kanonischen und nicht kanonischen Basenpaaren in jeder Sequenz verschieden ist. Für die misgepaarte 2T DNA beobachteten wir nicht nur Resonanzen mit einer chemischen Verschiebung im Bereich von Watson-Crick Basenpaaren (12-15 ppm), sondern auch vier Resonanzen bei etwa 11 ppm. Da man in dieser Region typischerweise Signale von Wobble-Basenpaaren findet, ist dies ein direkter Beweis für die Bildung von zwei stabilen T-T Basenpaaren in der DNA-Duplex 2T. (Abbildung 1.4). Darüber hinaus haben wir zweidimensionale, homonukleare und heteronukleare NMR-Experimente gemessen, die typischerweise aufgenommen werden, um die dreidimensionale Struktur von Nukleinsäuren mittels NMR zu lösen. Wir konnten alle aromatischen Protonen sowie alle H1 'und H2'/H2'' Zuckerprotonen in den 2D [^{1}H,^{1}H]-NOESY Experimenten mit Hilfe der "sequential walk" Strategie und zusätzlichen [^{1}H,^{1}H]-TOCSY und [13C,^{1}H]-HSQC Experimenten zuordnen. Ein Vergleich der chemischen Verschiebungen der nicht-austauschbaren Protonen ergab, daß die wenigen beobachteten Unterschiede nur im Bereich der veränderten Basenpaare oder in deren Nähe zu finden sind.

Obwohl die Strukturbestimmung der drei DNA-Doppelstränge noch nicht abgeschlossen ist, können wir bereits einige wichtige Schlussfolgerungen aus den NMR-Daten ziehen:

(I) Die beiden variierenden Basenpaare in der Mitte führen zu nur geringen Strukturunterschieden.

(II) Allerdings sind diese maginalen Strukturunterschiede der Hauptgrund für die verschiedenen Interkalationsmuster, die $[Ru(bpy)_2(dppz)]^{2+}$ mit den DNA-Sequenzen aufweist und welche zu den starken Differenzen in den Emissionsprofilen führen.

(III) In der 2T DNA-Sequenz werden zwei stabile TT-Wobble-Basenpaare gebildet.

(IV) Aufgrund der stabilen Anordnung der T-T Basenpaare kann davon ausgegangen werden, dass die die planaren dppz Liganden $[Ru(bpy)_2(dppz)]^{2+}$ sich in einer ähnlichen Art und Weise zwischen diese Basenpaare schieben wie sie es auch bei Watson-Crick Basenpaaren machen. Es kommt also wahrscheinlich zu keiner "Metalloinsertion" wie es für andere, aber weniger stabile, nicht-kanonische Basenpaare wie CA oder GG gefunden wurde.[14]

(V) Im Gegensatz zu den Watson-Crick Basenpaaren formen die T-T Wobble-Basenpaare eine flexible Bindungstasche, die beide Enantiomere in ähnlicher Weise unterbringen kann.

Die NMR-Daten haben unsere Hinweise aus den photophysikalischen Studien bestätigt, dass die erhaltenen Differenzen in den Emissionseigenschaften nur auf minimale Strukturänderungen im mittleren Bereich der DNA-Doppelhelixen zurückzuführen sind und eine Änderung der Interkalationsgeometrie der Komplexmoleküle zur Folge haben. Die

durchgeführten NMR-Experimente sind die Grundlage um die dreidimensionale Struktur der drei Doppelstränge zu bestimmen. Diese Strukturen können eventuell die strukturellen Unterschiede aufdecken, die für das unterschiedliche Bindungsverhalten verantwortlich sind. Unsere NMR Daten sind ausserdem die Voraussetzung für weitere NMR-Experimente, mit dem Ziel die genauen Bindungsstellen von $[Ru(bpy)_2(dppz)]^{2+}$ zu identifizieren. Dabei wird der Komplex direkt zu den DNA-Doppelsträngen titriert und die Änderungen der chemischen Verschiebung der Protonen analysiert.

Im letzten Teil der Arbeit untersuchten wir die Bindung von $[Ru(bpy)_2(dppz)]^{2+}$ an RNA-Doppelstränge mit Hilfe von UV-VIS und Fluoreszenzspektroskopie. Die RNA Sequenzen sind die strukturellen Gegenstücke der misgepaarten 2T und der Hg^{II}-modifiziertes 2THg DNA Sequenzen. Neben DNA, haben auch RNA-Moleküle Potenzial als Grundbaustein in der Bottom-up Methode. RNA besitzt die gleichen Selbstorganisationseigenschaften wie DNA und kann auch als Gerüst für die Anordnung von Metallionenin in vordefinierter Weise dienen. Darüber hinaus könnte ihre inhärent höhere thermische Stabilität ein zusätzlicher Vorteil für die Anwendung in der Nanotechnologie sein. Die verwendeten RNA-Sequenzen enthalten entweder 2, 3 oder 6 aufeinanderfolgende U-U Basenpaare, oder 2, 3 oder 6 aufeinanderfolgende U-Hg^{II}-U Basenpaaren. Als Ausgangspunkt, führten wir UV-Schmelzpuktuntersuchungen der fehlgepaarten Duplex-RNA in Gegenwart und Abwesenheit von Hg^{II} Ionen durch, um die Bildung von Hg^{II} modifiziertes RNA-Oligonukleotiden nachzuweisen. Unsere Ergebnisse belegen, dass die Destabilisierung durch die fehlgepaarten Basenpaaren vollständig durch die Zugabe von Hg^{II} Ionen aufgehoben wird. Dabei muss die Anzahl der Hg^{II} Ionen mit der Anzahl misgepaarter U-U Basenpaare übereinstimmen, um alle misgepaarten Basenpaare in U-Hg^{II}-U Basenpaaren umzuwandeln. Außerdem konnten wir zeigen, dass die Zugabe von $[Ru(bpy)_2(dppz)]^{2+}$ keinen Einfluss auf die thermische Stabilität der RNA Doppelstränge hat. Allerdings haben UV-VIS und Fluoreszenzemission Titration von RNA 2U, 2UHg, 2UN und 2UNHg (in Analogie zu den 2T, 2THg, 2TN und 2TNHg DNA-Doppelsträngen) keine Hinweise für eine interkalative Bindung von $[Ru(bpy)_2(dppz)]^{2+}$ an die RNA-Doppelstränge gezeigt, wie es für die DNA-Sequenzen gefunden wurde. Die beobachtete Hypochromie am dppz π-π^* Übergang ist mit rund 13-19% fast dreimal niedriger als die für die komplementären DNA-Sequenzen. Auch wenn die 2U und 2UHg Sequenzen eine etwas höhere Hypochromie zeigen (19%), wurde für keine der vier verwendeten RNA Sequenzen eine merklich erhöhte Lumineszenz des "DNA-light switch" Komplexes $[Ru(bpy)_2(dppz)]^{2+}$ beobachtet. Dies liegt wahrscheinlich an den strukturellen Merkmalen der A-Form-Duplex, so dass keine richtige Einlagerung des dppz Liganden in die RNA Struktur möglich ist. Dadurch kann die Wasserstoffbrückenbildung mit umgebenden Wasser nicht vollständig verhindert werden und der Komplex zeigt nahezu keine Emission. Der Grund dafür könnte die unterschiedliche Geometrie der A-Form Helix im Vergleich zur B-Form Helix sein, die einen kleinere Abstand pro Basenpaar aufweist (2.6 Å statt 3.4 Å in B-DNA) und andere Furchengrößen besitzt. Zusätzliche 1D [^{1}H] NMR-

Experimente in Wasser ergaben, dass die U-U Basenpaare eine ähnlich stabile Wobble-Konformation bilden, wie die T-T Basenpaare in der 2T-DNA Sequenz. Da wir auch keine erhöhte Lumineszenz von $[Ru(bpy)_2(dppz)]^{2+}$ mit den misgepaarten 2U RNA gefunden haben, scliessen wir auch hier eine "Metalloinsertion" an den U-U Basenpaaren aus. Wir vermuten stattdessen, dass ebenfalls wie in der DNA, die UU-Wobble Basenpaare zu keinen nennenswerten strukturellen Verzerrung der Helix führen, sondern vielmehr eine Struktur einnehmen, die der eines Watson-Crick Basenpaares ähnlich ist.

Obwohl sich RNA und DNA in vielerlei Hinsicht sehr ähnlich verhalten, sind die Unterschiede zwischen den A-und B-helikalen Struktur nicht zu vernachlässigen. Ergebnisse für DNA Strukturen können somit nicht direkt auf äquivalente RNA Strukturen übertragen werden. Um photoaktivierte Ladungstransferexperimente an Metall-modifizierten RNAs durchführen zu können, ist die Entwicklung von neuen Interkalatoren erforderlich, die spezifisch an RNA binden.

Die Ergebnisse dieser Dissertation beschreiben detaliert, wie kleinste Unterschiede der Nukleinsäurestruktur die Interkalationseigenschaften des "DNA light-switch" Komplexes $[Ru(bpy)_2(dppz)]^{2+}$ beeinflussen. Diese Abhängigkeit wird durch die sich ändernden Fluoreszenzeigenschaften des Komplexes verdeutlicht und verstärkt. Damit helfen die Resultate dieser Arbeit nicht nur den komplexen Mechanismus der Interkalation besser verstehen zu können, sondern bilden auch das erforderliche Fundament, um erfolgreich Ladungstransfer Experimente durchzuführen. Diese Experimente wiederum könnten aufzeigen, ob Metall-modifizierte Nukleinsäurestrukturen tatsächlich bessere leitende Eigenschaften besitzen als natürliche Nukleinsäuren.

3 Introduction

3.1 Nucleic acids: building blocks to scaffolds

In all living organisms, the nucleic acids deoxyribonucleic acid (DNA) and ribonucleic acid (RNA) are besides proteins the most important and central molecules in the cell. Structure and dynamics of these molecules are strongly related to their function and thus, obtaining three-dimensional structural information together with time-dependent changes in structure is very crucial to understand the various essential biological processes in which these molecules are involved. The genetic machinery of living systems is the most logical target for understanding the cause of various diseases such as of cancer. It is therefore also important to create novel molecules that bind to various genetic targets. On the other hand, technology drives the storage and processing of digital information. Computers are increasingly mimicking our body's smallest unit system, the cell. The hard disk stores the digital information along with the code for software to run, similar to the nucleus with DNA and RNA as the storage and decoder molecules in organic systems. To imagine an amalgamation of the two worlds is an achievable task. In fact, with the current advancements in chemistry and physics, the same genetic machinery found in living systems is poised to become the new organic analogue for storage of digital information.

3.1.1 DNA & RNA: structural and functional basics

DNA, the genetic material as we know it, is one of the most remarkable molecules to be studied.[17] It serves the very important function of information storage in biological systems. Nevertheless, the most fascinating fact about DNA is how exactly nature has designed it in order to enable it to deliver its functions. It started as a blur on an X-ray diffractogram in 1953, thereafter leading to the complete elucidation of its helical structure.[18] DNA is an organic polymer made of four different monomers. Each monomer (referred to as nucleotide) is composed of a phosphate group, a single-ring sugar and one of the four nucleobases: Adenine (A), thymine (T), guanine (G) and cytosine (C). These nucleobases are planar in structure and are differentiated by their single-ring or double-ring aromatic compounds also referred to as pyrimidines and purines, respectively. The nucleotides are bonded between the sugar subunit and the phosphate forming a long polymer (strand). The bases interact with each other, through the formation of hydrogen bonds and they pair each other following the Chargaff's rule where guanine pairs with cytosine and thymine pairs with adenine.[19] The bases A and T share 2 hydrogen bonds whereas G and C share 3 (Figure 3.1). An entire strand of the DNA forms base-pairs with its complementary strand to make double-stranded DNA. This is fundamental for information storage and retrieval in organisms. The helical structure of the DNA is formed as a result of the chiral sugar subunit

and the hydrogen bond angles between the bases (Figure 3.1-A). There are 10.4 bases per turn in the DNA helix.

An analogue of DNA, the RNA is another biomolecule that shares similar features with the DNA such as the adenine, guanine and cytosine nucleobases while thymine is replaced by unmethylated base analogue uracil in case of RNA (Figure 3.1-B). A main and important difference between the two nucleic acids is the sugar subunit (Figure 3.1-A). The RNA has an additional 2'-hydroxyl group on the sugar subunit, which in the case of DNA is deoxidized (Figure 3.1-A). In RNA, besides the canonical Watson-Crick base pairs, various other base pairing schemes are found. These comprise of the GU wobble or the (reverse) Hoogsten base pairs, which are common in ribozymes.[20,21]

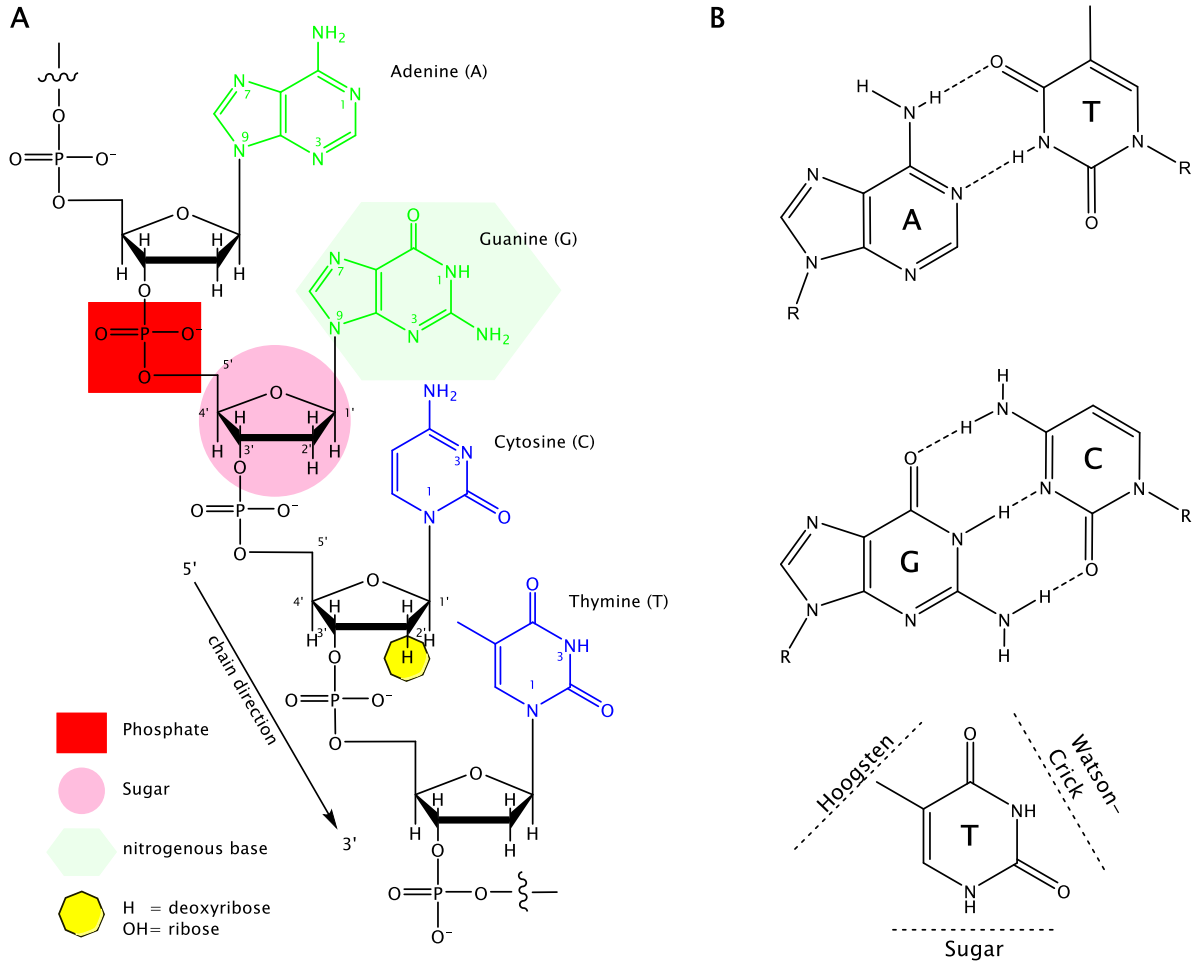

Figure 3.1: (A) The four DNA nucleobases with their connectivity to the phosphate sugar backbone. The purines are coloured green, pyrimidine in blue. The sugar-phosphate unit is marked in coloured shapes. (B) Canonical Watson-Crick base pairs A-T and G-C with their hydrogen bonds and a thymine base with indicated Watson-Crick and Hoogsten sites.

The hydrogen bond formation between the complimentary bases also imparts stability to the double helix. RNA, on the other hand forms secondary structures that includes single-stranded and double-stranded regions as well as hairpins, internal loops, bulges, and junctions within a singular polymer chain.[22] The DNA usually adopts the B-form helix as described by Watson and Crick.[18] On the other hand, double stranded RNA adopts an A-form helix (Figure 3.2). The formation of either A-form or B-form helix depends on several parameters (Table 3.1), the biggest factor being the sugar pucker conformation (Figure 3.2).[23]

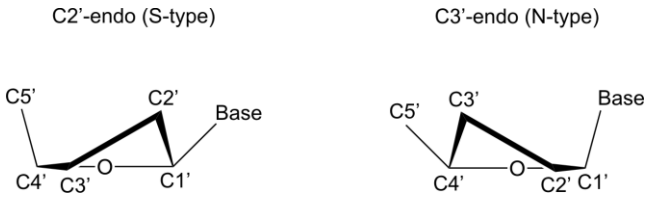

Figure 3.2: The sugar pucker conformations of deoxyribose and ribose sugars found in nucleotides. The S-type conformation is typically found in B-form DNA while the N-type is found in A-form RNA.

In B-DNA, the most typical conformation found is the C2'-endo (or South) while in RNA, only the C3'-endo (or North) is found because the C2'-endo conformation sterically hinders the B-form helix due to the presence of additional 2'-OH group.[24]

Table 3.1: Parameters for the A-helical and the B-helical form of polynucleotide helices.

	A-helical form	B-helical form
Helix Sense	Right handed	Right handed
Average base pairs / turn	10.7	10
Rotation / base pair	33.6°	35.9°
Pitch / turn of helix	24.6 Å	33.2 Å
Rise / base pair along axis	2.3 Å	3.32 Å
Propeller twist	+18°	+16°
Glycosyl angle	Anti	Anti
Sugar pucker	C3'-endo	C2'-endo
Diameter	26 Å	20 Å

In the B-form helix, the major and minor grooves are both available with the base pairs being on-axis. In other words, the depths of the grooves are similar. In comparison, the A-form helix has a very deep, narrow major groove and wide, shallow minor groove (Figure 3.3 A). In addition, the base pairs in A-form RNA are tilted with respect to helix axis thereby making a hole in the middle of the double helix when viewed from top along the helical axis (Figure 3.3 B).

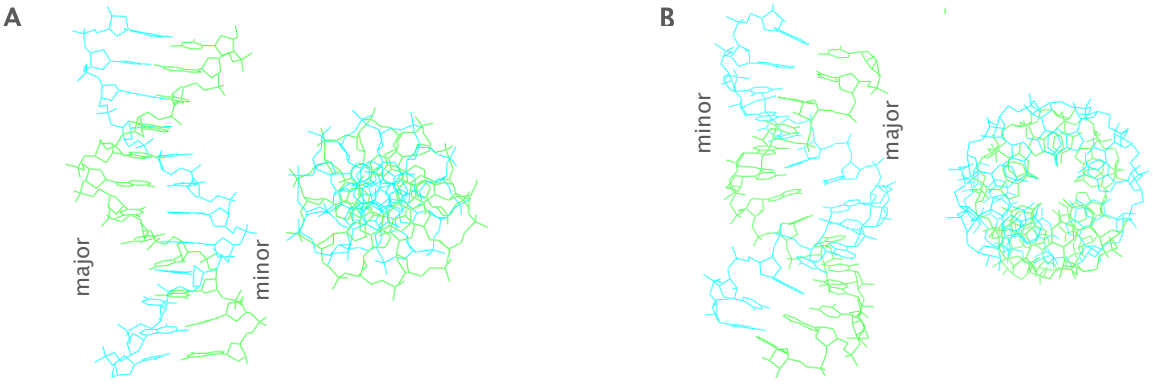

Figure 3.3: Nucleic acid helices formed through hydrogen bonding. (A) B-form DNA front-view (left) and top-view (right); compared to (B) A-form RNA duplex front-view (left) and top-view (right). The two separate strands are shown in blue and green. Note the differences in the grooves for each helix. In B-form DNA, the base pairs are aligned in the centre of the helix whereas in A-form RNA the base pairs are aligned around the z-axis of the helix with a distinct hole in the middle of the helix of the A-form RNA. The figures were prepared with Pymol[25] based on the PDB files 1BNA[26] and 1RNA[27] respectively.

The unique chemical properties of nucleic acids impart it fascinating abilities such as self-assembly along with robust structural features. In today's time, nucleic acid synthesis by both chemical or biochemical means is well established and has become less expensive. It is now possible to easily obtain short and long oligonucleotides with defined sequence and length for various biochemical and physical studies.

3.2 METAL-MODIFIED BASE PAIRS

Nucleic acids are highly versatile building blocks in all living systems. Besides being the genetic storage molecule, DNA also plays various other roles in biological systems such as in cell signalling through charge transport.[28] The most fascinating thing about nucleic acids is their ability to self-pair with their complimentary base pairs via hydrogen bonding. This highly specific and indeed very remarkable property could be exploited to create enhanced nucleic acid analogues. Moreover, nucleic acids can also accommodate metal ions at specific site, which enables greater functionalization of such modified oligonucleotides. Due to these novel physical and chemical properties of nucleic acids, the development of automated phosphoramidite chemistry has seen huge developments in the past decades.[29,30] Combined with various methods of PCR and ligation, it is also now possible to manufacture longer strands/ duplexes of nucleic acids functionalized with specific metal ions.[31-34]

Research on artificial base pairs is a relatively new field which started with a primary goal of augmenting the four letter code of the DNA.[35,36] Hitherto most of the efforts in the field of modified nucleic acids were dedicated to mimicking oligonucleotide components such as the phosphate or the sugar, the motives for which were driven by a quest to understand origin of nucleic acids and to search for antigene and antisense activities.[37-40] The ground-breaking work of Benner and co-workers established several unnatural nucleosides with altered hydrogen bonding schemes. More interestingly, Benner and co-workers were also able to demonstrate that such artificial nucleosides can indeed go unrecognised by proteins and enzymes involved in translation-transcription machinery leading to unnatural amino-acids.[41-44] The last decade has seen a new generation of nucleoside mimics that replace the hydrogen bonding pattern by metal-mediated base-pairing. Metal-modified base pairs form upon coordination of metal ion between nucleobases that are either natural or artificial. The first example of an artificial base pair was demonstrated by Tanaka and Shionoya in 1999.[45] The hydrogen-bond replacing metal ions have specific and high affinity for nucleobases.[46-50] Soon after 1999, in 2000 the trio of Meggers, Romesberg and Schultz demonstrated the incorporation of metal-mediated base pair in a DNA.[51] The following years saw plenty of metal-mediated base pairs introduced in DNA,[2,3,46,52-68] GNA[69] (glycol nucleic acid) and PNA[70-75] (peptide nucleic acid) containing up to three to 19 consecutive metal-modified base pairs. In our group efforts on the development of metal-modified RNA analogues also have been pursued to coordinate mercury metal ion between uracil-uracil mismatches.[3] The best examples of ingenious metal ion induced structural changes in DNA was observed in our group by Dr. Silke Johannsen where a hairpin structure containing artificial imidazole base pairs (3x) undergoes duplex formation upon addition of silver (Ag^{I}) metal ions. This was the first published work, which structurally characterised metal-modified DNA containing continuous stretch of metal-mediated base pairs.[4]

3.2.1 MERCURY MEDIATED BASE PAIRS (T–HG^{II}–T)

The oldest observations of the specific interaction of Hg(II) ions with the DNA were as early as 1950s.[76] Further work by S. Katz led to the confirmation of a 2:1 complex of deprotonated thymine and Hg^{II}.[77,78] Thereafter in 1990s, the interaction of Hg^{II} with DNA was revisited with NMR spectroscopic study revealing the dependence of the T–Hg–T base pair formation on the sequence and the conformation of the oligonucleotide.[79]

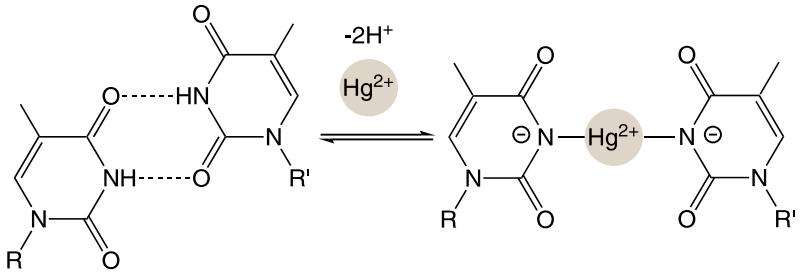

Figure 3.4: Formation of T–Hg^{II}–T base pairs as a result of mercury coordination.

A. Ono, Y. Tanaka and co-workers studied the stability of such T–Hg^{II}–T base pairs and established that the coordinative presence of Hg^{II} metal ion between the T–T base pairs leads to a strong stabilization of the oligonucleotide duplex. The thermal stability examined by UV melting studies revealed a 10°C increase in melting temperature of Hg^{II}–modified duplexes. The thermal stability of the Hg^{II}–modified duplex was also found to be 3°C higher than the sequence with canonical A–T base pairs. The isothermal titration calorimetry results indicated a binding constant of about 5 x 10^5 M^{-1} confirming the specific binding of Hg^{II} to T–T base pairs.[63,79,80] Through ^{1}H NMR, Ono and co-workers observed the replacement of imino protons from thymine residues by Hg^{II}.[79] Also, ^{15}N NMR spectroscopic studies by Tanaka and co-workers provided first direct proof of formation of a T–Hg^{II}–T base pair. They observed an interstrand $^2J(^{15}N, ^{15}N)$ coupling of 2.4 Hz.[63] The relevance of such T–Hg^{II}–T base pairs in biological systems has also been investigated. It has been demonstrated that DNA polymerases can utilize T–Hg^{II}–T base pairs during primer elongation. It was also demonstrated that the polymerases can also incorporate thymine triphosphate opposite a thymine base in presence of Hg^{II} to form T–Hg^{II}–T base pairs.[81] Other work by Park et. al showed that such T–Hg^{II}–T and C–Ag^{I}–C base pairs are considered as normal well-matched base pairs by polymerases and that the addition of metal ions can specifically trigger polymerase activity.[82] In essence, metal mediated base pairing broadens the scope of nucleic acid analogues allowing for widespread application of nucleic acids in biotechnology and material science.[83]

An analogous metal-modified base pair in RNA (U–Hg^{II}–U) has also been investigated.[3] The motivation for studying uracil based metal-mediated base pair is due to their close similarity. The only difference between thymine and uracil is the lacking methyl group in

uracil. This base pair brings the world of metal-mediated base pairing to RNA. ^{15}N NMR spectroscopic studies could confirm the similar coordination patter in U-Hg^{II}-U.[3] However, the structural differences between B-helical DNA and A-helical RNA reveal some challenges in metal ion binding to uracil bases. Moreover, a year later studies with differently substituted uracils revealed that specific changes in pH interestingly led to binding of either Hg^{II} or Ag^{I} metal ions.[84] These results signify that with slight changes at non-coordinating sites it is possible to tweak preferential binding of desired metal ion. This thesis deals with the interaction of metal-modified nucleic acids with ruthenium metal complexes unravelling insights into the intercalative binding of metal complexes with nucleic acids, focusing on the influence of metal-modified base pairs on intercalative binding. The binding characterisation employs various spectroscopic techniques such as UV-vis, Fluorescence emission, CD and NMR to unravel the differences in binding with various nucleic acid partners. The following sections further will discuss the various binding interactions with nucleic acids with focus on intercalative binding finally introducing the metal complex chosen for the studies with metal-modified DNA.

3.3 Binding interactions of Metal complexes with DNA

DNA represents an attractive target for metal complexes to bind.[85] Besides the classical organic molecules, several efforts have been put into the design of transition metal complexes that can bind selectively bind to nucleic acids based on their structural features.[85] Due to its central role in biological systems, investigating the interaction between artificial molecules and the DNA is very important. The structural perturbations induced as a result of binding have a significant influence on the biological activity of the double helical polymer. In addition, investigating binding interactions also reveals interesting information about the aberrations in the DNA such as mismatches and abasic base pairs. Such data is useful for further development of much more specific molecular probes that could be applied as diagnostic or therapeutic agents.

Straight away, transition metal complexes offer two main advantages. Firstly, they allow for a modular system where a stable metal centre acts as a rigid anchor holding the coordinated ligands, which could impart recognition or chemical properties to the complex. The ligands are interchangeable and thus the properties of the resulting metal complex can be tweaked easily. Secondly, transition metal centres possess unique electrochemical and photophysical properties, which provide direct benefit over passive molecular recognition systems. Such properties have allowed metal complexes to be used in a wide variety of applications ranging from fluorescent markers to DNA foot-printing agents to electrochemical probes.[86] Metal complexes can interact with nucleic acids via either covalent or non-covalent binding.[87,88] There are covalent interactions, which result in structural perturbations in the molecule resulting in disruption of its cellular activity like in the case of cisplatin binding to N7 atoms of guanines.[89,90] And, there are non-covalent interactions that provide multiple targets, with greater specificity, through various interactions in the grooves and base pair stack of the molecule. The non-covalent interactions can be categorized based on the involvement of the phosphate backbone, or the groove on the helix, or interaction with the base pair π-stack.

Surface binding: This binding interaction occurs as a result of the electrostatic or Van der Waals forces between the negatively charged phosphate backbone and cationic molecules. Such interactions are therefore limited to the surface of the double helix. Most common example are the histone proteins that bind DNA via interaction with negative phosphate backbone.[91]

Groove binding: This binding relies on the most accessible groove (major or minor) on the DNA molecule. The number of hydrogen bond acceptors and donors defines the grooves on the DNA. The Hoechst 33258 DNA binding dye is a well-known example of a minor groove binder.[92,93] Many transcription factors, polymerases and nucleases rely on a combination of surface binding via electrostatic potential

distribution to recognise nucleic acid backbone and bind via hydrogen bonding with either the phosphate backbone or nitrogen bases by accessing one of the grooves.

Intercalative binding: This binding occurs as a result of planar insertion of the ligand (of the molecule) between the base pairs of the DNA. Unlike the above two binding types, intercalation leads to physical changes in the DNA structure by the way of unwinding the helix and increasing its length.[94]

Non-covalent, DNA-binding metal complexes share a few important characteristics. Most of the complexes studied by other researchers are either photochemical or photophysically active. With a few exceptions, most of the metal complexes are also kinetically inert. This allows them to form stable complexes.[95] In fact, most of the complexes are d^6 octahedral or d^8 square planar. Apart from this, such metal complexes are also mostly structurally rigid with a defined three-dimensional structure. Too much flexibility could negate recognition of DNA targets. Furthermore, the stereochemistry of the complex if applicable can provide specificity as DNA targets are themselves chiral in nature. Thus, due to their unique electrochemical and photophysical properties, such metal complexes provide tremendous utility as nucleic acid probes or effecting chemistry at binding sites. In this thesis, the main focus is on characterizing the intercalative binding interactions of non-covalent transition metal complex $[Ru(bpy)_2(dppz)]^{2+}$ with nucleic acids.

Metallointercalation: This term was first coined by Lippard and co-workers from the studies of square planar Pt complexes intercalating into DNA.[96] Such planar complexes composed of aromatic heterocyclic ligands can stack amongst the nucleic acid base pairs in an unspecific manner. Being unspecific binding, obtaining meaningful structural characterization remains a challenge. Intercalators are small organic molecules or metal complexes that unwind the DNA in order to π-stack between the base pairs.[97] The metallointercalators are metal complexes that carry at least one intercalating ligand. These ligands are oriented parallel to the base pairs and are protruding away from the metal centre such that they readily π-stack in the DNA duplex. Upon intercalating, the other ancillary ligands, which do not participate in π-stack, help by anchoring themselves along the groove(s) thus stabilizing the helix and directing the orientation of the ancillary ligands with respect to the duplex. Two well-known examples of the intercalating ligands are the phi (9,10-phenanthroquinone diimine) and dppz (dipyrido [3,2-a: 2',3'-c] phenazine).[98-100] Ligand intercalation can easily be demonstrated by photophysical studies. The UV absorption for the intercalating ligand can be observed to decrease as it contributes increasingly in π-stacking with the DNA base pairs. Then again, depending on the metal centre and ancillary ligands, the intercalation could be observed as a result of the fluorescence luminescence from the complexes. Furthermore, NMR studies and high-resolution X-ray crystallography studies were able to reveal the structural basis of intercalative binding.[14,101] As a result of intercalation, the

intercalating ligand effectively acts as a new base pair. [88] Another effect observed is the increase in the DNA rise per residue and widening of the groove at binding site.[102] All these changes are minimal as the overall structure of the DNA is mostly unchanged. For example, in the case of B-DNA the sugar conformations (C_2' endo and anti) are maintained.[102] The only necessary requirement for intercalation is the opening of the phosphate angles.

3.3.1 $[Ru(bpy)_2(dppz)]^{2+}$

The DNA light-switch $[Ru(bpy)_2(dppz)]^{2+}$ (bpy=2,2'-bipyridine, dppz=dipyridophenazine) is a well-known transition metal complex categorized as metallointercalator. It is a sister analogue of the $[Ru(phen)_2dppz]^{2+}$.[100,103]

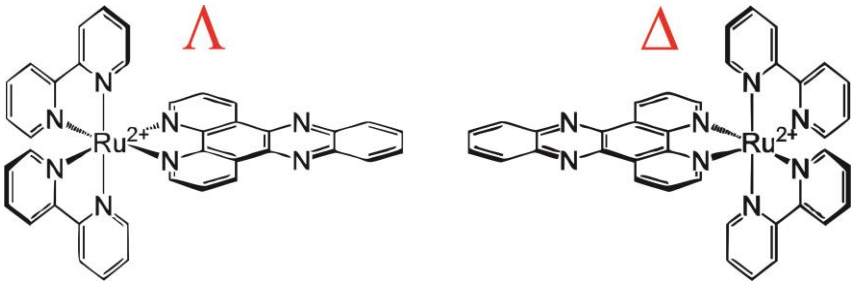

Figure 3.5: The DNA light-switch complex $[Ru(bpy)_2(dppz)]^{2+}$ (bpy = 2,2'-bipyridine, dppz = dipyrido[3,2-a:2',3'-c]phenazine) enantiomers. The light-switch effect occurs as a result of shielding of phenazine nitrogens from hydrogen bonding water.

These complexes show solvatochromic luminescence in organic solutions. However, in aqueous solutions, the excited state luminescence is deactivated by water and thus no emission is observed. This is followed by the hydrogen-bonding of the water with the endocyclic phenazine nitrogen atoms of the dppz ligand, which is the intercalating ligand in both cases. The interesting note here is that in the presence of DNA, the luminescence is restored and bright emission can be observed when these metal complexes are excited at their excitation wavelength at around 440nm. The bright emission occurs as a result of intercalation, where the dppz ligand slides between the DNA base pairs, thus the DNA surrounding the ligand prevents water from gaining access to the phenazine nitrogens. Thus, the DNA creates a region free of hydrogen bonding water for the complex to display its characteristic luminescence.[100,104,105] Due to their peculiar luminescence properties, such metal complexes have immense potential for being used as fluorescent probes of nucleic acids, in therapeutics and diagnosis of various diseases.[106-108] The aim of the thesis is to use the $[Ru(bpy)_2(dppz)]^{2+}$ as an electroluminescent probe that intercalates into metal-modified DNA and RNA duplexes and reports back the changes in binding sites on duplexes both in absence and presence of mismatched, metal-mediated and natural base pairs.

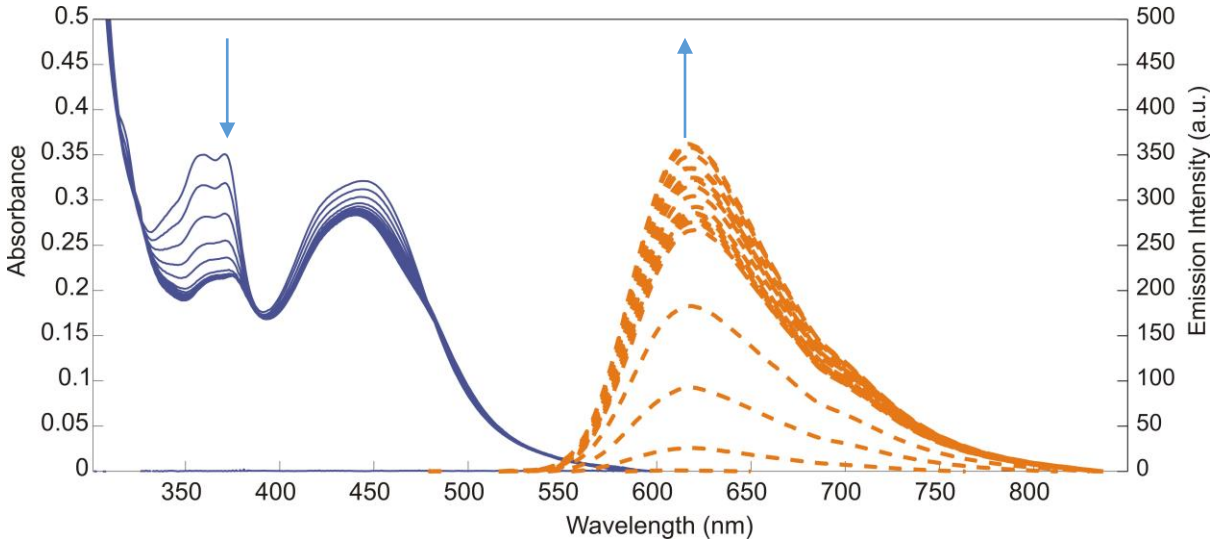

Figure 3.6: Typical absorption and emission profile of $[Ru(bpy)_2(dppz)]^{2+}$. Upon intercalation into duplex DNA, the absorption (blue) undergoes hypochromism with decreasing absorption saturating to a plateau. The emission (orange) increases with increasing DNA per complex and saturates to a plateau when all binding sites on DNA are occupied.

Figure 3.6 depicts the absorption and emission profile of the metal complex $[Ru(bpy)_2(dppz)]^{2+}$ in presence of increasing amounts of DNA. The figure summarises typical output of a titration experiment where upon increasing the concentration of DNA base pairs available per metal complex, the UV profile undergoes hypochromism at the MLCT and π–π* wavelengths, 444 nm and 370 nm respectively. The steady-state emission measured on fluorescence spectrometer shows an increase in intensity for the same DNA/Ru ratios with emission maxima at around 620 nm. Depending on the length of the DNA or number of binding sites available, the UV absorption and fluorescence emission intensities will saturate as all the binding sites are occupied by the available metal complex. The plots of emission maxima and π–π* wavelengths reveal qualitative information about the binding interactions and fitting the data provides quantitative information such as binding strength or stoichiometry. The thesis relies on such data to compare and correlate the findings in order to draw most important conclusions about the binding characteristics of the metal complex and it's separated enantiomers with various nucleic acid duplexes.

3.4 SPECTROSCOPIC TECHNIQUES

The main techniques used to characterise the binding interactions of the metal complex with metal-modified nucleic acids are briefly discussed in this section. Monitoring the changes in the absorption and the fluorescence emission of the metal-complex upo n interaction with nucleic acids as described in section 3.3.1 is easy way to obtain first-hand, qualitative binding information. The physical principles of fluorescence, absorption and circular dichroism are defined.

3.4.1 FLUORESCENCE

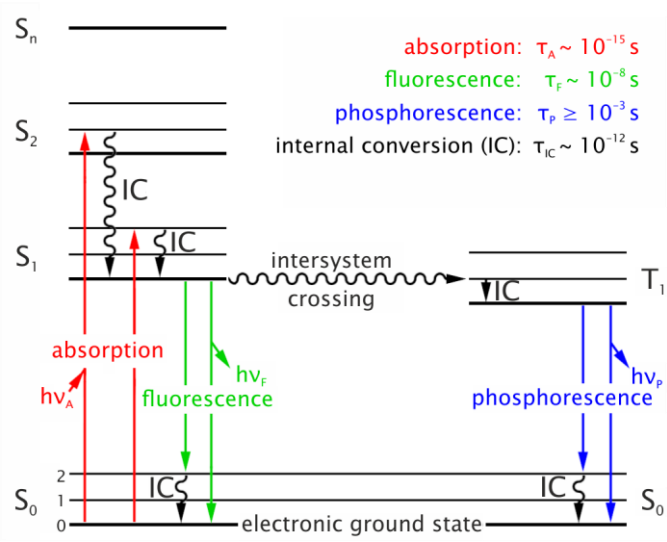

Figure 3.7: The photophysical principles underlying absorption, fluorescence and phosphorescence.

The emission of light upon relaxation of an excited electron leads to the phenomenon called Photoluminescence. The emitted photon via such relaxation, has similar energy to the difference in the energy of the ground and the excited state.

$$\Delta E = E_{\mathrm{Sn}} - E_{\mathrm{S0}}$$

$$\Delta E = h\nu$$

$$\Delta E = h\frac{C_0}{\lambda}$$

where, h is Plank's constant, C_0 is the speed of light and λ is the wavelength of the electromagnetic wave. Here, the energy, ΔE is in theory the δ-function at 0 K for molecules in the gaseous phase. However, for molecules in solution due to the solvent-chromophore interactions, spectral broadening is observed. This is often combined with excitations into more than one vibrational state. The Jablonski diagram (Figure 3.7) illustrates the processes in absorption, fluorescence and phosphorescence. Absorption of a photon (hν), leads to the excitation of an electron in the ground state S_0, to a higher singlet quantum state (S_1, S_2,

…S_n). This is time bound process generally very rapid taking place within $\tau_A \sim 10^{-15}$ s. This (excitation) is followed by vibrational relaxation (or internal conversion, IC) to the lowest vibrational energy level of the lowest excited state S_1 ($\tau \sim 10^{-12}$ s). This phenomenon is referred to as Kasha's rule.[109]

Fluorescence and phosphorescence are differentiated on the basis of the nature of the excited state prior to the radioactive decay. Fluorescence is a process where the excited state electron decays directly from S_1 to S_0 usually taking $\tau_F \sim 10^{-8}$ s. In phosphorescence, the excited state electron undergoes intersystem crossing to a triplet state (radiation-less) that leads to inversion of the electron spin. As a result, both, the electron in the triplet state and the electron in the ground state have identical orientation. Then, vibrational relaxation is followed by radiative decay to S_0. Such decay process involves a forbidden transition according to quantum-mechanics and thus phosphorescence is less likely to happen than florescence. The decay constants for phosphorescence are higher ranging from $10^{-3} \leq \tau_P \leq 10^{0}$ s.[110]

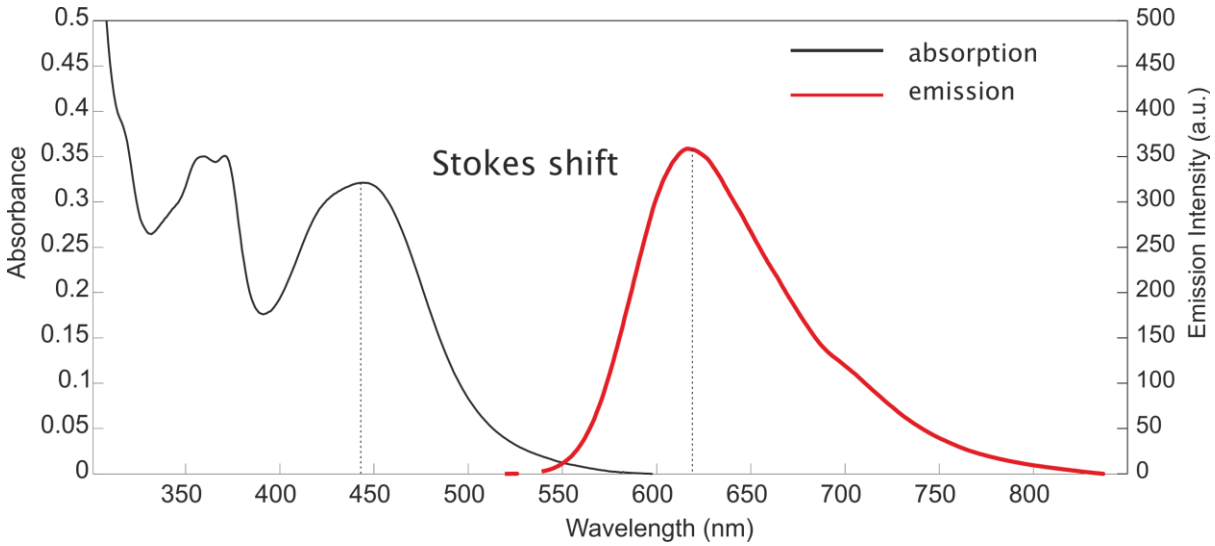

Figure 3.8: Typical absorption and emission profile of $[Ru(bpy)_2(dppz)]^{2+}$ depicting the large Stokes shift for $[Ru(bpy)_2(dppz)]^{2+}$. (emission occurs only in presence of DNA in aqueous solutions).

The energy of the absorbed photon ($h\nu_A$) is usually higher than that of the emitted photon ($h\nu_F$) in fluorescence and this phenomenon is referred to as Stokes shift.[111]

3.4.2 Circular Dichroism

Circular Dichroism is a spectroscopic technique used to study chiral molecules, and it finds many uses in the study of biomolecules such as DNA, RNA and proteins. The secondary structure of the biomolecules is particularly sensitive to changes in variables like pH, ionic strength, temperature and the ratio of ligand per biomolecule being studied. This is where CD finds its primary application. Circular dichroism is defined as the difference in the

absorbance of left circularly polarised light and the right circularly polarised light, where λ is the wavelength:

$$\Delta A(\lambda) = A(\lambda)L_{CPL} - A(\lambda)R_{CPL}$$

It can also be expressed as

$$\Delta\varepsilon = \varepsilon.L_{CPL} - \varepsilon.R_{CPL}$$

$$\Delta\varepsilon = \Delta A/(C * l)$$

Where, $\varepsilon.L_{CPL}$ and $\varepsilon.R_{CPL}$ are molar extinction coefficients for left circularly polarised light and right circularly polarised light, C is the molar concentration and l is the path length in centimetres (cm). This ($\Delta\varepsilon$) is molar circular dichroism. Circular dichroism can also be expressed as degrees of ellipticity (θ) and the relation of ΔA to θ is given by:

$$\Delta A = \theta/32.982$$

And, molar circular dichroism is given by:

$$\Delta\varepsilon = [\theta]/3298$$

DNA–Ligand Interactions

The ligands that bind to the DNA are usually cationic. Their binding is stabilised if the binding site adapted by the ligand is complementary to the DNA and ligand shapes. Planar aromatic molecules such as the $[Ru(bpy)_2(dppz)]^{2+}$ with its dppz ligand intercalates between the base pairs of the DNA. Also, certain bulky proteins adopt the major groove of the DNA. The CD signal of the DNA is dependent on the chirality of the helix and any changes in the component signal can be expected as a result of binding interactions via intercalation or groove binding. If the ligand happens to be achiral, meaning it has no intrinsic CD signal of its own before binding to DNA, the change in the CD signal of the component DNA is obvious. Thus, the CD signals induced upon binding of ligand to DNA are characteristic of interaction and could be interpreted to be used to obtain data such as binding constants. The most basic application of CD spectroscopy is to note the induced CD, ICD as a nonzero value indicates that the molecule must be binding to the DNA. It is possible to obtain more information from the CD data as discussed by Garbett et al. 2007.[112] In the case of DNA ligand interactions, if the measured ICD signal above 300 nm for the ligand does not change with relation to varying DNA:ligand ratio (the amount of ligand actually bound might have changed though) we may write:

$$L_b = \alpha * ICD$$

Where L_b is the concentration of the bound ligand and α is the proportionality constant. In the case where DNA is kept at constant concentration and increasing amounts of ligand is

added, at high DNA concentrations the concentration of bound ligand is approximately equal to the total ligand concentration. In case of excess ligand, it becomes difficult to judge the CD data since the ligand would most certainly adopt a second binding site with a different induced CD signal.[113–116] Interestingly, in the case when the ligands compete to occupy binding site as a result (of intercalative binding at low DNA per ligand concentrations) the ligands start stacking together (DNA serving as a scaffold) and hence, a significant number of ligand–ligand interactions occur. Such CD induced in ligand transitions as a result of binding to DNA takes place as a result of non-degenerate exciton coupling between the ligand's electric dipole transition moment and the electric dipole transition moments of the DNA bases.[114–116]

3.5 DNA-MEDIATED CHARGE TRANSPORT

The bottom-up approach to nucleic acid based nanoelectronics heavily relies on the structural integrity of the nucleic acid itself.[117] Often regarded as simplest of all chemical reactions, electron transfer (ET) is responsible for important life-sustaining processes such as respiration and photosynthesis.[118,119] Some of the earliest studies of ET in peptide systems and other σ-bonded networks revealed some of the most crucial and limiting aspects of ET. It is the dependence of ET on distance and the thermodynamic driving force. The σ-bond mediated ET is limited to short distances of 15-20 Å, due to a steep drop in the rate of electron transfer upon increasing distances.[120,121] In the more recent past, work done on extended molecular π-stacked systems have established that electron transfer can occur over much long distances in such systems.[117,122]

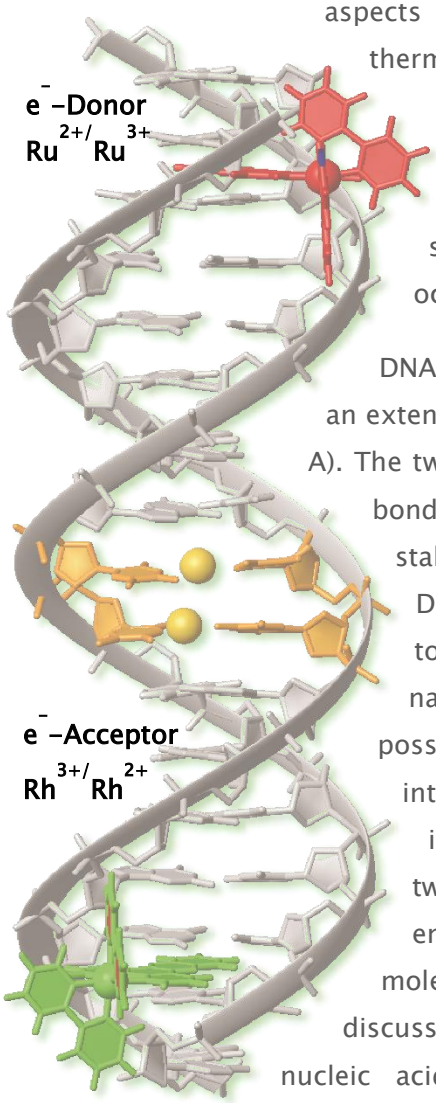

Figure 3.9: Set-up of a photo-activated charge transfer experiment using metal complexes as donor acceptor couple. Model of a Hg^{II}-modified DNA duplex representing the T-Hg^{II}-T base pairs in the middle of the sequence (yellow).

DNA represents a well-characterized molecular system containing an extended π-stack within the interior of its double helix (Figure 3.2-A). The two strands that make up the helix are held together hydrogen bonding between the complementary bases. The helix is further stabilized by their stacking interactions. The unique properties of DNA, such as self-assembly have made it an attractive molecule to be applied towards sophisticated molecular nanotechnology.[123] By following a bottom-up approach, it is possible to use the molecule as a scaffold for studying binding interactions of various complexes, for incorporation of metal ions in a predictable manner leading to fascinating structural tweaks in the molecule, and setting-up metal ion array to enable long distance charge transfer on a nanoscale, making molecular nanowires and nanomagnets possible.[123-127] Section 3.2 discussed the various possibilities to site-specifically functionalise nucleic acids to obtain metal-modified nucleic acids with unique properties such as enhanced charge conductance. The ruthenium metal complex can report back the differences in structural perturbations as a result of metal ion coordination. Although these studies give more insights into the mechanism of intercalative binding, the knowledge gained could be applied for setting up photoinduced charge transfer system (Figure 3.9). The ruthenium metallointercalator can also be applied as an electron injecting binder that can be used in conjunction with

another electron accepting molecule that can be bound at a specific distance from the donor molecule and the metal ion array. Using time resolved fluorescence spectroscopy one can determine the charge transfer rates in presence and absence of metal ion array. The thesis aims to establish results that can be used to ultimately allow setting-up of such a charge-transfer experiment.

3.6 Nuclear Magnetic Resonance (NMR) of nucleic acids

Besides X-ray crystallography, NMR is a principle method used for biomolecular structure determination. It allows for a three-dimensional structure determination at an atomic level. Unlike crystallography, NMR experiments are performed with the molecule of interest dissolved in a salt and/or buffer solution, which mimics approximately the physiological environment of these molecules. By contrast to X-ray crystallography, NMR provides the possibility to study not only structure but also dynamic properties of biomolecules. Using NMR, various types of information can be obtained:

- Information on distances between protons by the Nuclear Overhauser Effects (NOE),
- Chemical shifts
- Scalar coupling
- Relaxation times and
- Diffusion coefficients

A major disadvantage of NMR is the molecular size limit. The rotational correlation time, which is simply the tumble of a molecule while in solution, is proportional to the line width of the NMR signal. Therefore, larger the molecule, the slower it tumbles leading to unclear broad line widths. Despite various technical advances, nucleic acid NMR is still usable for short sequences only.[128-132] The vast majority of nucleic acid structures solved hitherto contain less than 50 nucleotides.

3.6.1 Initial steps for structure elucidation through NMR

From solution to structure: Nucleic acid structure determination by NMR can be divided into several steps. First, a series of NMR experiments are performed in 100% D_2O and in 10% D_2O / 90% H_2O to observe the non-exchangeable and exchangeable protons, respectively. The 2D [^{1}H, ^{1}H]-NOESY spectra in 100% D_2O comprises the "sequential walk" region that gives important first hand structural information. In NOESY experiments the magnetization is transferred through magnetic dipole-dipole coupling of protons close in space (with a maximum distance of up

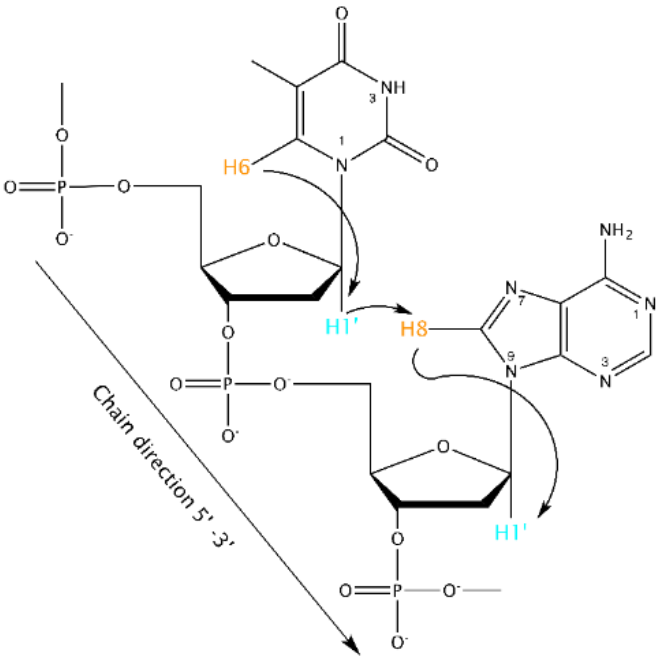

Figure 3.10: The "Sequential Walk". The important protons (nucleobase protons in orange and sugar protons in blue) and their through-space connectivities indicated by black arrows.

to 7 Å) to establish correlation. Each of these proton-proton correlations is visible as a cross peak in the spectrum with an intensity proportional to the interatomic distance by r^{-6}. Figure 3.10 depicts the typical through-space connectivities of nucleobase and sugar protons observed in double helical regions of nucleic acids. The H6 and H8 aromatic protons are spatially close to the H1', H2' and H2'' protons of the own deoxyribose and also to H1', H2' and H2'' of the 5' nucleotide sugar moiety. In layman terms the aromatic protons "can see" both its own sugar protons and the sugar protons of the nucleotide in the 5' direction and therefore the connectivities of consecutive nucleotides in a strand can be established. The sequential assignments are in principal the basis for all the further assignments.

2D [^{1}H,^{1}H]-NOESY spectra in H_2O provide information on the base pairing pattern as correlation of exchangeable proton resonances, like the amino and imino protons that are not visible in D_2O, can be observed. However, it should be noted that only amino and imino protons involved in base pairing or stacking interactions can be seen due to their slower exchange rate with water.[133] Exchangeable protons not involved in such strong interactions have a very fast exchange rate with water, which results in very strong broadening or even disappearance of the signals. Such signals would normally arise from the base pairs at the end of the helixes. In addition to NOESY experiments, several other multidimensional NMR experiments like [^{1}H,^{1}H]-TOCSY (Total Correlated Spectroscopy) and [^{13}C,^{1}H]-HSQC (Heteronuclear Single Quantum Coherence Spectroscopy) are conducted to facilitate and validate the assignments of the NOESY spectra. After all proton resonances are assigned and NOE correlations are integrated, the structure calculation can be performed using the distance restraints obtained by classifying the distances as very strong, strong, medium and weak. However, to fully describe the structure of nucleic acids information on sugar pucker and backbone conformation is required. The conformation of the nucleotide linkage in the backbone is described by five torsion angles α, β, γ, δ, ϵ, and ζ whereas the endocyclic torsion angles ν_0-ν_4 determine the furanose ring conformation of the sugar. In addition, also the glycosidic bond angle χ that determines if the nucleobase is syn or an anti to the sugar moiety can be verified by NMR. (Figure 3.11).

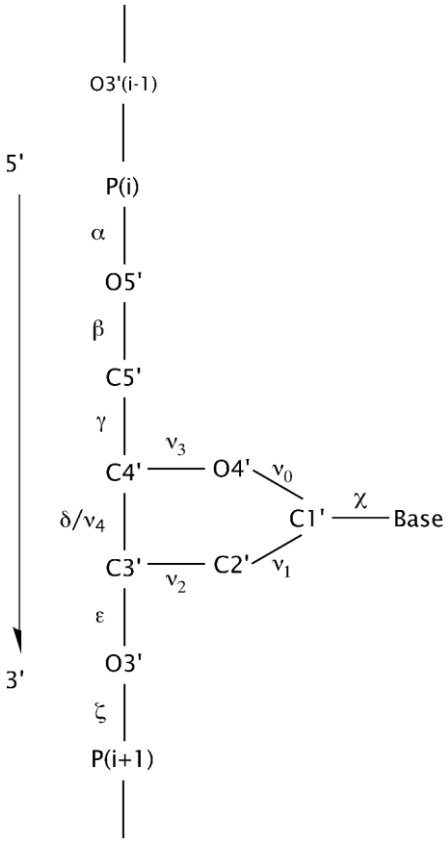

Figure 3.11: The various torsion angles in the sugar phosphate backbone: α, β, γ, δ, ϵ, and ζ; the glycosidic torsion angle χ, and the endocyclic torsion angles ν_0-ν_4 in the sugar ring.

3.7 Thesis Outline

This work deals with the characterisation of intercalative binding of the transition metal complex $[Ru(bpy)_2(dppz)]^{2+}$ with Hg^{II}-modified DNA and RNA duplexes. $[Ru(bpy)_2(dppz)]^{2+}$ is a well-known complex for its unique luminescence properties and several studies detail the interaction of the complex with several long and short oligonucleotide sequences. The first part of the work entails the influence of different sequences on the photophysical properties of the metal complex and its enantiomers, and most importantly gives insights into the influence of metal-mediated (T-Hg^{II}-T) base pairs on intercalative binding. The second part focuses on NMR spectroscopic studies performed with the various Hg^{II}-modified DNA and RNA sequences comparing them with the natural duplexes. The differences between the natural and metal-modified DNA are discussed with a final outlook for the ongoing structural studies. The comparison of the sequences via NMR clearly shows the formation of metal-mediated base pairs in both DNA and RNA. The sequence assignment further tells us about the structural differences between the natural, mismatched and Hg^{II}-modified DNA duplexes revealing that the mismatched base pairs exist in the wobble conformation. The last part of the thesis deals with the thermal stability of the mismatched and Hg^{II}-modified RNA duplexes and discusses the interaction of $[Ru(bpy)_2(dppz)]^{2+}$ with RNA duplexes. The metal coordination leads to a significant increase in the melting temperature of the RNA duplexes demonstrating the strong influence of metal coordination on the overall stability of the duplexes. The results shine light on the intercalative binding interactions with metal-modified DNA / RNA duplexes for the first time.

4 INSIGHTS INTO INTERCALATION OF $[Ru(bpy)_2(dppz)]^{2+}$ ENANTIOMERS WITH Hg^{II}-MODIFIED DNA

4.1 INTRODUCTION

The seminal work by Barton and co-workers on the transition metal complex $[Ru(bpy)_2(dppz)]^{2+}$ (bpy=2,2'-bipyridine, dppz= dipyrido[3,2-a:2',3'-c]phenazine disclosed its peculiar luminescence properties to act as a light switch for DNA (Figure 4.1). It exhibits bright luminescence in presence of DNA, but not otherwise as the luminescence is quenched in aqueous solution.[100,134]

The metal complex $[Ru(bpy)_2(dppz)]^{2+}$ and its sister analogue $[Ru(phen)_2(dppz)]^{2+}$ (phen=1,10-phenanthroline) are well studied for their distinct photophysical properties in particular when their interaction with duplex DNA.[100,104] Their ability to intercalate between DNA base pairs and their extraordinary luminescent properties led to an increased interest towards development of various similar dppz based molecules, which could potentially act as reporter molecules for DNA.[88,135]

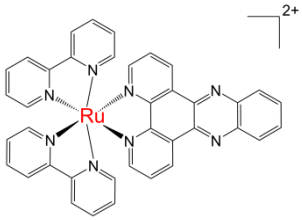

Figure 4.1: The DNA light switch complex $[Ru(bpy)_2(dppz)]^{2+}$.

The unique light-switch effect is considered to occur due to the protection of the phenazine nitrogens of the dppz moiety from hydrogen bonding with water, upon intercalation into DNA.[100,134] Apart from the use in DNA binding studies, the light-switch effect has also been exploited largely in various interdisciplinary fields - from the use of such molecules as reporters of structural aberrations in nucleic acids to their increasing use as components of functional supramolecular assemblies.[136,137] Some established examples are their application in light harvesting antennae and photo-induced charge separation modules in artificial photosynthesis systems.[138]

Recent studies reveal that the intercalative binding of such $Ru(L_2)$dppz complexes does not only depend on the conformation, sequence of the nucleic acids and the enantiomer species of the complex, but is also influenced by sample conditions such as pH, ionic strength and temperature.[8-10] The chiral nature of such complexes also affects the intercalative binding especially as nucleic acid duplexes are themselves chiral biomolecules.[139,140] These new insights reveal the complexity of the intercalation with a binding geometry that is exceptionally sensitive to small changes. For example, planar dppz/phen/bpy based metal complexes readily target the thermodynamically weaker mismatched base pairs on DNA.[16,141,142] Mismatches can occur as result of UV irradiation, polymerase errors or genotoxic substances.[143-145] Hence, probes for mismatched DNA would be very useful as diagnostic tool for detection of mismatches. Another example demonstrated by McKinley et

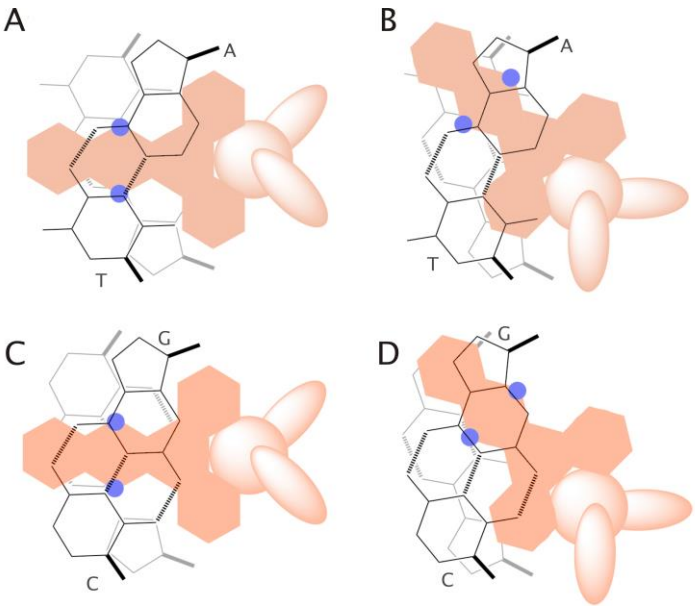

Figure 4.3: A, C depict the symmetrical binding geometry and B, D show the angled (canted) binding geometry upon intercalation of $[Ru(bpy)_2(dppz)]^{2+}$ with poly[dT-dA] and poly[dC-dG] base pair sites respectively. Adapted from Andersson, J.; Fornander, L. H.; Abrahamsson, M.; Tuite, E.; Nordell, P.; Lincoln, P. *Inorg. Chem.* **2013**, *52* (2), 1151.

the single enantiomers of $[Ru(bpy)_2(dppz)]^{2+}$ and $[Ru(phen)_2(dppz)]^{2+}$ by Lincoln and co-workers suggest two different intercalative binding geometries which are governed by the two distinct fluorescence lifetimes (Figure 4.3).[8] They studied time-resolved fluorescence emission data to understand the biexponential excited state lifetime of ruthenium complexes. The two different emission lifetimes have been proposed to originate from two different binding orientations of the complex. This again heavily depends on the enantiomer and the sequence at the binding site of the DNA. Long emission lifetime is assigned to the canted intercalation binding geometry and the shorter lifetime component is assigned to the symmetrical binding geometry (Figure 4.3).[8] Since the emission and lifetimes are directly related to the binding geometry assumed by the complex during intercalation, the complexes could be deployed to report the local DNA structure.

al. describes the influence of nucleic acid sequence on the emission of dppz based metal complexes.[9] The Δ-$[Ru(phen)_2(dppz)]^{2+}$ is shown to emit more strongly with AT-rich polynucleotides than with GC-polynucleotides. In case of $[Ru(bpy)_2(dppz)]^{2+}$ the Δ enantiomer has higher steady-state emission compared to the Λ enantiomer, however both enantiomers bind through intercalation and there is no enantioselectivity noticed when either binds to ctDNA.[146] Recent ITC and photophysical studies of

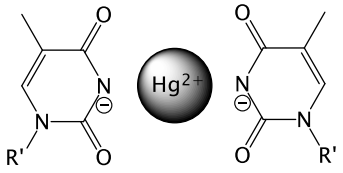

T- Hg^{2+} -T

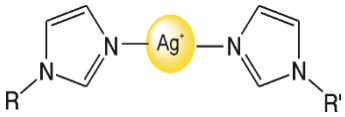

Im- Ag^{+} -Im

Figure 4.2: Metal-mediated base pairs with the natural nucleobases thymine (top) and artificial imidazole nucleobase (bottom) coordinating Hg^{II} and Ag^{I}, respectively. Adapted from Johannsen, S.; Megger, N.; Böhme, D.; Sigel, R. K. O.; Müller, J. *Nature Chemistry* **2010**, *2* (3), 229.

On the other hand, metal modified DNA is increasingly gaining importance in interdisciplinary research as the robust structural properties of DNA allow it to be employed as a scaffold for building molecular wires and magnets on a nano scale.[3,4,147] This application relies heavily on a firm structural confirmation of the nucleic acids itself. The site-specific functionalization of nucleic acids with metal ions that coordinate between either natural base pairs or artificial base pairs is one of the most promising methods to incorporate metal ions within the nucleic acid helix. We started with the aim to set-up photo-induced charge transfer experiments. By employing the DNA light-switch effect of the $[Ru(bpy)_2(dppz)]^{2+}$ we studied the enhancement in charge transfer properties of the Hg^{II}-modified DNA duplexes. Our studies incorporate the Ruthenium metal complexes as probes to gain insights into the influence of presence of metal ions in functionalized nucleic acids (Figure 4.2). The site-specific binding and luminescence characterisation studies impart a greater importance to this transition metal complex demanding further deeper investigation into its intercalative binding properties.

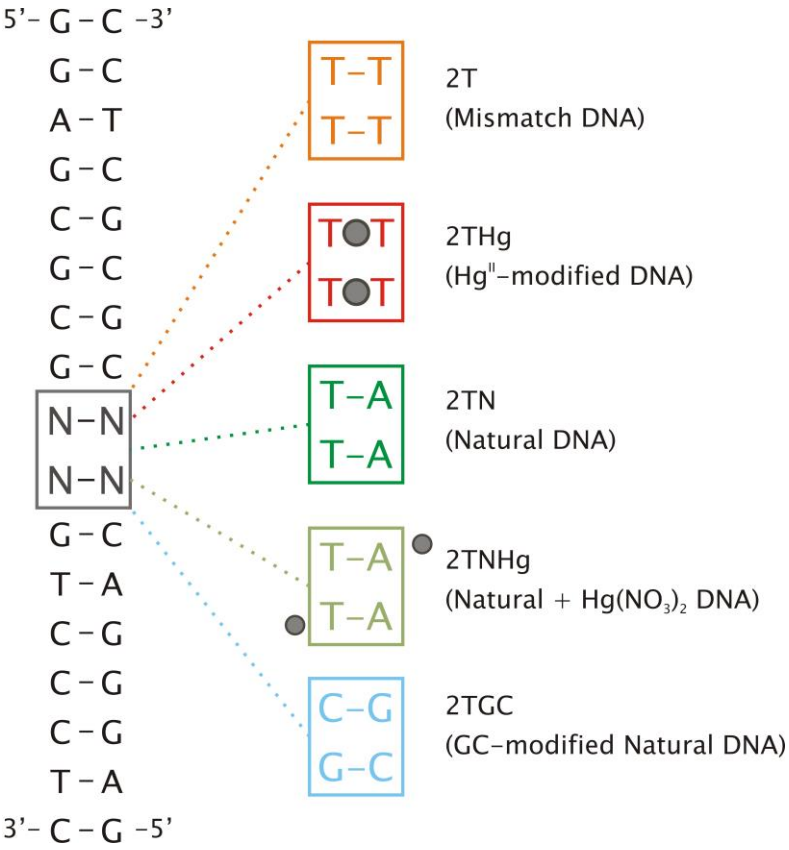

Figure 4.4: Design of the various DNA duplexes employed to study the intercalative binding of Ruthenium complexes with metal-modified oligonucleotides. The duplexes are the same except for changes at N_9, N_{10}- N_{25}, N_{26} bases in the middle. The T-T base paired duplex (mismatch duplex) becomes T-Hg-T (Hg^{II} modified) upon Hg^{II} coordination. To use as a control DNA duplex, the T-A (natural) and G-C (GC-modified natural) are used. The overall length of the duplexes is 17 base pairs.

We performed series of spectroscopic studies including UV-vis, Fluorescence emission, CD and time-resolved single photon counting techniques to understand the intercalative binding with mismatched DNA duplexes, metal-modified duplexes and duplexes with Watson-Crick base pairs with slight modification at the preferential binding site of the intercalating metal complex. These studies formed a part of the bigger goal of setting-up photoinduced charge transfer experiment as described in Section 3.5. The aim of setting up robust charge transfer experiments led us to first investigate the binding characteristics of DNA light-switch complex with metal-modified DNA duplexes on an individual enantiomer level. The chapter deals with the necessary insights obtained in order to gain a deeper understanding of the intercalative binding itself as well as the subtle influences on binding brought about by Hg^{II} ion coordination between mismatch base pairs.

4.2 RESULTS

4.2.1 UV-Vis Absorption titrations

UV-vis absorption titrations were conducted with the aim to determine the hypochromism and to compare the binding constants across the various DNA duplexes. Comparing the results with literature would offer evidence for intercalative binding and the strength of binding itself. First, we measured the titrations keeping the racemic mixture of $[Ru(bpy)_2(dppz)]^{2+}$ constant at 17 μM. The results are summarised in Figure 4.5 and Appendix 2. Thereafter, the titrations were performed with separated enantiomers of $[Ru(bpy)_2(dppz)]^{2+}$ (Figure 4.5 and Appendix S4).

The intercalative binding of the planar dppz ligand between the DNA base stack causes a decrease of the absorption intensity of the dppz π- π* and the MLCT transition at around 370 nm and 440nm (Figure 4.5). The π* orbital of the dppz moiety that interacts with the DNA bases π orbitals is partially filled with electrons. The transition probabilities are limited and thus effectively result in an hypochromic effect at the dppz π- π* wavelength.[148] The Table 4.1 summarizes the percentage hypochromism (Section 7.5.1) observed for various DNA duplexes and their interaction with $[Ru(bpy)_2(dppz)]^{2+}$.

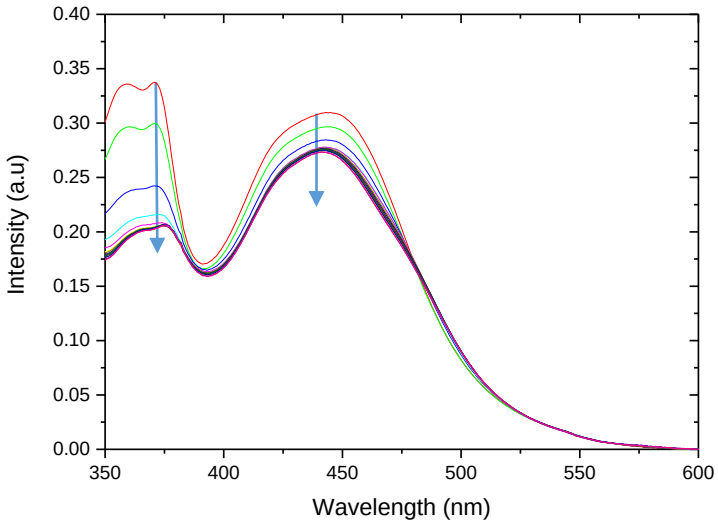

Figure 4.5: Absorption profile of $[Ru(bpy)_2(dppz)]^{2+}$ under experimental conditions. Upon addition of increasing amounts of 2T DNA, the absorption at 370nm and 440nm decreases finally reaching a plateau.

The initial set of titrations were done using only the 2T, 2THg, 2TN and 2TNHg duplexes keeping the racemic metal complex at constant concentration. Table 4.1 summarises the hypochromism observed in each case of DNA used when $[Ru(bpy)_2(dppz)]^{2+}$ binds to them. As observed, the % hypochromism (see Section 7.5.1) upon binding to the metal complex is more or less similar across all the different DNA duplexes studied with slightly less % observed in the case of the 2T duplex. These values are also similar to previously obtained values for $[Ru(bpy)_2(dppz)]^{2+}$ intercalating into ctDNA.[11]

Table 4.1: The percentage hypochromicity observed for all the DNA duplexes used for studies with a racemic mixture of the complex and individual enantiomers. Note that for the 2TGC DNA, no titrations were conducted with *rac*-$[Ru(bpy)_2(dppz)]^{2+}$.

% Hypochromism	Racemic $[Ru(bpy)_2(dppz)]^{2+}$	Δ	Λ
2T	37	39	37
2THg	40	38	39
2TN	41	42	40
2TNHg	41	42	40
2TGC	-	40	37

To further elucidate the contribution of each of the isomers during the intercalation, we conducted the titrations with separated enantiomers (see Table 4.1). With only UV-vis spectroscopy, the subtle differences between the various DNA duplexes cannot be expected to be observed directly. However, based on the data obtained, we still see an overall higher % hypochromism in the case of Δ-$[Ru(bpy)_2(dppz)]^{2+}$ compared to its mirror analogue Λ-$[Ru(bpy)_2(dppz)]^{2+}$. Also what can be observed is that the highest hypochromism is consistently observed for the perfectly matched natural DNA duplex (both with and without $Hg(NO_3)_2$ in solution). The second highest hypochromism is observed for the GC-modified natural duplex as this is also well-matched duplex with an exception of C-G base pairs instead of A-T. The least % hypochromism is observed in the case of the mismatch DNA followed by the Hg-modified duplex. The mismatched DNA due to its flexible thymine-thymine mismatch region can in principle, accommodate more of the ruthenium metal complexes. The hypochromism values are also much more similar to GC-modified duplex, however, the presence of Hg^{II} might be influencing the intercalative binding in interesting ways that can be investigated in further results from other techniques.

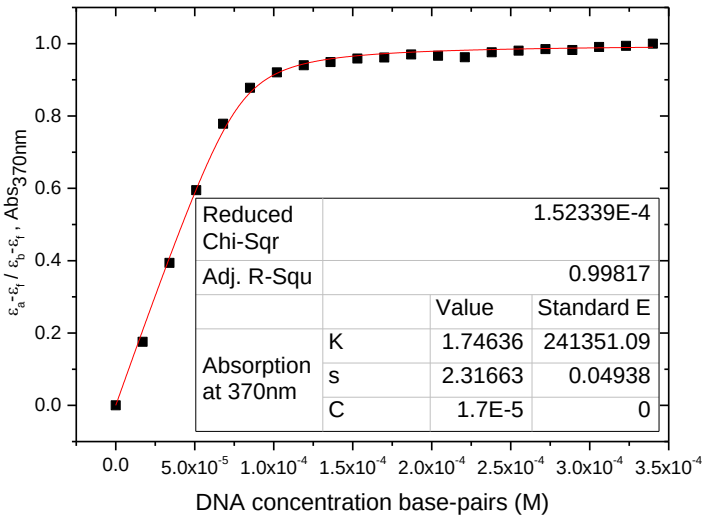

Figure 4.6: The fitted absorption titration data of Δ-$[Ru(bpy)_2(dppz)]^{2+}$ (with 2TN) at 370nm. The hypochromicity saturates after 8 additions of DNA aliquots.

The absorption data for all the duplexes were fitted using the equation developed by Bard et al. for the non-cooperative binding (Figure 4.6) of a metallointercalator to DNA of infinite length (Figure S4 for the remaining fitted data).[12,149]

$$\frac{(\epsilon_a - \epsilon_f)}{(\epsilon_b - \epsilon_f)} = \frac{b - \left(b^2 - \frac{2K^2 C_t [DNA]}{s}\right)^{\frac{1}{2}}}{2K}$$

$$b = 1 + KC_t + \frac{K[DNA]}{2s}$$

Where, ϵ_a, ϵ_f, and ϵ_b are the extinction coefficients of the metal complex at a given DNA concentration, the metal complex free in solution, and the metal complex fully bound to DNA, respectively, K is the equilibrium binding constant, C_t is the total metal complex concentration, [DNA] is the DNA concentration in base pairs, and s is the binding site size. The fitting revealed few interesting observations. Firstly, one obtains a set of binding constants that are in the order of magnitude of 10^6 M^{-1} for all the duplexes as also reported in previously done studies. However, the s (binding-site size) value seems to differ amongst the binding constant obtained from either of the enantiomers and amongst the different duplexes studied. This equation caters only to oligonucleotides of infinite length since it is based on Original McGhee von Hippel model for a non-cooperative binding mode, which does not consider the cooperativity between neighbouring ligands, as well as the increased affinity of the ligands for abasic, mismatched or flexible binding pockets on duplex.

4.2.2 Steady-state fluorescence emission titrations

Racemic $[Ru(bpy)_2(dppz)]^{2+}$

The emission intensity titrations were carried out keeping racemic mixture of the metal complex constant at 17 μM in 5 mM MOPS 10 mM $NaNO_3$ (pH 7.5) buffer and to it, increasing amounts of duplex DNA were added in 1 μL aliquots (1 μM of DNA concentration- calculated in base pairs). The ratio of Ru: DNA was monitored from 1:0 (one Ru: No-DNA), 1:0.06 (one Ru complex per one base pair) to 1:1.18 (one Ru per > 1 duplex). Between each incremental additions, absorption and fluorescence emission were acquired. The peak emission intensity was observed at around 620 nm which is the emission maxima for the $[Ru(bpy)_2(dppz)]^{2+}$ and thus the emission data across the 2T, 2THg, 2TN and 2TNHg duplexes were compared at this wavelength (see Appendix S3 for emission spectra and individual plots of emission maxima at 620 nm for each duplex).

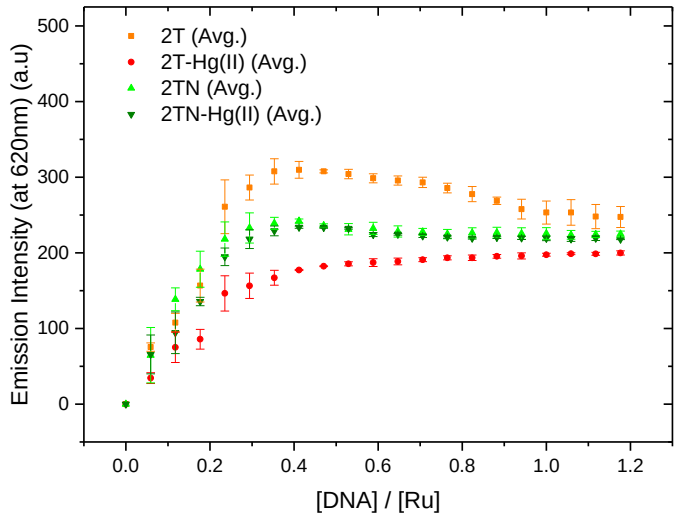

Figure 4.7: Steady-state emission of $[Ru(bpy)_2(dppz)]^{2+}$ at 620nm against increasing DNA/Ru with mismatch DNA duplex (orange squares), Hg^{II} modified DNA duplex (red dots), Natural DNA duplex (green triangle) and natural DNA duplex + $Hg(NO_3)_2$ in buffer (olive green triangles). The buffer used was 5mM MOPS with 10mM $NaNO_3$ at pH 7.5.

The aim of these experiments was to qualitatively compare the emission intensity from the $[Ru(bpy)_2(dppz)]^{2+}$ when it is intercalated into each of the various duplexes. The emission intensities observed for the racemic mixture reveals highest intensity when intercalating into 2T, followed by the 2TN duplex (with and without Hg^{II} in the buffer) and the least intensity observed for the 2THg duplex. In all the cases, the emission is observed to reach a plateau after addition of 8 – 9 (1 µL) aliquots. The emission intensity was 1.5 times higher when the metal complex intercalates into the 2T DNA compared to 2THg indicating a certain influence of T-Hg^{II}-T base pairs on intercalation. The emission intensity for the 2TN and 2TNHg duplexes was 1.3 times lower than that of 2T.

The mismatch DNA 2T with thymine-thymine mismatched base pairs seems to accommodate the Ru^{II} metal complex much more readily than a natural DNA duplex like 2TN/2TNHg could. As observed from the data, both 2TN and the 2TNHg duplex were equal in emission intensity when the racemic Ru intercalates into them. This means that the free Hg^{II} in the buffer does not have an influence on intercalation of racemic mixture of Ru metal complex. However, interestingly the lowest emission from the metal complex was observed in the case of the 2THg, the Hg^{II} modified DNA duplex. The T-Hg^{II}-T base pairs are formed as result of deprotonation as the charge held by Hg^{II} ion are lost as a result of coordination between the N3H of the two consecutive thymine nucleotides. This leads to formation of a neutral stable base pair that is thermodynamically comparable to a normal Watson-Crick base pair.[45,79,150,151] Hence, one would assume that the emission for a Hg^{II} modified duplex should be comparable to the natural duplex. Since in this case we were observing the emission from a racemic mixture of the metal complex, the observed intensity enhancement in case of 2T could be due to the cooperative binding. As described by Andersson et al.[8], such binding between the enantiomers could lead to a situation where one prefers to bind a

specific site on the duplex in a certain binding geometry to which, another enantiomer binds adjacently close assuming slightly different binding geometry. The two binding geometries lead to either higher or lower emission depending on the degree of shielding offered to the phenazine nitrogens. The distance between the adjacently bound enantiomers would be dictated by the sequence of the DNA and the confirmation. Thus, it seemed necessary to study the emission of individual enantiomers.

Δ AND Λ-$[Ru(bpy)_2(dppz)]^{2+}$

In order to investigate and characterise the intercalation of the individual enantiomers, the titration experiments were conducted with separated enantiomers in similar manner as previously described for the racemic mixture. The concentration of each metal complex enantiomer was kept constant at 17 μM while increasing amounts of DNA were added.

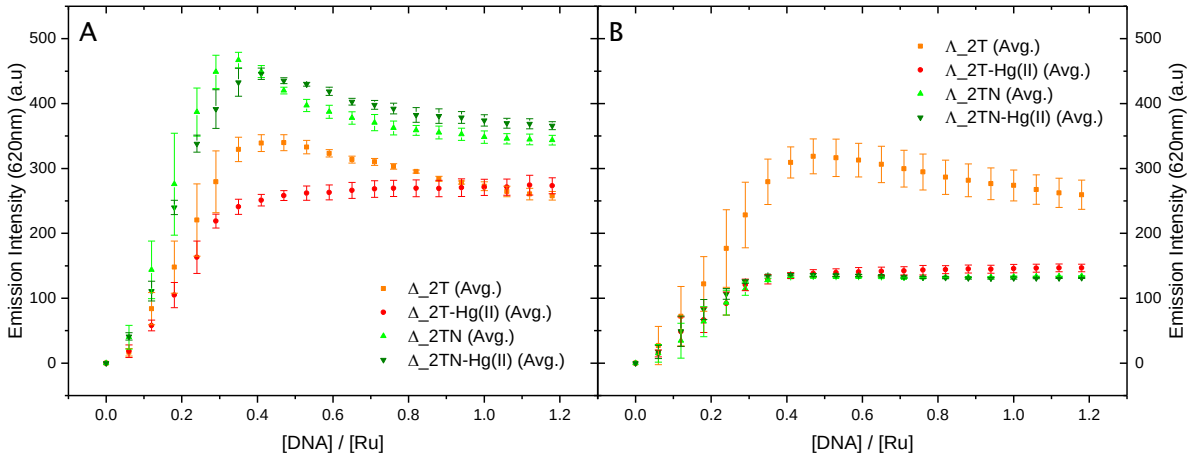

Figure 4.8: Emission intensity of individual isomers of $[Ru(bpy)_2(dppz)]^{2+}$. The graph in (A) depicts the emission intensity of the Δ-$[Ru(bpy)_2(dppz)]^{2+}$ at 620 nm and in (B) depicts the emission intensity of Λ-$[Ru(bpy)_2(dppz)]^{2+}$ at 620 nm when intercalated into 2T, 2THg, 2TN and 2TNHg.

Figure 4.8 compares the emission intensity of Δ and Λ-$[Ru(bpy)_2(dppz)]^{2+}$ with 2T, 2THg, 2TN and 2TNHg duplexes. We observe that the emission intensities of the Δ and Λ enantiomers are significantly different. The Δ enantiomer depicts higher intensity almost in all cases except with 2T where both enantiomers are able to emit with similar intensity. The emission intensity of the Δ enantiomer varies across 2T, 2THg and 2TN duplex. Unlike the previous studies with *rac*-$[Ru(bpy)_2(dppz)]^{2+}$, the highest intensity was noted for the 2TN duplex (both in absence and in presence of Hg^{II} in buffer), but with a decrease in emission maxima which then saturates at duplex/Δ-Ru ratios 1:1. A similar pattern was observed also for the 2T duplex in both the cases of Δ and Λ-$[Ru(bpy)_2(dppz)]^{2+}$. In the case of Δ-$[Ru(bpy)_2(dppz)]^{2+}$ intercalating into 2THg duplex, the emission intensity at 620 nm is albeit a bit lower, but without the decrease in emission maxima. In the case of the Λ enantiomer,

we observe a predictable binding behaviour with all the DNA duplexes except the mismatch DNA 2T. The emission intensities are similar when Λ-$[Ru(bpy)_2(dppz)]^{2+}$ intercalates into either 2THg, 2TN and 2TNHg indicating similar binding behaviour of the isomer irrespective of the difference in sequence or the presence of Hg^{II} in the 2THg duplex. Only in the case of 2T, either of the enantiomers shows a similar emission intensity indicating similar binding geometries assumed by the isomers. The mismatch region being structurally undefined could accommodate the Λ enantiomer with a binding geometry favouring comparable shielding of phenazine nitrogens as also with the Δ enantiomer. The structural features of the T-T mismatch region also offer least hindrance to the Λ enantiomer by reducing the backbone interaction with the ancillary bpy ligands, which might result in the enhanced luminescence observed. Compared to other duplexes, it is clear that the Λ enantiomer is unable to intercalate deeply inside the base pair pockets of natural duplexes due the hindrance from the backbone. It seems to intercalate, but is being forced to assume a symmetric geometry. Moreover, for the same reason, the intercalation of the Λ enantiomer is shallow leading to insufficient shielding of phenazine nitrogens of the bound complex resulting in lowered emission. The presence of Hg^{II} seems to impart a well-defined structure to 2THg, which is comparable to natural duplex 2TN as indicated by the data.

To understand the decrease in emission at higher DNA/Ru ratios (in the case of Δ-$[Ru(bpy)_2(dppz)]^{2+}$), the emission titrations were once again conducted with lowered (constant) concentration of metal complex in order to rule out any possibilities of inner filter effects. Figure 4.9 summarizes the steady-state emission titration results. There was no significant difference between the two experiments except the lowered intensity as a result of lowered concentration of the metal complex. Clearly, it could be observed that the decrease in the emission maxima was still apparent and the individual enantiomers depicted similar binding behaviour. This excluded the possibility of inner filter effects as the decrease in emission maxima was observed at both high (17 μM) and low (5 μM) concentrations of the metal complex isomers. The sequences for the DNA duplexes, which are rather similar, differ in the centre. The natural DNA duplex, has contiguous T-A Watson-Crick base pairs which are also the preferred binding site for the Δ enantiomer.[9] McKinley and co-workers observed the highest emission intensity when the Δ-$[Ru(bpy)_2(dppz)]^{2+}$ binds to $[poly(dAdT)]_2$. Therefore, we introduced another DNA duplex- 2TGC, differing only in the centre of the sequence (Figure 4.4. The contiguous $(T-A)_2$ base pairs were replaced by a non-contiguous C-G, G-C (for nucleotides 9-26 and 10-25 respectively). The titration experiments were conducted in similar conditions as for all the other duplexes and their emission intensities were compared (Figure 4.9). The result now was rather contrasting. The decrease in emission intensity observed in the case of 2TN was not visible with the GC modified DNA duplex 2TGC. Swapping the middle contiguous sequence altered the binding behaviour of the enantiomer in a way that affected the preferential binding. As G-C base pairs are not the preferred binding sites[10], the occupation of the middle region was scarce.

As a result, the closely bound metal complexes at lower DNA/Ru ratios were less. In addition, the distribution of the metal complexes on the duplex was more uniform which leads to occupation of preferred A-T base pairs first followed by the rest of the regions. Hence, the decrease in emission intensity was not observed.

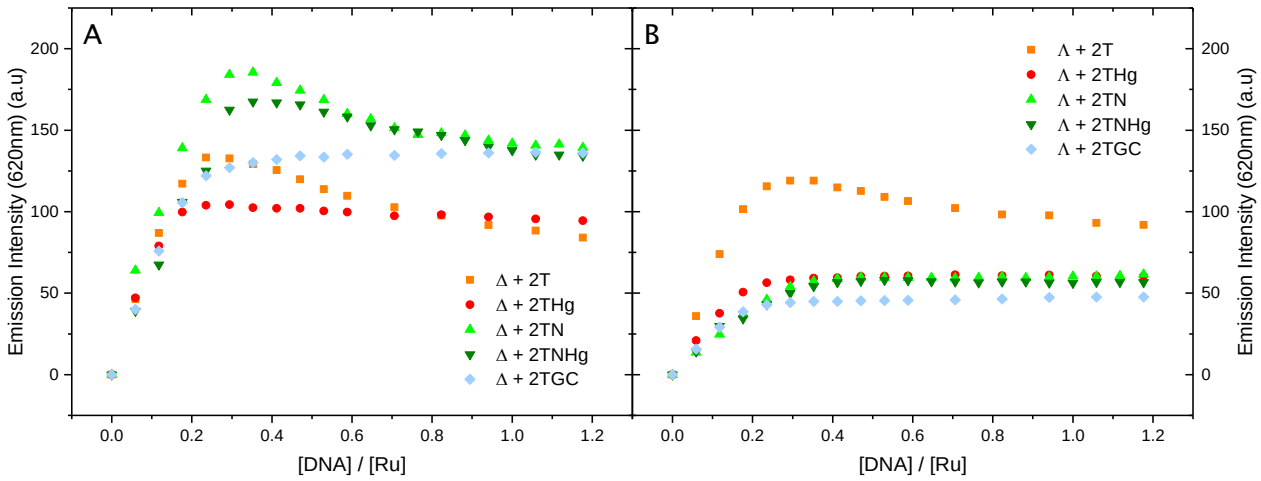

Figure 4.9: Steady-state emission at 620 nm of 5μM Δ-$[Ru(bpy)_2(dppz)]^{2+}$ (A) and Λ-$[Ru(bpy)_2(dppz)]^{2+}$ (B) when bound to 2T, 2THg, 2TN, 2TNHg and 2TGC. The decrease in the emission maxima is still apparent at lower metal complex concentration.

Overall, we observed that lowering the concentration of the metal complex had no effect on the binding behaviour of the individual enantiomers. Modifying the sequence from 2TN to 2TGC lead to the disappearance of the decrease in emission maxima indicating that the contiguous $(T-A)_2$ base pairs were favourable binding sites for the Δ enantiomer.

Since the DNA being added is a complete 17bp long duplex, the steps of titration in the beginning leads to an excess of Δ-$[Ru(bpy)_2(dppz)]^{2+}$ per duplex. Hence, the Δ-$[Ru(bpy)_2(dppz)]^{2+}$ is in essence competing for every binding site (base pair) on the duplex. The experiments were carried out at 5 mM MOPS with 10 mM $NaNO_3$ with neutral pH 7.5 conditions to ensure that the favourable electrostatic interactions between the complex and DNA are not hindered.

4.2.3 Job-plot for stoichiometry determination

To determine the number of metal complexes bound per unit duplex, we employed the method of continuous variations where, the molar ratios of complex/ duplex was varied but the total sum of both concentrations was constant to 2 μM. The emission from Ru^{II} metal complex at 620 nm was monitored at each measurement (ratio) and the highest emission intensity reported the most favourable stoichiometric conditions at that ratio. The results for both the enantiomers across all the DNA duplexes are summarized in Table 4.2 (Appendix S6 for fitted graphs).

Table 4.2: Number of Ru^{II} complex bound per each duplex. Note the difference between the capacity of mismatch DNA and the Hg^{II}-modified DNA.

	Mismatch	Hg^{II}-modified	Natural	Natural + Hg^{II}	GC-modified-Natural
Δ-$[Ru(bpy)_2(dppz)]^{2+}$	5	3	4	4	3
Λ-$[Ru(bpy)_2(dppz)]^{2+}$	5	3-4	3	3-4	3-4

The emission measurements were performed at Ru/DNA ratios that report the stoichiometry as precisely to unit number as possible. Monitoring the emission from the $[Ru(bpy)_2(dppz)]^{2+}$ reports back the most accurate binding capacity of a particular duplex. We observed from our measurements that the mismatch DNA 2T accommodates a total of 5 Δ-$[Ru(bpy)_2(dppz)]^{2+}$ as well as Λ-$[Ru(bpy)_2(dppz)]^{2+}$. Whereas, the control DNA duplex 2TN could accommodate a total of 4 Δ-$[Ru(bpy)_2(dppz)]^{2+}$, only 3 Λ-$[Ru(bpy)_2(dppz)]^{2+}$ were observed to bind. These results were in agreement with the previously observed stoichiometry by Barton and co-workers.[7,141] Interestingly, the results for 2THg were directly comparable to that for the GC modified duplex 2TGC, where a smaller binding stoichiometry was recorded for both enantiomers. The results complement the steady-state data obtained, particularly true especially in the case of the Δ-$[Ru(bpy)_2(dppz)]^{2+}$. The comparable stoichiometry of 5 complexes bound to 2T also support the similar emission intensity observed during the steady-state studies with the two enantiomers (Section 4.2.2). The presence of 2x T-T mismatches seems to offer extra binding sites probably due to the undefined structure in the middle of the duplex. The presence of Hg^{II} most likely hinders the binding leading to lesser number of metal complexes binding.

4.2.4 LIFETIME MEASUREMENTS

It has been previously reported that both enantiomers of $[Ru(bpy)_2(dppz)]^{2+}$ exhibit two different lifetimes when intercalated into duplex DNA.[8,9,152-154] Typically the excited state lasts for 10 – 100 ns for the short-lived and the long-lived component respectively. The lifetime itself depends on the enantiomer under consideration but factors such as the sequence and confirmation further influence the distribution of shorter and longer components. Figure 4.10 shows the overall analysis for time correlated single photon counting experiments across all the different duplexes (see Table S1 in Appendix for tabulated values).

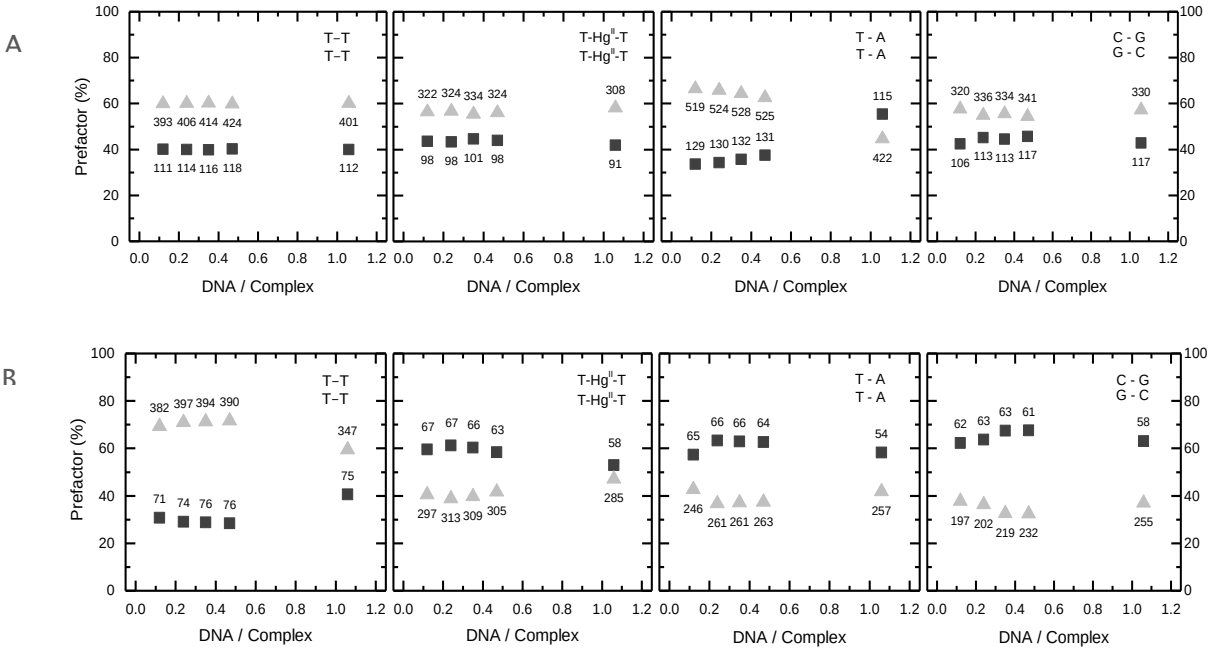

Figure 4.10: Lifetime pre-exponential factors α_S (dark grey closed squares) and α_L (light grey, triangles) for (A) Δ-$[Ru(bpy)_2(dppz)]^{2+}$ and (B) Λ-$[Ru(bpy)_2(dppz)]^{2+}$ with 2T, 2THg, 2TN and 2TGC (from left to right) respectively.

The lifetime decay obtained for each of the enantiomers yielded two different lifetimes and their % distribution upon fitting. We observe that with all the DNA duplexes, the Δ-enantiomer yielded a more pronounced longer lifetime component (α_L) suggesting an intercalative binding, which favours canted binding geometry. The lifetimes were measured by time correlated single photon counting at DNA/Ru that mimics the same ratios used in steady-state measurements described in Section 4.2.2. For the particular case of the natural DNA duplex 2TN, we observed that the lifetime distribution as well as the lifetime itself (ns) is greater for the longer component until the DNA/Ru ratio is 1:1. At this ratio, we see a flip-change in the trend where now the shorter component (α_S) is favoured over the longer. This trend is not observed in any other case except the 2TN and 2TNHg duplexes. This behaviour is well in agreement with the trend observed for the duplexes from the steady-

state results. Interestingly, we observed a striking similarity in the lifetime data upon comparing the Hg^{II} modified 2THg duplex with the GC modified 2TGC duplex. It seems that for the Δ-$[Ru(bpy)_2(dppz)]^{2+}$, both the T-Hg^{II}-T base pairs and the G-C Watson-Crick base pairs present a similar binding target in terms of structure and base-pairing energy.

In the case of the Λ enantiomer (Figure 4.10- B), we again see a similar trend as observed from the steady-state studies. The lifetime data for the Λ enantiomer is predictable when binding to all the DNA duplexes, with an exception of the mismatch DNA 2T. The distribution of the shorter and longer components is opposite to that observed with Δ-$[Ru(bpy)_2(dppz)]^{2+}$ except in the case of mismatch DNA 2T, where the longer component is still more pronounced than the shorter component. The more pronounced shorter component (α_S) justifies the lowered steady-state emission observed in the case of Λ enantiomer as lowered emission is associated to symmetrical binding geometry where both the phenazine nitrogens are partially exposed to water.[8,10]

4.2.5 Circular Dichroism experiments

We performed CD spectroscopic investigations to follow structural patterns characterizing DNA intercalation. CD is an important tool in structural biology for observing structural changes in biomolecules such as protein as well as nucleic acids.[97] For our studies particularly, CD spectroscopy provides invaluable insights into the mode of binding, along with the orientation of the bound ligand. DNA-drug interactions typically lead to what is known as an Induced CD signal into ligand transitions upon intercalative binding to DNA as a result of non-degenerate exciton coupling between electric dipole transition moment of the ligand and that of the DNA bases.[115,116,155,156] Below, in Figure 4.11 is depicted a raw CD spectra of DNA in absence (1:0) and presence of increasing concentration of *rac*-$[Ru(bpy)_2(dppz)]^{2+}$. Note that the CD of the DNA (in absence of ligand) is not subtracted.

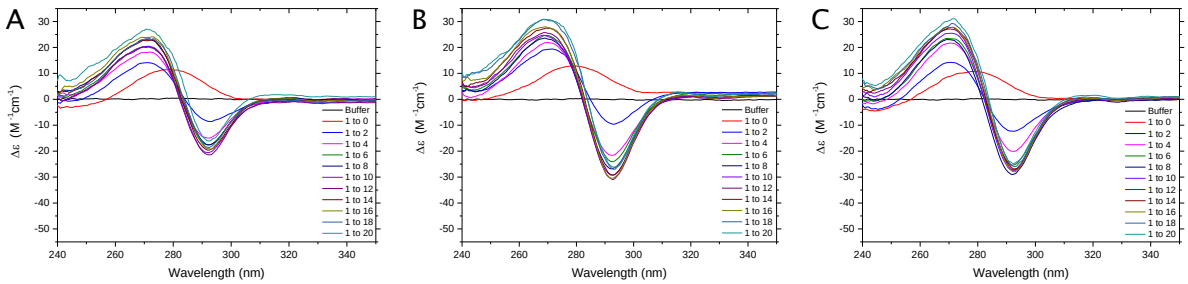

Figure 4.11: Differences in the CD spectra of Mismatch (A), Hg^{II}-modified (B) and Natural (C) DNA when titrated with increasing amounts of racemic-$[Ru(bpy)_2(dppz)]^{2+}$ metal complex per duplex. The ratios are mentioned in the inset. The lone DNA CD signal (red) undergoes shift where upon intercalation with Ru^{II} metal complex, there is an increasing negative CD signal at 290 nm and the CD signal from the DNA undergoes blue shift from 280 nm to 270 nm with slight increase in intensity.

As observed from the results in Figure 4.11, the CD signal of the DNA duplex alone (red) undergoes changes upon binding by *rac*-$[Ru(bpy)_2(dppz)]^{2+}$ (from DNA:Ru ratio 1:2 onwards) resulting in a blue shift (270 nm) of the positive signal. We observe another negative CD signal at 290 nm which increases slightly at higher *rac*-$[Ru(bpy)_2(dppz)]^{2+}$ per DNA ratios. This is due to the intercalative binding between the dppz ligand and the DNA base stack. As a result of intercalation, the interaction between the electric transition dipole moments of the DNA base stack with that of the long axis of the dppz give rise to different induced CD spectra.[114,156-158] Interestingly we can observe differences in the intensity of both the positive and the negative ICD signals from mismatch, Hg modified and the natural DNA duplexes (Figure 4.11). The intensity of the induced CD signals in the case of mismatch DNA (Figure 4.11, A) is smallest compared to Hg^{II}-modified (Figure 4.11, B) or the natural DNA duplex (Figure 4.11, C). In all the cases, upon increasing the metal complex concentration the ICD signal intensity also increased steadily before saturating.

4.3 DISCUSSION

SEQUENCE AND STRUCTURE DEFINE THE BINDING GEOMETRY AND STOICHIOMETRY

Our studies incorporated the use of DNA light-switch complex $[Ru(bpy)_2(dppz)]^{2+}$ to reveal differences between a natural, mismatched and a metal-modified DNA duplex. All these sequences differed only at 2 base pairs in the middle of the duplex. We combined various photophysical techniques to unravel the nuanced differences between the binding of two individual enantiomers of the $[Ru(bpy)_2(dppz)]^{2+}$ with the DNA duplexes. Figure 4.12 compares the measured fluorescence intensity with the calculated emission intensity using the lifetime data. The relative steady-state emission intensity can be calculated as the sum of the lifetimes multiplied by their pre-exponential factors as:

$$I(calc) = \Sigma(\alpha_i \times \tau_i)$$

Since the lifetime and steady-state measurements were conducted using similar conditions and ratios, the equation above was applied to the lifetime data, compensated for the measured binding stoichiometry and normalised to compare with (normalised) emission intensity.

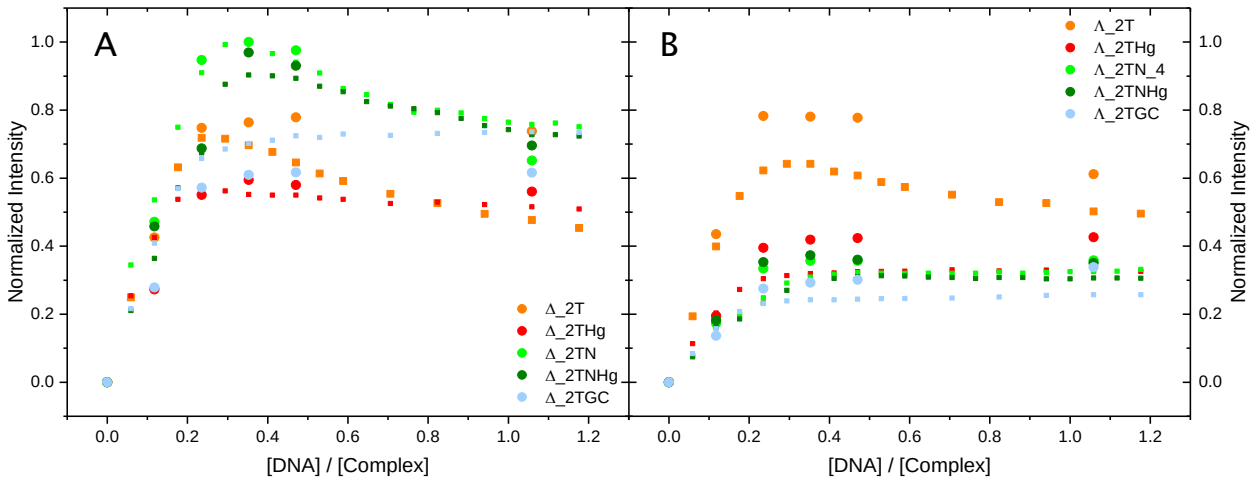

Figure 4.12: Emission intensity titrations of (A) Δ-$[Ru(bpy)_2(dppz)]^{2+}$ and (B) Λ-$[Ru(bpy)_2(dppz)]^{2+}$ (filled squares) compared to the calculated emission using the lifetime data (dots).

It can be clearly seen from the above figure that the calculated emission follows the same pattern with change in DNA/Ru ratios in mostly all the cases of DNA duplexes with an exception being the Δ-$[Ru(bpy)_2(dppz)]^{2+}$ interacting with the 2T DNA. Since the experiments were performed with slightly different aliquot volumes and time intervals (between addition and measurement), the calculated emission intensities are higher from the lifetime measurements compared to the steady-state intensities.

2TN AND 2TGC DNA: SEQUENCE DEPENDENT EMISSION

In case of the Δ-$[Ru(bpy)_2(dppz)]^{2+}$ it has been observed from various photophysical studies that it prefers to bind isolated on a $[poly(dA-dT)]_2$ oligonucleotide.[8,10] It's preference for $(T-A)_2$ base pairs is also well documented in previous studies.[153] The cooperativity of Δ-$[Ru(bpy)_2(dppz)]^{2+}$ with adjacent complexes is also lowest compared to the Λ-$[Ru(bpy)_2(dppz)]^{2+}$.[8,10] Therefore, we expect the complex to bind with a symmetrical geometry, in an isolated arrangement, at least in the middle region of the duplex. This does not seem to be the case however. Especially, when one compares the steady-state, TCSPC and the stoichiometric data for the 2TN duplex. At lower DNA/Ru ratios, the difference in the emission intensity shows that the Δ-$[Ru(bpy)_2(dppz)]^{2+}$ is binding in a canted mode which allows for a higher overall emission. The single photon counting data directly supports canted binding geometry at lower DNA/Ru ratios (Figure 5). The competition to occupy a binding site, leads to intercalative binding that allows for more adjacently close: duplets of canted or triplets with canted-symmetrical-canted binding. Therefore, in the beginning of the titration, at low Duplex/Ru, the emission for natural duplex is higher; compared to GC modified duplex or even mismatch and Hg^{II} modified DNA duplexes. The low availability of DNA base pairs and high competition for $(T-A)_2$ base pairs and DNA base pairs in general leads to the occupation of $(T-A)_2$ sites in duplet or triplet configuration. The decrease in the emission intensity at 1:1 DNA/Ru ratio is also observed from lifetime data; as more base pairs are easily available, the Δ-$[Ru(bpy)_2(dppz)]^{2+}$ goes back to its non-cooperative isolated binding arrangement and thus the emission intensity stabilizes as a result of saturation of preferred binding sites. In the case of Λ-$[Ru(bpy)_2(dppz)]^{2+}$, it was observed by Lincoln and co-workers that both the lifetimes for longer and shorter components were much less compared to the lifetimes for Δ-$[Ru(bpy)_2(dppz)]^{2+}$ when intercalating into $[poly(dA-dT)]_2$.[8,10] At high DNA/Ru ratio, the shorter component is pronounced much more than the longer component.[10] Moreover, the sister complex Λ-$[Ru(phen)_2(dppz)]^{2+}$, has been shown to have mixed sequence preference when binding to natural DNA.[9] From our data, we observe a very predictable and similar behaviour when Λ-$[Ru(bpy)_2(dppz)]^{2+}$ binds to various duplexes. The only exception here is the mismatch DNA 2T. Across the various photophysical techniques, it can be observed that the binding behaviour of Λ-$[Ru(bpy)_2(dppz)]^{2+}$ is comparable across DNA duplexes such as Natural, Natural+Hg^{II} and the Hg^{II}-modified DNA. Unlike the Δ-$[Ru(bpy)_2(dppz)]^{2+}$ we see a high cooperativity between ligand-ligand (complex-complex) interactions, and also complex-DNA interactions. The predictable and similar binding from the Λ-$[Ru(bpy)_2(dppz)]^{2+}$ can be attributed to the difficulty of the left-handed Λ-$[Ru(bpy)_2(dppz)]^{2+}$ to intercalate deeply as Δ-$[Ru(bpy)_2(dppz)]^{2+}$ which renders both of the phenazine nitrogens partially exposed to water. The ancillary ligand (bpy) hinders the entry of the dppz by hindrance from the phosphate backbone of the DNA. This seems to be the only logical explanation of comparable steady-state emission from the enantiomer across various duplexes. The

explanation is further supported by the lifetime measurements and the stoichiometric data (See Figure 4.12, Section 4.2.4 and Section 4.2.3). One should note that guanine oxidation could also lead to quenching of the emission which in turn yields slightly lower steady-state luminescence especially in case of the Λ-$[Ru(bpy)_2(dppz)]^{2+}$.

Note on the fitting of the absorption data (Section 4.2.1 and Appendix S4): The binding site size (s) value should be taken with a grain of salt. The original McGhee Von Hippel model for non-cooperative binding mode assumed the duplex of infinite length, which in our case is not. In addition, the cooperativity between the two enantiomers of the complex was not considered. We now know from our photophysical studies that the binding itself is heavily sequence dependent.[10] The preference for mismatch base pairs, both in case of DNA and RNA are well established in literature.[14,159] The sequence dependence is driven by the fact that the two enantiomers are left handed and right handed structures with the difference at the positioning of the ancillary ligands accounting for most of the difference in intercalative binding.

Mismatch DNA- 2T: Structurally undefined flexible binding pocket

From the various photophysical studies, we can conclude that in the absence of Hg^{II} ions, the $(T-T)_2$ mismatched site serves as a flexible binding pocket as the emission for both Δ and Λ enantiomers is comparable. In previous studies from Lim et al. it was shown that the mismatched base pairs serve as a preferential binding site for the Δ-$[Ru(bpy)_2(dppz)]^{2+}$.[14,16] The lowered thermodynamic stability of the mismatched base pairs leads to such preferential binding. They compared the luminescence behaviour across various base mismatches and observed highest intensities with A-A, A-C and C-C mismatches. These base pairs are destabilized base pairs compared to Watson-Crick base pairs.[160] With the stable mismatches like G-G, G-A and G-T they observed that the metal complex luminesces similar to that of well-matched DNA with A-T base pairs. Interestingly, they observed similar luminescence for C-T and T-T mismatches as that from well matched DNA. They attributed this observation to a possibility of quenching due to intermolecular hydrogen bonding between thymine and the phenazine nitrogens of the dppz moiety. However, they still observed a difference between the two enantiomers when intercalating into single base mismatched DNA duplex. The Λ enantiomer only showed enhanced luminescence in presence of an abasic site.[16] Furthermore, the CD studies with the *rac*-$[Ru(bpy)_2(dppz)]^{2+}$ indicate the presence of the flexible binding pocket. On comparing the induced CD signals for the mismatch DNA with natural and Hg^{II}-modified DNA, we can clearly observe the less intense signals from the intercalative binding. This is however not an indication of less or partial binding with mismatch DNA as otherwise the emission results also would indicate significantly lowered emission intensity upon intercalation. In fact, both of the enantiomers are welcomed without any enantio-bias as indicated by the highly enhanced emission of *rac*-$[Ru(bpy)_2(dppz)]^{2+}$ with mismatch DNA duplex (Appendix S6-A).

Hence, it is safe to assume that the Δ enantiomer is binding at the mismatch site. Interestingly, the same can be said about the Λ enantiomer as otherwise, the Λ enantiomer does not show such enhanced luminescence and does not follow an emission pattern similar to the Δ enantiomer. When their individual emission profiles are studied with the control DNA duplex, it is observed that the Δ enantiomer is preferably binding at $(T-A)_2$ sites in the centre of the duplex. Being a preferable site, the other T-A base pairs are also occupied before the G-C sites are.[9,10] The consecutive sites in the middle allow for a particularly close arrangement of Δ enantiomers such that the quantum yield is enhanced much more than it would normally be. This is due to an arrangement of the three Δ enantiomer in a triplet arrangement of two canted isomers sandwiching a symmetrically intercalated Δ enantiomer at the $(T-A)_2$. The symmetrically intercalated complex in the middle is already in its' preferred site while at lower DNA/Ru ratios, the adjacent complexes surround this complex and form a triplet arrangement by intercalating at T-A | G-C sites. As a result, this arrangement allows for a higher luminescence, which is a cause of the hump in the emission at 620nm. This hump then gradually decreases at higher base pair to metal complex ratio, as more intercalation sites are available, the Δ enantiomer falls back to its isolated binding preference. The decrease in emission intensity observed with the natural DNA also indicates that the Δ enantiomer is able to achieve a triplet binding arrangement only in presence of contiguous sites (strand a: 5'-GTTG-3'; strand b: 5'-GAAG-3') as the phenomenon is no more observable when these consecutive T-A base pairs are replaced with C-G G-C base pairs. Therefore, the mismatch site seems to be structurally undefined. Not collapsed entirely but just flexible enough to incorporate both left handed and right handed enantiomers. This revelation is unlike the previous studies by Barton et. al where upon interacting with mismatched binding sites, the metal complex inserts itself into the pocket pushing out the mismatched nucleobases (metalloinsertion).[14] This probably is due to the relatively more stable thymine-thymine wobble base pair formation combined with the more stable G-C neighbouring base pairs. This is an important consideration as it has been shown that the presence of mismatch base pairs like C-A or even abasic sites on duplexes leads to much enhanced luminescence compared to that from binding at canonical sites.[16] The recently published crystal structure of Δ-$[Ru(bpy)_2(dppz)]^{2+}$ provides proof for such a type of binding.[14] From our studies however, we observe no such enhancement in the luminescence as the emission for both the enantiomers is similar and comparable to the emission from natural duplex with being only slightly lower for the Δ-$[Ru(bpy)_2(dppz)]^{2+}$, further indicating that no metalloinsertion is happening at the mismatch sites.

T-Hg^{II}-T BASE PAIRS ARE COMPARABLE TO G-C BASE PAIRS

During the course of our studies we always expected that natural DNA duplex 2TN and the Hg^{II} modified DNA duplex 2THg would exhibit similar luminescence characteristics. In fact, studies hitherto characterizing the thermodynamic stability of such Hg^{II} modified base pairs

suggest that the T-Hg^{II}-T base pairs are comparable to normal Watson-Crick base pairs.[63] Also, the mercury nuclei are neutral when coordinated between T-T.[78] Upon comparing the van der Waals radius of Hg^{II} (1.44 Å) and the base pair spacing in DNA (3.4 Å), it is clear that Hg^{II} can incorporate between the mismatched T-T bases without any alterations in the double helical structure of the duplexes.[79] The fact that we saw a clear difference between the steady state and excited state lifetime data between the Hg^{II} modified and the natural DNA suggests that the light-switch complex is indeed sensitive to the presence of Hg^{II}. Considering the case of the Λ enantiomer, it is clear that because of hindrance from the phosphate backbone of the duplex, the complex is not able to intercalate as deeply as the Δ enantiomer could. Hence, the similar photophysical response across the various DNA duplexes with only exception of the mismatch duplex. However, the Δ enantiomer with its right-handed configuration and long dppz moiety, is able to assume flexible binding geometries. The binding geometries are evidently dictated by the nucleic acid sequence[10], but since we have a mixed sequence make-up of all the duplexes, we used the excited state lifetime data to reveal the average binding geometry it assumes in given DNA duplex. Upon either comparing the photophysical response of the Δ enantiomer when intercalated into the Hg^{II} modified 2THg or the GC modified 2TGC, we observed a significantly similar output across various experiments performed. The average distribution of the longer component (τ_L) for Hg^{II} modified duplex is 57 % which is directly comparable to that of 2TGC at 56 %. The same can be observed for the lifetime itself that are 322ns and 332ns for the Hg^{II} modified 2THg and the GC modified 2TGC respectively. This means that in both cases, the Δ enantiomer is able to assume a similar binding geometry with a slightly higher bias towards canted binding geometry (on average distribution). The similarities from the stoichiometric data also strongly support the argument as in both the cases clearly 3 Δ enantiomers are bound per duplex. Compared to natural duplex which can accommodate up to 4 complexes per duplex (corresponding to 4.25 base pair site size), this indicates that replacing the contiguous $(T-A)_2$ sites with either $(G-C)_2$ or $(T-Hg^{II}-T)_2$ induces a significant difference affecting the distribution of complexes intercalated per duplex. The other significant question then is about the intercalation site in case of $(G-C)_2$ or $(T-Hg^{II}-T)_2$ base pairs. On the 2TGC, there are 3 A-T base pairs which could provide a favourable site for intercalation. This explanation justifies the stoichiometric data obtained for the duplexes. However, the steady-state emission data for the Hg^{II} modified duplex is slightly lower compared to that of GC modified duplex.

In the case of the 2TNHg no significant differences were observed for photophysical studies with enantiomers of $Ru(bpy)_2(dppz)]^{2+}$. The free Hg^{II} in buffer has no coordination sites on the natural DNA duplex and thus we expect random interactions with the negatively charged phosphate backbone to take place. These interactions are much weaker compared to the coordinative binding and thus would not significantly affect the intercalative binding nor induce any structural perturbations in the duplex.

The difference in the intensity of the signal could be attributed to the distribution and the orientation of the metal complex concerning the base stack of the duplexes. The induced CD signal is sensitive to the distance between the electric transition dipole moment of the dppz ligand and that of the DNA base pair's long axis. In addition to the distance, it is also influenced by the angle between the two parallel dipole moments. Thus, in the case of the dppz long axis dipole moment coupling with the base pair long axis dipole moment, any perturbations in the orientation of dppz could lead to the changes we observe in the case of mismatch DNA duplex.

4.4 CONCLUSION

Application of polypyridyl based metal complexes for use as anticancer agents that bind DNA is rapidly gaining increasing importance. Various studies hitherto explore the binding of such metal complexes with nucleic acids and especially DNA. DNA represents an attractive target to such complexes due to it's central role in the dogma of life sciences. The intercalative binding mode provides more number of targets for planar metal complexes to bind providing in addition greater specificity for a particular site. We performed photophysical studies across various DNA duplexes which only differ at the middle, using the famous light-switch complex $[Ru(bpy)_2(dppz)]^{2+}$. Generally, both Δ and Λ enantiomers prefer the A-T Watson Crick base pairs over G-C simply because of the lower thermodynamic stability of the A-T base pairs compared to G-C base pairs. Nevertheless, we observe differences between the enantiomers' binding site preferences, which, are governed by various factors. One of the main factor being the sequence. Per Lincoln and his co-workers were able to establish, based on the photophysical studies with $[poly(dA-dT)]_2$ the less cooperative binding of the Δ-$[Ru(bpy)_2(dppz)]^{2+}$ compared to the Λ enantiomer. In addition, the preferential binding of the Δ enantiomer to A-T base pairs is also thoroughly discussed in the literature. From our photophysical studies with the Natural DNA 2TN, we observe that the Δ enantiomer clearly intercalates between the $(T{=}A)_2$ as both the steady state and the lifetime data indicates. The higher more pronounced emission maxima observed only in the case of natural duplex 2TN and not in case of the GC-modified duplex 2TGC, indicate that the $(T{=}A)_2$ site offers a possibility of a triplet arrangement which is forced upon at lower DNA/Ru ratios. The Δ enantiomer prefers to bind in a canted geometry indicated by the longer lifetimes. At lower ratios of DNA/$[Ru(bpy)_2(dppz)]^{2+}$, it is forced to bind in a closer configuration, which leads to triplet arrangement of adjacent Δ enantiomers. As more DNA is available per $[Ru(bpy)_2(dppz)]^{2+}$, the non-cooperativity is more expressed, leading to a steady decrease in the pre-exponential factor from the longer component. At 1:1 ratio, the longer lifetime component, which dictates the canted binding geometry for the intercalated $[Ru(bpy)_2(dppz)]^{2+}$, is observed to shift to lower values indicating the isolated bound Δ-$[Ru(bpy)_2(dppz)]^{2+}$. However, upon comparing the lifetime at this ratio with the lifetimes for other DNA duplexes, it is clear that the Δ enantiomer is targeting the $(T-A)_2$ site as the lifetimes and the pre-exponential factors are higher in case of natural DNA 2TN compared to the GC-modified DNA sequence 2TGC. The absence of $(T-A)_2$ sites in GC-modified sequence leads to lifetime values that are firstly, less and secondly, the distribution of pre-exponential factors show no variation at lower or higher DNA/$[Ru(bpy)_2(dppz)]^{2+}$ ratios. In the case of Λ enantiomer, the left-handed enantiomer with its ancillary bpy ligand faces hindrance from the phosphate backbone to intercalate completely and deeply between the base pairs. It is rational to think that this hindrance forces the Λ enantiomer to assume a symmetrical binding geometry. The fact that it shows more cooperativity compared to Δ is true but binding with exposed phenazine nitrogens

leads to overall lower emission compared to the Δ. The only exception is observed in the case of the mismatch duplex. The flexible $(T{=}T)_2$ allows the Λ to intercalate deeply into the pocket leading to effective shielding of its' phenazine nitrogens. This holds true also for the Δ enantiomer. This is evident from the steady state emission studies and the lifetime data. Fitting the lifetime decay into bi-exponential equation does indicate that the Λ enantiomer is offered a binding pocket to completely shield at least one the two phenazine nitrogens. This is clear from the highly expressed longer component in the single photon counting experiment. In case of Hg^{II}-modified duplex, we see from the lifetime data that the distribution of the pre-exponential factors are unchanged across various ratios of DNA/$[Ru(bpy)_2(dppz)]^{2+}$. This is comparable to the GC-modified lifetimes and its' pre-exponential factors. The leads to another interesting conclusion that for the Δ $[Ru(bpy)_2(dppz)]^{2+}$, the T-Hg^{II}-T base pairs are similar to G-C Watson Crick base pairs.

5 NMR STUDIES OF Hg^{II} MODIFIED DNA DUPLEXES

5.1 INTRODUCTION

From the steady-state photophysical studies, we observed that the enantiomers of the ruthenium(II) metal complex have different binding behaviours towards the DNA duplexes except towards the DNA duplex 2T, which with its two thymine-thymine mismatched base pairs shows no bias to either of the Δ- or Λ-$[Ru(bpy)_2(dppz)]^{2+}$ isomer. In the presence of Hg^{II} however, the bias is restored (Section 4.2.2). On the other hand, the Hg^{II}-modified duplex 2THg has similar excited state lifetimes as the natural duplex 2TGC, signifying a similar make-up of T-Hg^{II}-T base pairs and G-C Watson crick base pairs. However, detailed structural information is needed to confirm and understand these findings. From the lifetime measurements we were able to follow the changes in the distribution of lifetime prefactors α_1 and α_2 and reveal the subtle differences in the intercalative binding geometries at various ratios of Ru^{II} / duplex. In addition, the Job plot revealed the difference in the binding stoichiometry of the two enantiomers. The presence of Hg^{II} certainly has a profound effect on the stoichiometry and the lifetime distribution and is mostly comparable to 2TGC (Section 4.3). A more detailed structural outlook is necessary to support the findings from the various photophysical studies.

Hence, we employed a series of NMR experiments to determine the 3D structures of the DNA duplexes 2T, 2THg and 2TN and to disclose those small structural differences. NMR spectroscopy is one of the few techniques to gain three-dimensional structural data on the atomic level. We recorded 1D [^{1}H] and 2D-[^{1}H, ^{1}H]-NOESY NMR experiments in H_2O and D_2O to obtain first information on the exchangeable and non-exchangeable protons and to compare the results among the three different DNA duplexes. Furthermore, the 2D-[^{1}H, ^{1}H]-NOESY experiments in 100 % D_2O with the sequential walk region were necessary to start the assignment of the protons (see Section 3.4). The full assignments, which are later needed for the structure calculation process, were cross-validated and completed using [^{1}H,^{1}H]-TOCSY and [^{13}C,^{1}H]-HSQC experiments. After having the structures at hand, the intention is to map and compare the chemical shift changes of the duplex resonances in the presence and absence of the two $[Ru(bpy)_2(dppz)]^{2+}$ enantiomers. Such data may disclose preferential binding sites and binding geometries which would permit a detailed view on the intercalative binding of the $[Ru(bpy)_2(dppz)]^{2+}$ enantiomers to natural and metal-modified nucleic acids.

5.2 Results

5.2.1 1D [^{1}H]-NMR in 100 % D_2O

Figure 5.1 depicts the 1D [^{1}H]-NMR spectra of the 2TN, 2THg and 2T DNA duplexes in 100 % D_2O. Upon a quick glance it is already clear that all duplexes adopt one distinct stable structure as in all cases sharp resonances in the aromatic (7 – 8.5 ppm) and sugar proton regions (6.4 to 5 ppm) can be observed. Moreover, as the chemical shift distribution as well as shape and peak sizes look very similar for several regions it can be assumed that the three constructs share also many analogies within their structures. This is not surprising as only the central part of the three sequences is different (Figure 4.4).

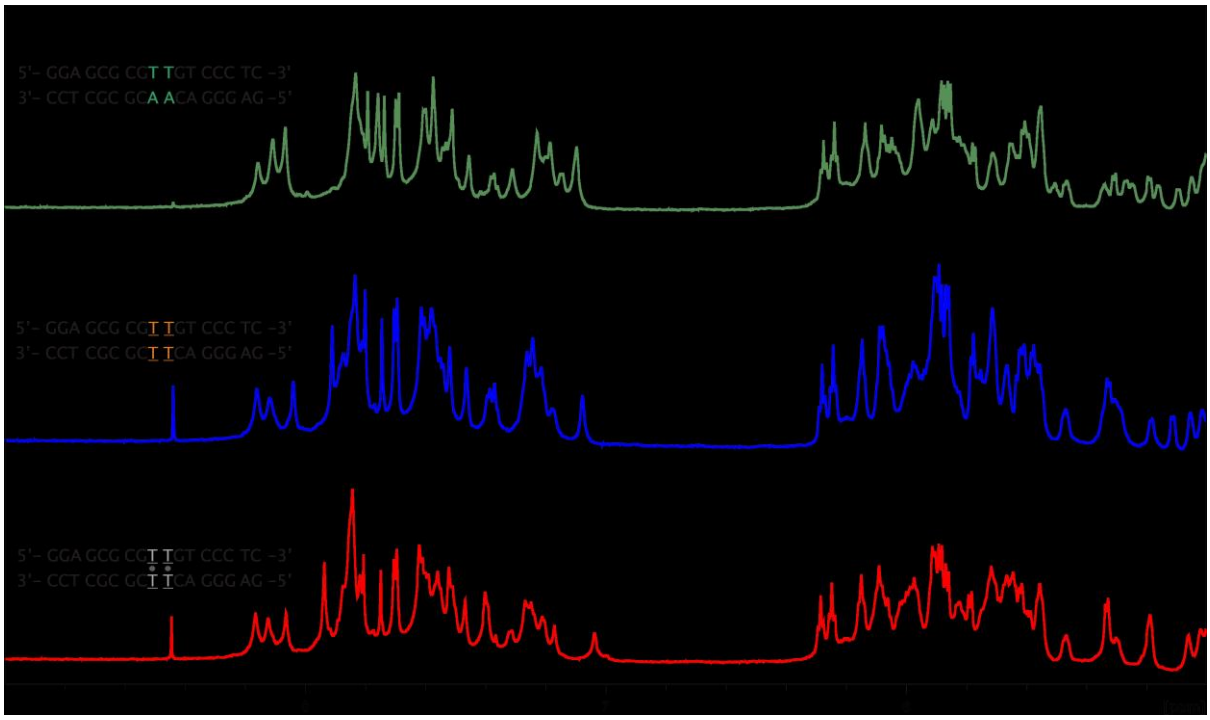

Figure 5.1: Stackplot of 1D [^{1}H] NMR spectra in100 % D_2O of the DNA duplexes 2TN, 2T and 2THg. The spectra look very similar indicating quite a few similarities within their structures.

5.2.2 1D [^{1}H]-NMR in H_2O

1D [^{1}H]-NMR in 10 % D_2O/90 % H_2O offers a quick and easy way to gain information on the base pairing scheme of the duplexes by looking to the exchangeable imino proton. As only the nucleobases guanine and thymine possess imino protons, we expect to observe 12 imino proton resonances from the guanine NH1 per each duplex. In addition depending on the DNA duplex either 5, 7 or 3 peaks from the thymine NH3 protons are expected in the case of 2TN, 2T and 2THg, respectively (Figure 4.4).

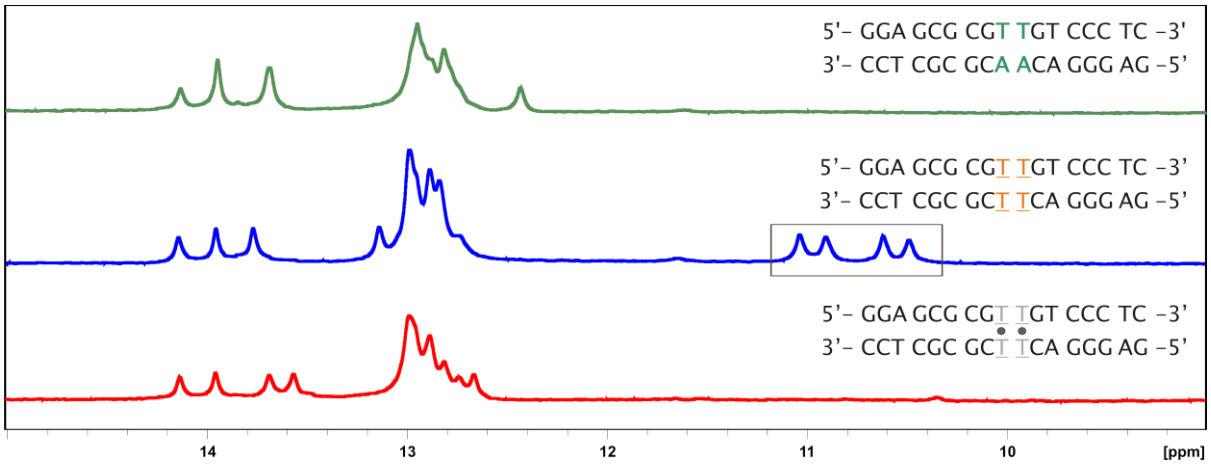

Figure 5.2: Stackplot of 1D [^{1}H]-NMR (10 % D_2O, 90 % H_2O) spectra of the DNA duplexes 2TN, 2T and 2THg. In the case of 2T DNA four imino protons resonate in the typical wobble base pairs region indicating the formation of two T-T wobble base pairs (Figure 5.6).

The imino resonances of Watson-Crick base paired guanines mainly appear in the region around 13 ppm whereas the ones of the thymine nucleobases are generally found more downfield shifted around 14 ppm. Looking at the 14 ppm region of 2TN we observe three peaks with a signal intensity of 1:2:2 that arise from the five thymine bases. In the case of the mismatched DNA duplex 2T, the nucleobases A25 and A26 are replaced with thymines to form upon addition of Hg^{II} ions the metal-modified thymine-Hg^{II}-thymine base pairs (Figure 4.4). Hence, apart from the three thymine bases of the Watson-Crick base paired region, we expect to observe additional four resonances in case of thymine-thymine wobble base pair formation. Indeed, three peaks in the 14 ppm region and four additional peaks around 10.5-11 ppm (see grey square) are visible in the spectrum. The three downfield shifted peaks with an intensity ratio of 1:1:1 correspond to the NH3 protons of T12, T16 and T32. The four strongly highfield shifted resonances belong to the four mismatched thymine NH3 protons. The chemical shift of 11 ppm is typically for imino protons involved in wobble base pairing and are frequently observed in RNA structures.[133] Upon addition of Hg^{II} the formation of the T-Hg^{II}-T base pairs is induced and the 2THg duplex is formed. The NH3 protons of the mismatched thymines disappear as Hg^{II} coordination leads to deprotonation of the thymine N3 nitrogens.[63,80] In the 14 ppm region of the 2THg spectrum, we observed the three NH3 resonances of T12, T16 and T32. The extra peak visible in the same region most probably belongs to the neighbouring guanine- G11 NH1 proton that is shifted due to conformational changes of the duplex centre.

5.2.3 2D [^{1}H, ^{1}H] NOESY NMR FOR SEQUENTIAL WALK ASSIGNMENTS

The 2D [1H, 1H]-NOESY spectrum in 100 % D_2O displays well-resolved and separated peaks for all the DNA duplexes 2TN, 2T and 2THg (Figure 5.3). Moreover, the sequential walk starting from the 5'- end to the 3'- end can be followed through the whole sequence for all

duplexes. The NOESY experiments also allows for the observation of stacking peaks between aromatic protons thereby indicating the presence of a well-defined helix.

The DNA duplexes 2TN, 2T and 2THg differ only in the middle region of their sequence with the nucleobases A25 and A26 in 2TN that are swapped to thymine in the 2T and 2THg constructs (Figure 4.4). Therefore, we expect that structural differences between the DNA duplexes arise mainly from the central part. Straightaway, looking to the sequential walk region of the duplexes (Figure 5.3) we can observe that correlations of nucleobases belonging to the helix ends like G1 to G6, C14 to C17, G18 to G21, and G30 to C34 (Figure 4.4) have very similar chemical shifts and intensity properties (see Section 5.2 for comparison of the chemical shifts). By contrast, nucleobase belonging to the modified middle region like T9, T10, A/T25 and A/T26 with the neighbouring nucleobases show very strong variations amongst the different duplexes. For example, the peaks of the nucleobases C24 and C27 experience a strong downfield shift upon exchange of A25 and A26 to T25 and T26. This indicates that indeed the helical structures of the DNA duplexes 2TN, 2T and 2THg are very similar except for the middle region. In the next section the chemicals shift variations upon changes of the middle part are evaluated and described in more detail.

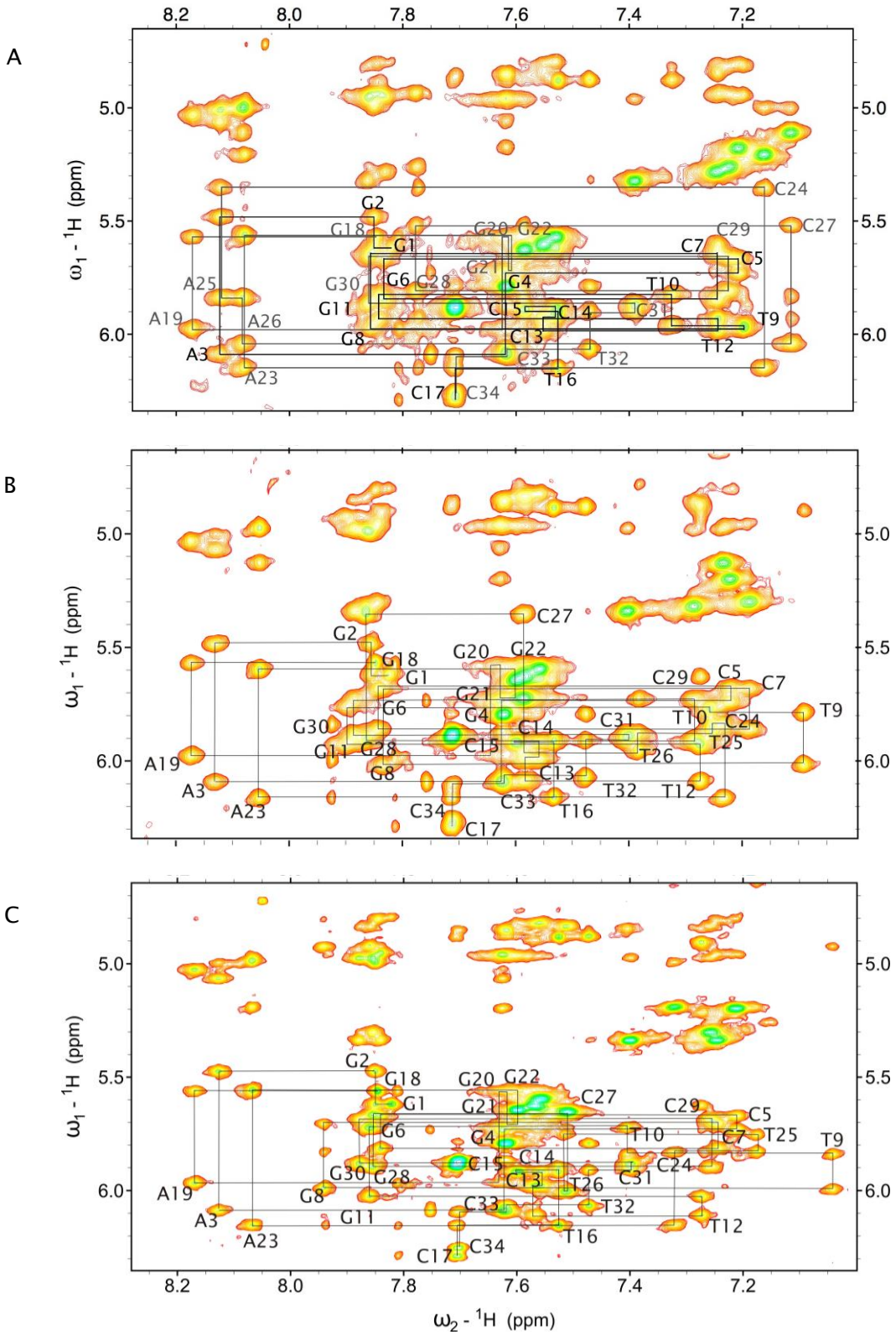

Figure 5.3: Comparison of the 2D [^{1}H, ^{1}H]–NOESY spectra of the natural (A), mismatch (B) and Hg^{II}–modified (C) DNA duplexes showing their corresponding sequential walk regions. All the DNA duplexes were measured at pD 6.85 (100 % D_2O, 303K). The sequential walk is indicated in solid lines. The correlation between the aromatic proton and the own sugar proton is labelled accordingly to the nucleotide number in the sequence.

5.2.4 CHEMICAL SHIFT PERTURBATIONS

To better visualize the differences in the proton chemical shifts amongst the three duplexes we mapped the changes in chemical shift (Δδ) of 2T and 2THg compared to 2TN for the residues G6-C13 of strand a and G22-C29 of strand b (Figure 5.4 and 5.5). Since the adenines A25 and A26 of 2TN are replaced with thymines in 2T and 2T-Hg, it has no meaning to compare the chemical shift changes of the aromatic protons of those nucleotides. Therefore, these nucleotides are not considered in panel (B) of graph 5.4 and 5.5. However, we included their sugar protons to get an overall impression of the variations. Residues belonging to the mismatched region or which are close by showed the strongest differences. For the sugar protons, we see for example a strong upfield shift of T9 and T10 along with very slight perturbations of the neighbour nucleotides G8 and G11 especially in the case of 2THg. However, the strongest chemical shift differences was observed for protons of the residues C24 and C27. Both, are neighbouring nucleobases of T25 or T26 and exhibit a strong downfield shift compared to duplex 2TN, most likely due to the lowered stacking interactions with thymine instead of the adenine in 2TN.

Comparing the chemical shifts changes of 2T/TN with 2THg/2Tn we also observe interesting differences (compare Figure 5.4 with 5.5). For example, the sugar proton H2' of T25 in 2THg has the largest Δδ (0.97 ppm which in case of 2T is only 0.77 ppm. On the other hand, the Δδ for H2' of 2THg T26 (0.34 ppm) is smaller than in the case for 2T T26 (0.6 ppm). These differences are most likely due to the rearrangement of wobble base pairs upon addition of HgII forming the T-Hg^{II}-T base pairs.

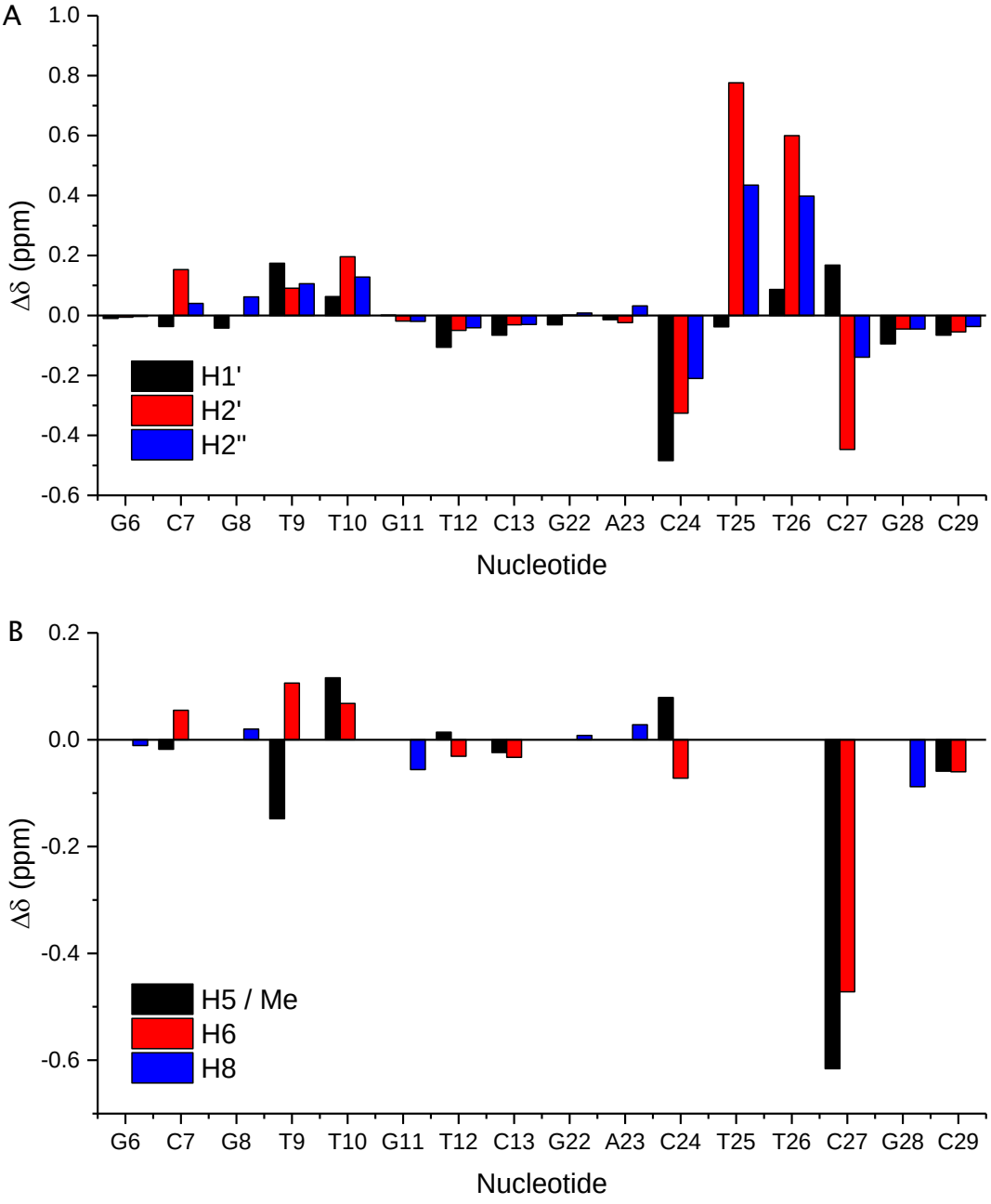

Figure 5.4: Chemical shift variation between the central nucleotides G6–C13 and G22–C29 of the 2T and 2TN duplex. (A) shows the differences of the sugar protons (H1', H2' and H2'') and (B) of the aromatic protons (H5, H6 and H8). Positive values imply an upfield shift and negative values a downfield shift of 2T protons compared to 2TN protons.

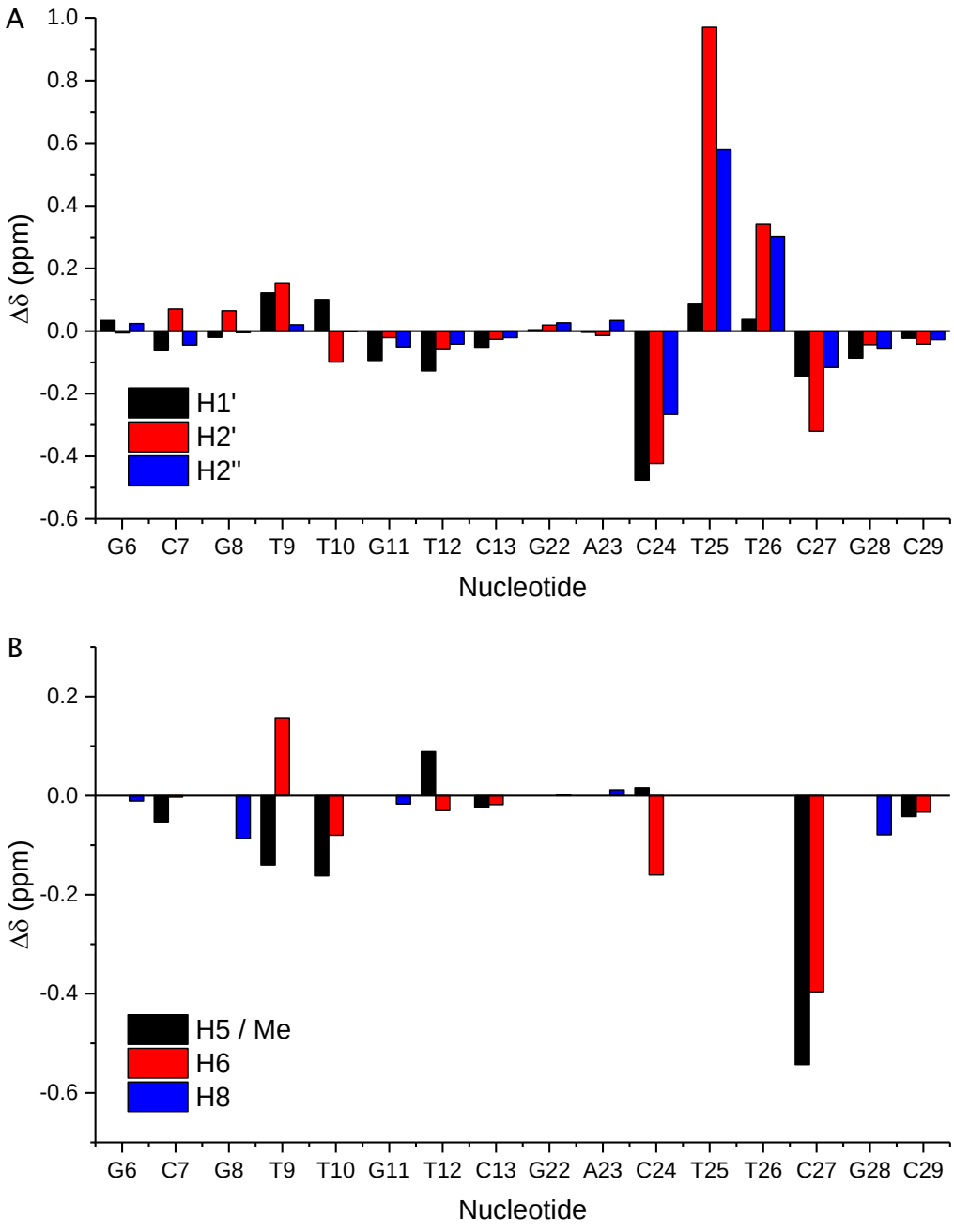

Figure 5.5: Chemical shift variation between the central nucleotides G6–C13 and G22–C29 of the 2THg and 2TN duplex. (A) shows the differences of the sugar protons (H1', H2' and H2'') and (B) of the aromatic protons (H5, H6 and H8). Positive values imply an upfield shift and negative values a downfield shift of 2THg protons compared to 2TN protons.

5.3 Discussion

5.3.1 Duplex formation observed through NOESY experiments

The structure determination of the three DNA duplexes is still in progress. Nevertheless, we can draw some conclusion about their three-dimensional structures just from analysing the 1D and 2D proton NMR spectra. As in the three cases we were able to assign all proton resonances needed to follow the sequential walk, we can conclude that all duplexes adopt a stable distinct conformation. Even the 2T duplex containing two mismatched base pairs yields only well-defined and sharp NMR resonances implying also a quite rigid structure for the mismatched region. Moreover, looking to the imino proton region of 2T we observed four sharp resonances around 11 ppm (Figure 5.2) that suggest the formation of two stable T-T wobble base pairs. This is in accordance with work done by Ono et al that studied a 10nt long DNA duplex by NMR which sequence corresponds exactly to the middle part of 2T (C5-C14 and G21-G30) including the two mismatched thymine-thymine base pairs.[79] They as well observed four sharp resonances at 11 ppm and the non-exchangeable protons have the same chemical shifts signature.[79,161] Another example of thymine-thymine wobble base pairing was demonstrated by Kuklenyik et al that studied DNA hairpins with 2, 3 or 4 consecutive thymines in the loop.[162] In the case of four thymines they observed proton resonances at around 11 pm and suggested the formation of a T-T wobble base pair between the first and the last thymine. However, as their resonances were very broad and undefined the loop probably does not adopt one fixed conformation. In general the T-T wobble can exist in two conformation (Figure 5.1).[163]

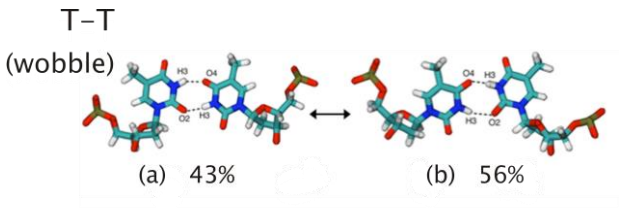

Figure 5.6: Possible wobble conformations for T-T mismatch base pairs shown with their percentage chance of formation. Adapted from (163) Rossetti, G.; Dans, P. D.; Gomez-Pinto, I.; Ivani, I.; Gonzalez, C.; Orozco, M. Nucl. Acids Res. 2015, gkv254.

Comparing the different examples in literature, it seems that the stability and conformation of the T-T mismatched base pairs strongly depends on the direct surrounding.[79,161,162] For example the crystal structure published by Kondo et al of a 12nt long DNA duplex with also two mismatched T-T base pairs in the middle, but surrounded by the energetically weaker A-T base pairs lead to a completely collapsed, heavily distorted non-helical conformation.[150] In their case, two T-T mismatched base pairs in absence of Hg^{II} show no wobble base pair formation, in fact they do not participate in any sort of hydrogen bond formation. The

weaker neighbouring A-T base pairs also do not form Watson-Crick base pairs, but form an A-T*_T* triplet (* indicates base from opposite strand). The terminal part of the duplex with canonical base pairs (G-C) assume a left-handed twist corresponding to a Z-form and thus it seems that the whole middle part of the duplex has been collapsed with the mismatched thymine bases pushed out.[150] Such comparisons indicate a strong dependence of tandem T-T mismatched base pairs on their immediate neighbouring base pairs for the overall structural conformation of the helix.

Also in the case of the Hg-modified duplex 2THg we observed well-resolved spectra. The 2THg too adopts a stable conformation as indicated by the similar resonances observed between 2TN and 2THg. The most immediate difference however, is the absence of four imino proton resonances from the 11 ppm region. These observations are again comparable to the previous work by Ono et al where upon the addition of Hg^{II}, they also observed similar effects on the imino proton resonances. As the changes in the imino proton resonances and the chemical shift perturbations are comparable with previous studies, the Hg^{II} coordination leading to the formation of metal-mediated base pairs T-Hg^{II}-T can be easily confirmed. In fact, even the chemical shifts for the nucleobases are in accordance with that observed previously with 10nt long DNA duplex studied by Yamaguchi et al (Section 5.2.4).[164]

5.3.2 Chemical shift perturbations

We took the 2TN DNA as a control DNA and used its assignments to set a standard against which we mapped chemical shifts for 2T and 2THg. Indeed, the most apparent observation is that for the majority of the duplex parts all of them share similar structural features with no strong distortion. Since the two adenines A 25 and A26 from 2TN are replaced by thymines for 2T and 2THg (Figure 4.4), we cannot not directly compare the chemical shift differences between 2TN with 2T and 2THg. Keeping 2TN chemical shifts as standard, we can compare the $\Delta\delta$ obtained for 2T with that obtained for 2THg. As a result of the Hg^{II} coordination, we observe slight up-field shift in the T25 resonances and downfield shifts in the T26 resonances most likely reflecting the rearrangement due to the presence of metal ion. In fact, comparing the chemical shifts for the 2THg with the chemical shifts for the published NMR structure of a similar Hg^{II}-modified DNA (Yamaguchi et al)[164] we observe striking similarities.[164] The sequence they used also carries 2 thymine mismatches flanked by G-C base pairs similar to the middle region of 2THg (Figure 4.4). This in addition to the CD studies conducted with 2T and 2THg (see Section 4.2.5) already gives us sufficient hints to the successful formation of a B-helical structure complete with perfectly aligned Hg^{II} ions.

On an overall basis, we observe that the proton chemical shifts for both 2T and 2THg duplexes are similar with exception of T9, T10, T25 and T26 and their neighbouring bases. This compared to the photophysical studies reveals some interesting facts. Firstly, the differences in the steady-state emission and the excited-state lifetimes of the

$[Ru(bpy)_2(dppz)]^{2+}$ enantiomers are due to the intercalative binding in the middle of the duplex, which is highly regulated by the structural variations due to the presence of either natural T-A/ G-C base pairs, mismatched T-T or Hg^{II} mediated T- Hg^{II}-T base pairs. It is apparent from the studies that indeed the mismatched T-T sites are favoured binding sites by both the enantiomers and in further investigation via NMR we expect to observe the changes due to interaction. The lowered binding stoichiometry of the Δ-enantiomer in the case of 2THg could be due to the non-favourable binding of the ruthenium(II) metal complex away from the Hg^{II} mediated site. Considering the ionic radius of the Hg^{II} (116 pm) and the positive charge, it is possible that the electrostatic repulsion between the Hg^{II} ion and the ruthenium(II) metal complex might be responsible for this. Further NMR studies of 2THg with administered metal complex would be useful in solving these queries.

5.4 Conclusion

In conclusion, we observed through NMR the formation of well-defined duplexes in all the cases of 2T, 2THg, and 2TN. All duplexes assume a B-helical conformation with slight differences for the central region that was altered (T9-T10 and A/T25-A/T 26) and it's direct surrounding. Comparing 2T and 2THg with 2TN, we confirm that both of the duplexes are structurally similar to each other with slight modifications to T25 and T26 that are induced by the coordination of Hg^{II}. This also means that only the middle part of the duplexes is different which is in accordance with the results from the photophysical studies from Chapter 4 (see Section 4.3). This concludes that indeed the central part from each of the duplex is responsible for the observed intercalation behaviour from the metal complex isomers. These subtle differences in the structure might be clearer once the solution structures are solved and compared. In addition, comparing the photophysical data of 2THg with 2TGC duplex we concluded that the 2THg duplex with T-Hg^{II}-T base pairs was more similar to the 2TGC duplex which instead of T-A canonical base pairs, had G-C base pairs in the middle of the duplex. Since the lifetimes for the Δ-$Ru(bpy)_2(dppz)]^{2+}$ intercalating into 2THg are comparable to those intercalating into 2TGC, it would be also nice to compare 2TGC via NMR studies.

6 Exploring RNA as target for $[Ru(bpy)_2(dppz)]^{2+}$ intercalation

6.1 Introduction

RNA is an important molecule possessing many complex roles in the cellular machinery of all living systems. The field of RNA biology has advanced steadily following landmark discoveries like the role of mRNA and tRNA in the DNA translation, discovery of RNA viruses, as well as the discovery of non-coding RNA with catalytically and/or regulatory functions.[165-168] The important role of RNA as an information shuttle between DNA, the genetic code, and the proteins, which execute the code is well established.[165,169] Since the 1980s, RNA is seen more and more as a biomolecule with numerous diverse functions. The 1989 Nobel Prize winners, Thomas Cech and Sidney Altman demonstrated for example the self-splicing activity of RNA enzymes (ribozymes) which require no assistance from proteins.[167,168,170,171] Such catalytic functions of ribozymes often rely on intricate 3D structures of the biomolecule. Therefore, detailed structural studies of RNA are a prerequisite to understand its immense catalytic and regulatory functions.

Structural studies using techniques like NMR or X-ray crystallography can give information on the atomic level but heavily rely on intricate sample preparation processes. To obtain "one sufficient diffracting crystal" can last up to many years and is linked to the preparation of numerous different constructs and to find the appropriate crystallization conditions. Moreover, X-ray crystallography has two main drawbacks. The crystallization conditions are frequently far away from the natural environment of the biomolecules, and the final construct is often a strongly modified/truncated version of the wildtype molecule. On the other side, the successfully application of NMR for structural investigations depends strongly on the molecule size and the presence of one distinct conformation. Thus, also, NMR often requires a long process for improvement of the construct and optimisation of the sample conditions until spectra with well-resolved and

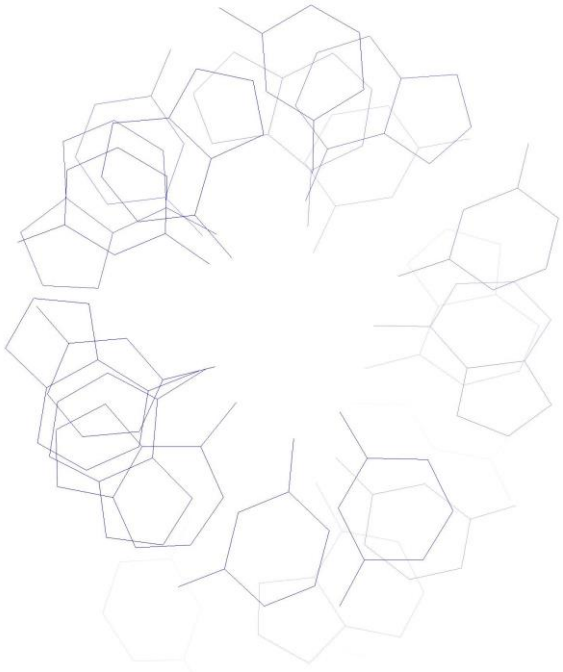

Figure 6.1: Top view of an A-form RNA duplex depicting the empty space in the middle of the helix. The figure was prepared with MOLMOL.[32] Adapted from PDB file 1RNA.[33]

sharp resonances can be obtained. Unlike X-ray crystallography and NMR that require a long elaborated process until conclusions can be drawn, the usage of intercalating luminescent probes is an easy and fast method to obtain valuable structural information that augments the information obtained from NMR and such advanced techniques.[100,107] Although the application of fluorescent probes such as the DNA light-switch complex $[Ru(bpy)_2(dppz)]^{2+}$ will not yield such details on the structure like X-ray and NMR, this method offers many advantages. For example, it can be administered both in-vitro and in in-vivo studies. Therefore, the biomolecule of interest can in principle also be studied in its natural conditions. There are many approaches for tagging RNA motifs with fluorescent probes.[172-176] However, the biggest hurdle is the development of RNA probes that selective and non-covalent bind to complex RNA structures (Figure 3.2). Although DNA and RNA share many, chemical and structural features the additional 2'-OH group on the sugar ring in RNA induces many differences. RNA is more susceptible to hydrolytic decomposition than DNA but on the other hand strongly facilitates the formation of very complex structures using the OH-group as additional hydrogen-bond partner.[177] These complex structures formed from a single RNA strand comprise not only single-stranded and A-helical regions but also loops, bulges, junctions and many other structural motifs. One of the biggest reasons for the various RNA structures is the important role of various metal ions which are the most abundant and crucial cofactors that determine their folding.[178-180] However, the A-form double helical RNA is much less prone to the hydrolytic decomposition than other various forms of RNA due to the geometry of the 2'-OH being altered.[181,182] In addition, the thermal stability of RNA duplexes is also greater compared to DNA duplexes. Therefore, A-form RNA double helices can also be used to serve as scaffolds for aligning metal ions in an array along the helical axis.

In this chapter, we investigate RNA duplexes containing mismatched uracil-uracil base pairs that are analogues of the DNA duplexes described in Chapter 4. Previous studies on such mismatched RNA duplexes revealed that similar to the T-T mismatched base pairs, U-U base pairs are able to coordinate Hg^{II} leading to formation of U-Hg^{II}-U (Figure 6.2).[3] Such metal-modified RNA duplexes have been proposed as well, as potential molecular wires due to their ability to incorporate a specific metal ion array.[183]

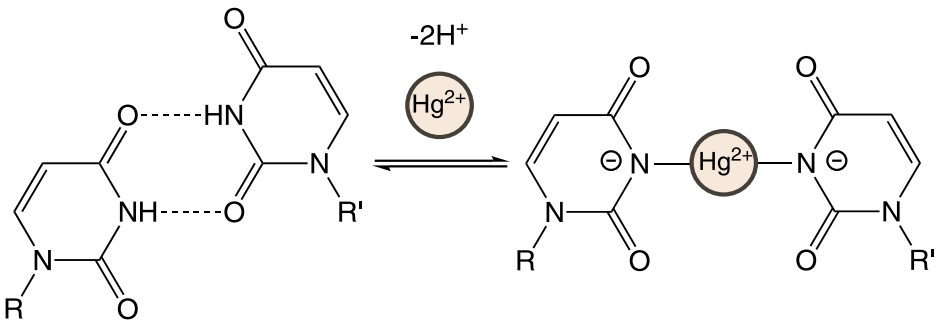

Figure 6.2: Proposed formation of U-Hg^{II}-U base pairs upon Hg^{II} ion coordination.

Therefore, the aim is to apply the same methods applied in Chapter 4 to probe the charge transfer properties of metal-modified RNA duplexes and to compare and draw differences to the metal-modified DNA analogues.

We initiated by first investigating the binding of the $[Ru(bpy)_2dppz]^{2+}$ to the various RNA sequences (Figure 6.3). Metal complexes such as $[Ru(bpy)_2dppz]^{2+}$ with their unique fluorescence emission properties could be immensely useful in probing the charge transfer properties as they are sensitive to their binding environment. However, so far there have very few studies regarding such interactions. The studies conducted by McConnell et al. indicate that while the emission enhancement upon binding of $[Ru(bpy)_2dppz]^{2+}$ with well-matched RNA hairpin is negligible, the presence of a mismatched base pair leads to several fold luminescence enhancement followed by the metalloinsertion of the complex in the mismatched site.[159] The RNA duplexes are complements of the DNA analogues discussed in chapter 4 and comprise of 2, 3 and 6 uracil-uracil mismatch base pairs that in the presence of Hg^{II} form U-Hg-U base pairs (Figure 6.2). At first, UV-vis thermal melting experiments were conducted to characterise the thermal stability of the mismatched and metal-modified RNA duplexes (Figure 6.2), both in the absence and presence of the intercalating metal complex $[Ru(bpy)_2dppz]^{2+}$. These studies are an continuation to previous work performed in our group.[3]

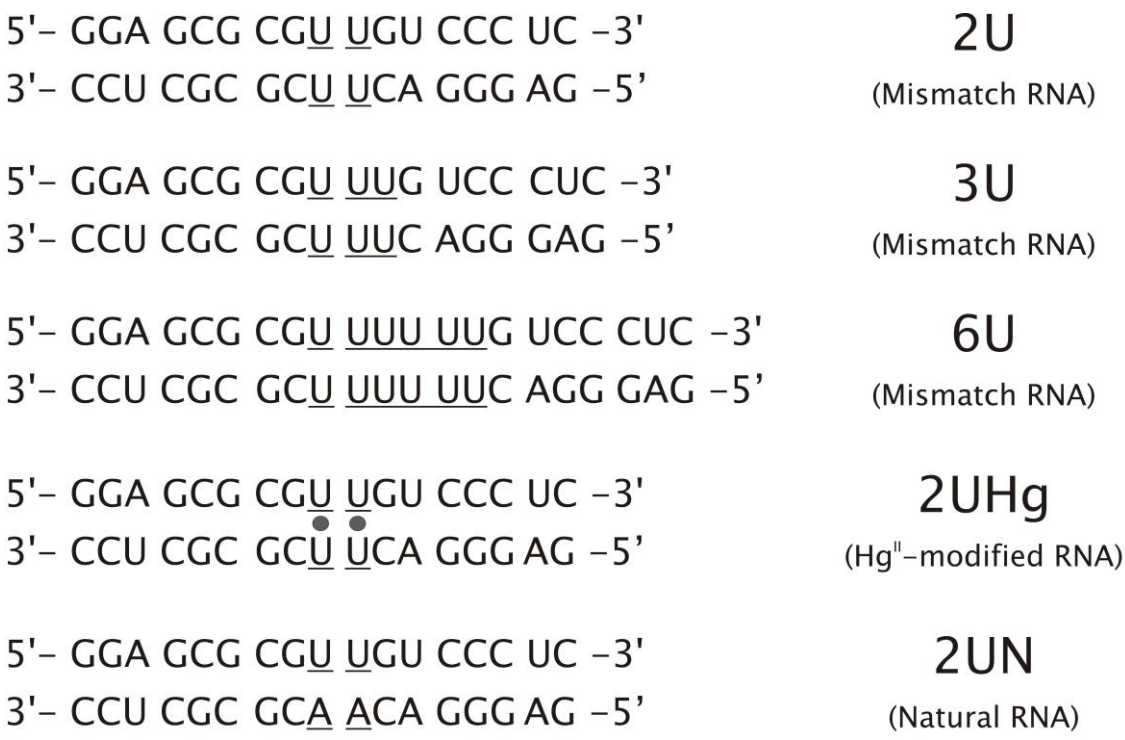

Figure 6.3: RNA sequences used for spectroscopic studies. From top: 2U, 3U and 6U are RNA duplexes with increasing number of U-U mismatches. As an example for Hg^{II}-modified RNA, 2UHg is shown with grey dots signifying coordinated mercury. A natural RNA duplex 2UN was used as a control. Not shown here are Hg^{II}-modified 3UHg and 6UHg for the sake of simplicity.

6.2 Results

Most of results discussed below were conducted with RNA strands directly purchased from IBA Life sciences (Germany). Initially, the RNA strands were in vitro transcribed but as the sequences are very short (17 bp), only low transcription yields were obtained.[184,185] For transcription details please refer to the Experimental section (see Section 7.2.1).

To investigate the thermal stability of the RNA duplexes 2U, 3U and 6U in absence and presence of Hg^{II} we conducted UV melting experiments by varying pH conditions and concentration of the duplexes. In addition, we study the effect of $[Ru(bpy)_2dppz]^{2+}$ on thermal stability of the 2UHg, 3UHg and 6UHg RNA duplexes. To follow the intercalative binding of $[Ru(bpy)_2dppz]^{2+}$ into the RNA duplexes, we employed UV-Vis titrations where to a constant metal complex concentration, increasing amounts of RNA duplex was added. The intercalative binding typically leads to hypochromism at the MLCT wavelength (370 nm) of the $[Ru(bpy)_2dppz]^{2+}$ metal complex. Therefore, mapping the drop in the absorption can yield information in two regards. First, how well the complex can enter in between the base stacks which is illustrated by the % hypochromism as it is defines as the ratio between bound and unbound metal complexes (Section 7.5.1) and second, the obtained data can be fitted into an equation to calculate the strength of the binding (refer to Section 4.2.1). Steady-state emission titrations were also performed. The emission titrations and absorption titrations were performed in conjunction to avoid wasting more sample for measurements. Hence, all the samples mentioned above (UV-Vis titrations) were subjected to both measurements and the buffer conditions for the samples were similar. Finally, we investigated via 1D $[^1H]$-NMR in 10 % D_2O, 90 % H_2O the preliminary structural information of the mismatched and the Hg^{II}-modified RNA sequences. We compared the imino resonance spectra of the RNA sequences with the DNA spectra.

6.2.1 Thermal melting studies

First we wanted to investigate the thermal stability of RNA duplexes in presence and absence of Hg^{II}. UV-vis melting studies allow for a convenient determination of the oligonucleotide melting temperature T_m, the mid-point of the transition from ordered helical structure to single strands. Therefore, the T_m contains information on the thermal stability of nucleic acid secondary structures. This involves heating the nucleic acid sample, which leads to changes in the absorption properties of the molecule. The changes in the absorption properties are caused due to the lowered stacking interaction between the base pairs of the oligonucleotide and thus the absorption of the nucleic acid duplex is plotted vs. temperature. Upon cooling, the nucleic acid duplexes typically undergo reannealing; therefore, one can obtain one or more heating and cooling ramps in order to obtain the temperature of midtransition. In the case of typical DNA/ RNA duplexes, the absorption at 260 nm is plotted against temperature, which is revealed as a sigmoidal curve, from which the melting temperature can be determined. We conducted melting studies with transcribed RNA as well as purchased RNA. The results are summarised in Figure 6.4. Clearly, we observe that as the number of U-U base pairs increases, the melting temperature recorded for such duplexes is lower (in absence of HgII). This is evident upon comparing the black squares from A, B and C (Figure 6.4). The order of the melting temperature follows this trend: 2U> 3U > 6U with T_m of 6U being lowest.

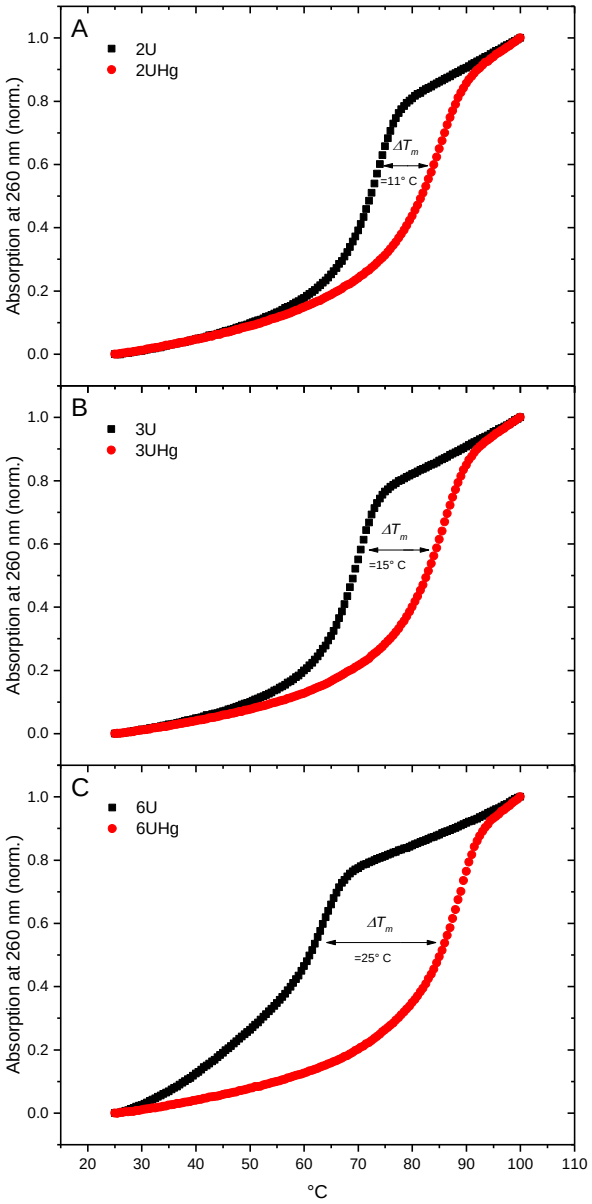

Figure 6.4: Melting profiles of RNA duplexes in absence (black filled squares) and presence (red filled circles) of Hg^{II} (A) 2U, (B) 3U and (C) 6U depicting the difference in melting temperature, ΔT_m (ΔT_m = T_m in presence of Hg - T_m no Hg, in RNA) brought about by stabilization of the duplex due to mercury coordination.

In presence of Hg^{II}, we observe that for each of the RNA duplex, the recorded T_m is higher and in the same range at around 84° – 88° C. The graphs in Figure 6.3 compares the difference in the melting temperature ΔT_m for each duplex with and without Hg^{II} (T_m (2UHg) – T_m (2U)). The graphs clearly show the increasing ΔT_m in the order 6U> 3U> 2U.

In the second set of UV melting experiments we compared the melting temperature of each of the duplexes in absence and presence of 1 equivalent of Hg^{II} at two conditions of pH (6.8 and 7.5) and concentration of the duplex (0.5 and 2 μM). The results of these experiments are summarized in Figure 6.5. Firstly, the influence of varying concentrations of duplex RNA was studied. We saw that consistently, for all the duplexes (mismatched and Hg^{II}–modified) at 2 μM concentration the T_m was slightly higher than the T_m of duplexes at lower 0.5 μM concentration. This was true at both lower and higher pH conditions. This observation is typical for duplexes as the separation of two strands leads to higher absorption, which is because of lesser stacking interactions. Such first order transitions are dependent on the concentration of the molecule unlike in the case of hairpin melting where it is not concentration dependent.

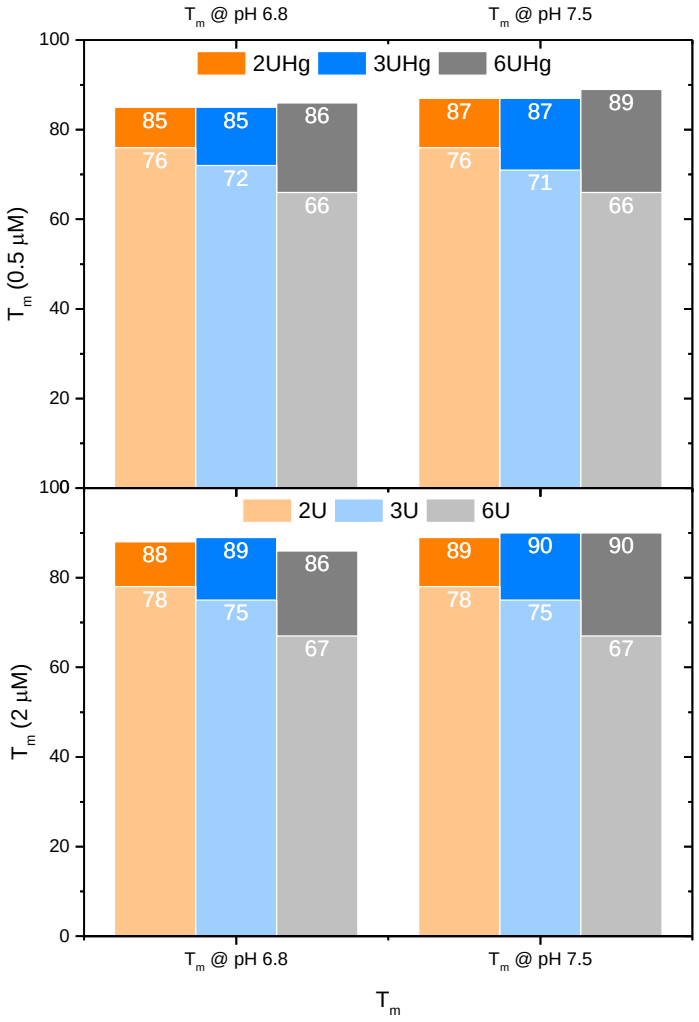

Figure 6.5: Melting temperatures for 2U, 2UHg, 3U, 3UHg, 6U and 6UHg at an RNA duplex concentration of 0.5 μM (top) and 2 μM (bottom) at pH 6.8 (left) and at pH 7.5 (right).

Secondly, we observed that while the varying pH does not affect the melting temperature of the mismatched duplexes (in absence of mercury) (Figure 6.5, lighter coloured bars), the presence of mercury (Hg^{II}–modified RNA duplexes certainly shows slight variations in the T_m. At lower pH 6.8 the T_m for the Hg^{II}–modified duplexes is 1–2° C lower than at pH 7.5 (Figure 6.5). We know from the Figure 6.4 that for each of the lone RNA duplex (in absence of Hg^{II}), the melting temperature decreases in the order 2U > 3U > 6U, with the melting temperature

of 6U being the lowest. An overall drop of 9° C in the melting temperature is observed going from 2U (78° C) to 6U (67° C). This observation is not surprising as the number of mismatches translates to increased thermal instability of the duplex. Interestingly, the presence of Hg^{II} completely flips the situation. The mercury coordination leads to an overall increase of at least (ΔT_m) 11° C (in the case of 2U). In the case of 3U, the ΔT_m is even higher (15° C) due to an extra coordination site for the mercury ion. The highest ΔT_m is observed for the 6U RNA duplex (25° C) indicating a strong influence of metal ion coordination on the overall duplex stability. This is a similar trend at both pH 6.8 and pH 7.5. To test the influence of the intercalating metal complex, the Hg^{II}-modified RNA duplexes were subjected to melting studies in presence of metal complexes at 1) low concentration such that 1 metal complex is available per duplex and 2) high concentration such that 1 metal complex is available per base pair of duplex. In the final series of melting experiments (Figure 6.6), we studied the influence of intercalating metal complex $[Ru(bpy)_2(dppz)]^{2+}$ on the melting profiles of Hg^{II}-modified duplexes. Hence, we collected the melting data for duplexes 2U, 3U and 6U in presence of Hg^{II}, in presence of Hg^{II} and ruthenium(II) metal complex (1 complex per 1 duplex) and in presence of Hg^{II} and ruthenium(II) metal complex in excess (1 complex per 1 base pair). Figure 6.6 summarises this data with melting temperatures mentioned per each sample. The results indicate that the presence of metal complexes have no significant influence on the melting temperature. The T_m in presence of metal complex both in low concentration and in high concentration cases is comparable.

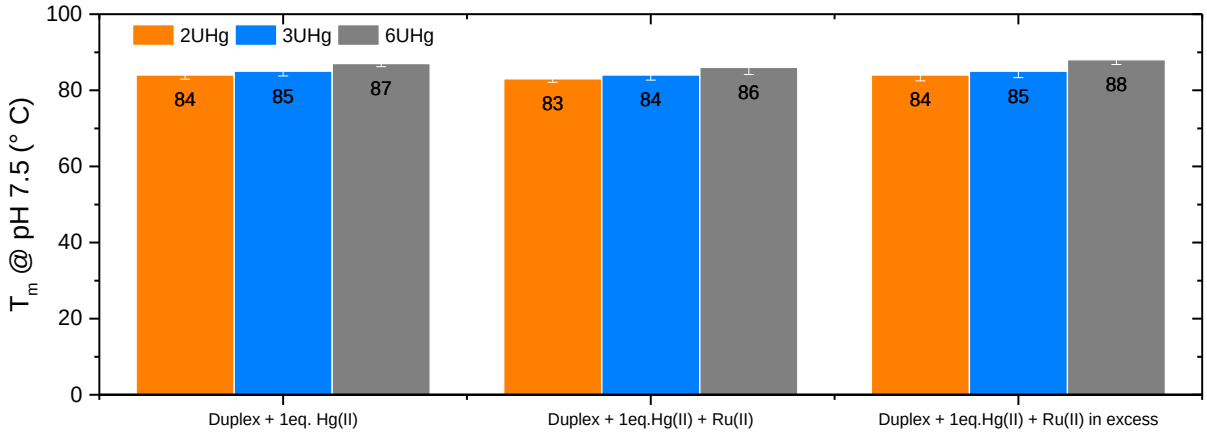

Figure 6.6: Duplex melting temperatures recorded for 2U, 3U and 6U in the first lane, Hg^{II} modified duplexes in second lane, Hg^{II} modified duplexes with 1 equivalent metal complex in third lane and finally Hg^{II} modified duplexes with metal complex in excess.

6.2.2 UV-Vis Absorption Titrations

Similar to the previously discussed results with DNA analogues (see Section 5.2.1), here we also expected to observe and map the % hypochromism upon interaction of rac-$[Ru(bpy)_2dppz]^{2+}$ with the analogous RNA sequences. Figure 6.7 shows a typical UV absorption profile of $[Ru(bpy)_2dppz]^{2+}$ undergoing hypochromism upon addition of RNA

duplex 2UN. On the right side, the percentage hypochromism values obtained for the duplexes are summarised. It can be observed that the drop in the absorption is small compared to similar experiment conducted with DNA analogues (see Section 4.2.1). Straightaway, we observe that the titrations do not reach a plateau as they did in the case of DNA and in addition, the fitting of the data is also not possible due to the absence of a plateau. Upon comparison with hypochromism values derived from titrations with the DNA analogues (Figure 4.3), it becomes clear that there is less intercalative binding of rac-$[Ru(bpy)_2dppz]^{2+}$ to RNA duplexes. As discussed in the Section 4.2.1, the hypochromism observed at the MLCT wavelength of the $[Ru(bpy)_2dppz]^{2+}$ is a direct proof of intercalative binding as upon increasing the RNA concentration, the π* orbital of the dppz moiety contributes to the DNA π orbital of the base pairs leading to the observed hypochromic shift at the MLCT wavelength. For example, the % hypochromism observed for 2T DNA duplex is around 38 % whereas for the RNA analogue 2U this value drops down to 18 %. Similarly, in the case of Hg^{II}-modified DNA 2T and 2U RNA duplexes, we observe the same differences. Interestingly there is a difference in the % hypochromism between the mismatched RNA 2U (18 %) and the control RNA 2UN (13 %). The value recorded for both 2U and 2UHg is 18 % while it decreases to 13 % for 2UN and 2UNHg. This trend is opposite of that observed from the DNA counterparts where the % hypochromism for 2TN DNA duplex was the highest at 40 % only with a slight increase from the 38 % recorded for 2T and 2THg DNA duplexes. Clearly, the 2U RNA duplex seems to behave like the 2UHg at least in terms of accommodating the metal complex.

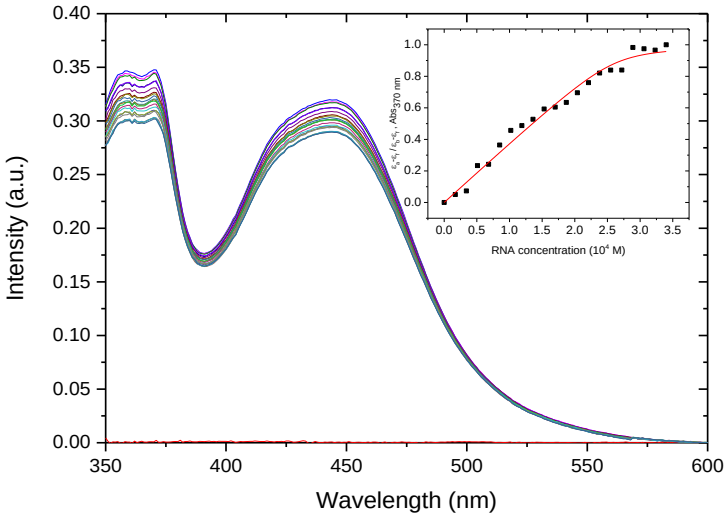

% Hypochromism	
2U RNA	18.3
2UHg RNA	18.7
2UN RNA	13.2
$2UNHg^{II}$ RNA	13

Figure 6.7: (Left) UV absorption profile of rac-$[Ru(bpy)_2dppz]^{2+}$ mapped upon titrating increasing amounts of RNA duplex. The inset shows the absorption at 370 nm fitted using equation developed by Bard et al. for non-cooperative binding of metallointercalator to DNA (Section 4.2.1). (Right) summary hypochromism in % recorded for the various RNA duplexes.

Also, the significant differences between the hypochromism values observed for 2UN and 2U means that the presence of mismatch base pairs has a significant influence on the intercalative binding as depicted by the increased hypochromism values.

6.2.3 Fluorescence emission titrations

To study the intercalative binding using the unique light-switch properties of the rac-$[Ru(bpy)_2dppz]^{2+}$ we performed steady-state fluorescence emission titrations keeping the concentration of the metal complex constant and adding RNA. For a direct comparison with previously performed studied with DNA duplex analogues (see Section 4.2.2) the experiments were performed in a similar manner as for the DNA duplexes.

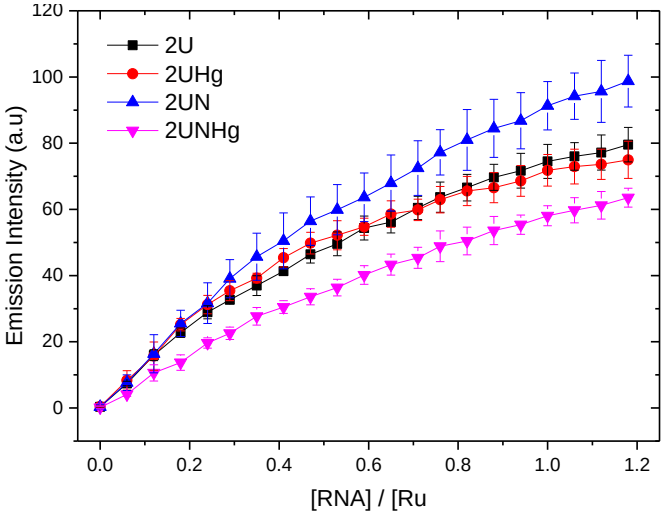

Figure 6.8: Fluorescence emission intensity of rac-$[Ru(bpy)_2dppz]^{2+}$ at the MLCT wavelength 620 nm upon increasing amount of 2U (black), 2UHg (red), 2UN (blue), and 2UNHg (pink) RNA duplexes.

The emission titrations shown in Figure 6.8 reveal that indeed the intercalative binding is significantly influenced when the $[Ru(bpy)_2dppz]^{2+}$ interacts with an A-form RNA. We expected this would be the case but surprisingly we observe no significant emission from the mismatched RNA duplex 2U. In the presence of mismatch base pairs the metal complex is known to prefer binding at such sites as indicated by previous studies.[159] Interestingly, from the emission titration data for 2U, 2UHg, 2UN and 2UNHg we can observe a much lowered emission intensity across all the duplexes irrespective of the presence of mismatched base pairs or not. In fact, the instrument's PMT detector voltage settings were set to high in order to capture the emission from the sample, as it was too low. The results when compared to that from DNA reveal a stark difference between the intercalative binding with DNA and RNA.

6.2.4 1D [^{1}H] H_2O NMR

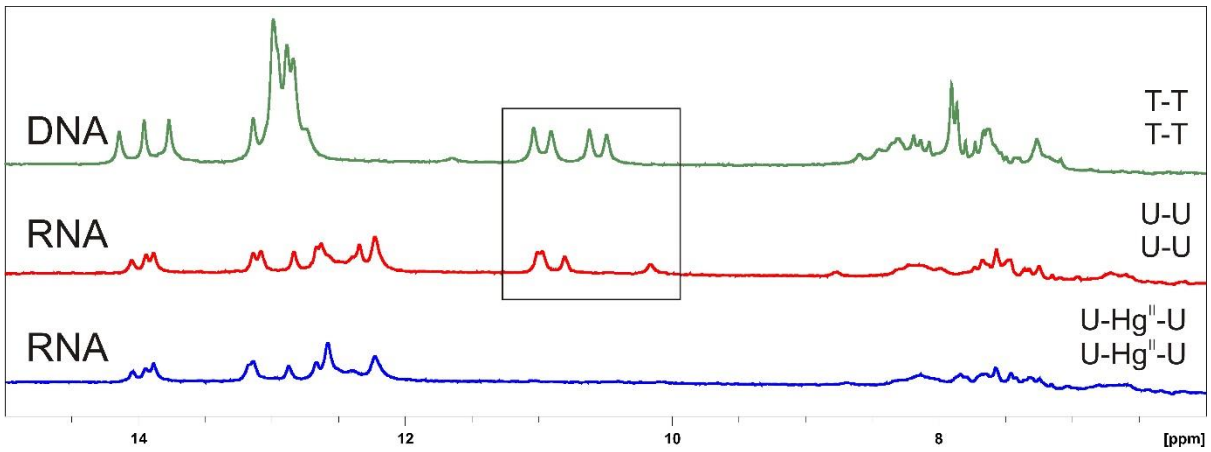

Figure 6.9: 1D NMR spectra measured in H_2O compared for RNA duplexes 2U and 2UHg with DNA duplex 2T. The peaks for 2x mismatched bases pairs T-T (DNA) and U-U (RNA) appear in the region where one would observe wobble base pairs. Hg^{II} coordination leads to shifting of the peaks from uracil/thymine-N3H otherwise appearing in the wobble base-pair region. Note that the peaks for the RNA duplexes are less intense compared to DNA due to compact folding of the RNA duplex.

To receive preliminary structural information on the mismatched and Hg^{II}-modified RNA, some simple 1D [^{1}H]-NMR spectra in H2O were recorded and compared with the DNA analogue. Figure 6.9 compares the NMR spectra of 2T DNA duplex in H_2O with 2U RNA duplex and 2UHg RNA duplex. For a well-defined nucleic acid duplex, the imino proton resonances from the Watson-Crick paired guanine and uracil nucleobases appear within the 12 – 14 ppm range. Indeed, we can clearly see the resonances from the guanine nucleobases at around 12 – 13 ppm followed by the imino resonances from the uracil nucleobases around 14 ppm. Here again, similar to the DNA analogues, we expect to see at least 3 imino resonances from the uracil bases that are involved in Watson-Crick base pairing in the case of 2UHg. In the case of 2U, we expect to see 7 imino resonances (3 from Watson-Crick bases and 4 from the mismatched bases). In the Figure 6.9, we can clearly observe the 3 imino resonances from the uracils involved in Watson-Crick pairing for both 2U and 2UHg. Interestingly, we also observe 4 peaks for 2U the range of 10 – 12 ppm matching with the wobble base paired T-T peaks observed at same place for the 2T DNA duplex. Upon addition of Hg^{II}, these peaks at 11 ppm disappear just like they did in the case of 2THg (Figure 5.2). Otherwise, upon comparing the spectra of 2U with 2T, we can see the peaks being slightly less intense than in the case of DNA. However, no significant differences are observed between the 2U and 2UHg 1D spectra.

6.3 Discussion

6.3.1 Hg^{II}-mediated base pairs lead to increased thermal stability of RNA duplexes

The thermal melting studies compared the influence of metal ion coordination on two varying conditions. In the first series of experiments, we studied the influence of different pH on duplexes at 0.5 μM and 2 μM concentrations. We observed that the thermal stability of the mismatched RNA duplexes 2U, 3U and 6U remained unchanged at both pH levels of 6.8 and 7.5 (Figure 6.5) even at lower or higher concentrations. However, from Figure 6.4 we see that the presence of mercury ion shows significant differences in T_m at pH 6.8 and 7.5, which is dependent on the concentration of the duplexes. At lower concentration and pH 6.8, the 2UHg, 3UHg and 6UHg duplexes all show the lowest melting temperature. As pH is increased, the melting temperature also rises. The highest differences between the melting temperatures across all the Hg^{II}-modified duplexes are observed at concentrations of 2 μM and at pH 7.5. The melting temperature is affected minimally between pH 5 -9. However, considering that Hg^{II} coordination between the U-U mismatched base pairs leads to deprotonation of Hg^{II}, the slight increase in acidity should account for the lowered T_m of the duplexes as there are more protons competing with the uracil bases at lower pH than there are at pH 7.5. Here again, the more the number of Hg^{II}-mediated base pairs, higher is the melting temperature which demonstrates the stabilizing effect caused due to the Hg^{II} coordination between the mismatched uracil-uracil bases affected due to the basic conditions at pH 7.5 and higher concentration of the nucleic acid duplex. In fact, the stability imparted to the overall duplex is also slightly dependent on the number of U-Hg^{II}-U base pairs a duplex has. This is very clearly demonstrated in Figure 6.4. The Figure 6.4 shows the differences in ΔT_m between 2U and 2UHg (A), 3U and 3UHg (B) and 6U and 6UHg (C). As observed, the higher number of mismatched base pairs dramatically leads to lowered melting temperature. The differences across the RNA duplexes is in the range of 10° C going from 2U to 6U. In presence of Hg^{II}, the difference in melting temperature decreases to 3° C between 2U and 6U. This is very interesting demonstration with strong evidence of the enhancement in thermal stability brought to the mismatched RNA by metal ion coordination.

Furthermore, in the last series of the melting experiments (Figure 6.6) we tested the effects of metallointercalator on the thermal stability of the RNA duplexes 2U, 3U and 6U (both with and without Hg^{II}). Intercalative binding leads to an overall positive effect on the thermal stability of the nucleic acid duplexes leading to increased melting temperature of the duplexes. For our Hg^{II}-modified RNA duplexes, we observed no change in the melting temperature in presence of rac-$[Ru(bpy)_2dppz]^{2+}$. One conclusion to be made out of this study is that the metallointercalator did not affect the Hg^{II} coordinated to the uracil-uracil

base pairs. We performed emission studies to determine the reason for this that are discussed further in the next section.

6.3.2 Binding of $[Ru(bpy)_2dppz]^{2+}$ with RNA duplexes

We tried to observe the luminescence of the metal complex $[Ru(bpy)_2dppz]^{2+}$ exhibited in presence of the RNA duplexes 2U, 2UHg, 2UN and 2UNHg. These RNA duplexes are direct analogues of the DNA duplexes discussed in Chapter 4. We expected to observe luminescence at least from the mismatched RNA duplex 2U due to the presence of U-U mismatched base pairs, which based on their weaker thermodynamic strength could be an easy target for intercalative binding. Surprisingly, we saw very little to negligible luminescence enhancements when $[Ru(bpy)_2dppz]^{2+}$ intercalates into the 2U, 2UHg, 2UN and 2UNHg duplexes. One reason could be that the intercalation does not take place. However, this is least likely to be true as otherwise we would see absolutely no emission from the complex (Figure 6.8). In addition, we would also not observe any hypochromism from the UV-vis studies (Figure 6.7). It could be rather weak intercalation or even capped intercalation which offers the phenazine nitrogens of the metal complex some shielding from the hydrogen bonding water thus leading to slight emission observed. Second reason could be an incomplete or partial intercalation leading to the observed low emission. To test this, we will need to investigate further the binding using advanced spectroscopic methods such as NMR. The binding could differ too based on the duplex.

In the case of 2UN, we observe a low % hypochromism at 13 % which compared to the DNA analogue is almost 3 times lower. In addition, the emission observed for the DNA duplex 2TN was significantly higher than that observed for 2UN (Section 6.2.3). From the previous studies of Barton and co-workers with the DNA light-switch complex $[Ru(bpy)_2dppz]^{2+}$, it was shown that the metal complex shows little to no luminescence when intercalating into an A-form RNA duplex.[100] The A-form conformation leads to weaker emission due to the exposed phenazine nitrogens of the metal complex to water. Compared to B-form conformation, it provides least stacking interactions due to the lowered overlap from the neighbouring base pairs dictated by the binding geometry assumed by the intercalated $[Ru(bpy)_2dppz]^{2+}$ into A-form RNA duplex.[104] This also holds true in the case of 2UN as observed from our spectroscopic studies.

With the 2U duplex however, one could speculate to observe intercalation right at the mismatch sites due to the flexible mismatch region. We expected this as again from the DNA counterpart 2T, we indeed observed intercalation at the mismatched sites (see Section 4.2.2). It could be very well that this indeed happens but we observe no emission. This could be explained using the same reasons as above for the 2UN. Looking at the intercalated complex from top-view, we see the differences between the A-form and the B-form duplexes where in one case, intercalation leads to bright emission and in other case it might

be minimal due to the exposed phenazine nitrogens in the cavity of the helical axis of the A-form RNA.[104] This idea is further supported by the slightly higher hypochromism observed for 2U and even 2UHg (Figure 6.7) when compared to natural 2UN RNA duplex. Interestingly, McConnell et al. were able to observe significantly enhanced luminescence (for $[Ru(bpy)_2dppz]^{2+}$) with mismatched RNA hairpin having in one case a C-A mismatch and in other case having a G-G mismatch; when compared to emission from well-matched RNA hairpin.[159] They attributed the emission to arise from metalloinsertion at the mismatched sites and concluded that the $[Ru(bpy)_2dppz]^{2+}$ emits more when intercalating at C-A mismatch sites than at G-G mismatch sites. Upon comparison with the 2U steady-state emission, we do not observe any significant enhancement despite the presence of 2x U-U mismatched base pairs. In fact, also with the mismatched DNA duplex 2T, we did not see any enhancement in steady-state luminescence from Δ-$[Ru(bpy)_2dppz]^{2+}$ indicating that the U-U/ T-T mismatch base pairs are not as thermodynamically weak as some other mismatch base pairs like C-A or G-G are. Upon comparing the emission from rac-$[Ru(bpy)_2dppz]^{2+}$ for 2T with the DNA counterpart used by McConnell et al. (with a C-A mismatch)[159], we observe similar luminescence enhancements (1.4 times) between 2T and 2TN, and McConnell's matched and mismatched DNA. It is not clear in their case whether the emission enhancement they observe is contributed from which of the isomer of $[Ru(bpy)_2dppz]^{2+}$. In the case of 2T, from our studies we now know that both of the isomers are able to intercalate similarly at the T-T mismatch sites. Thus, the enhancement observed in Figure 4.7 is likely due to the combined effect of both the isomers able to intercalate similarly (and in close proximity due to the mismatch) leading to higher quantum yield observed. Furthermore, the possibility of metalloinsertion in the case of 2U and even the DNA analogue 2T is negated, as we are not able to observe any enhanced luminescence when either of the isomer or the racemic mixture binds to the mismatched RNA / DNA duplexes (Figure 6.8 for RNA and Figures 4.7 & 4.8 for DNA). The strength of the resulting U-U/ T-T mismatch base pair could be higher compared to various other mismatch base pairs like C-A or G-G. This is further supported by the NMR studies conducted with the RNA and DNA duplexes 2U and 2T respectively which reveal the formation of wobble base pairs for each mismatched base pair (Figure 6.9). This could be very well the reason that we might not observe metalloinsertion in either case of 2U and 2T. The structural variations between the 2U and 2UN could be small due to the formation of wobble base pairs leading to the observed results.

In the case of Hg^{II}-modified RNA duplex 2UHg, we observe similar hypochromism effects as for 2U suggesting similar kind of binding of $[Ru(bpy)_2dppz]^{2+}$ with 2UHg (Figure 6.7). From the steady state emission data, we see no difference in emission compared to the 2U or 2UN (Figure 6.8). Interestingly, from the NMR studies the Hg^{II} coordination leads to disappearance of the imino proton peaks observed in the wobble region in absence of Hg^{II}.

These results are comparable to the NMR data from DNA duplex 2THg (Figure 5.2) revealing similar behaviour of the U-Hg^{II}-U to T-Hg^{II}-T.

RNA plays several important roles in the cellular processes. The development of cellular probes to target RNA is a powerful tool to understand in depth the diverse role of this biomolecule. Adapting from the DNA studies with the light-switch complex $[Ru(bpy)_2dppz]^{2+}$, we studied the interaction of duplex RNA helices with the metal complex. $[Ru(bpy)_2dppz]^{2+}$. Metal complexes including $[Ru(bpy)_2dppz]^{2+}$ are known to preferentially bind at the abasic, mismatched or at bulged site on the oligonucleotide.[14,15,141,159] The reason for this behaviour being the lowered thermodynamic stability of such base pairs.[16] The binding at mismatched site leads to the insertion of the ligand from the minor groove following the ejection of mismatched bases out into the major groove.[14,141,186] While most of such studies for characterising binding interactions between nucleic acids and octahedral metal complexes have been carried out with DNA, there are very few known examples of such binding interaction with RNA. The tilted base-pair stack present in RNA duplexes due to the C_3-endo ribose sugar-pucker conformation leads to the formation of an A-form helix. The ancillary ligands on the $[Ru(bpy)_2dppz]^{2+}$ also influence the intercalation as they are hindered due to the narrow major groove and shallow, wide minor groove of the A-form RNA. In the presence of mismatched sites however, one could expect intercalative binding as the unstable mismatched site paves way for metalloinsertion. From our studies this is most likely not the case as supported by the absorption and emission data. No luminescence enhancement is observed upon binding of $[Ru(bpy)_2dppz]^{2+}$ with 2U indicating that metalloinsertion is not taking place. What seems most likely so far is that the intercalation at the U-U site does take place as indicated by the hypochromism enhancement, but the metal complex shows low emission due to the exposed phenazine nitrogens in the binding pocket.

6.4 Conclusion

The formation of U-Hg^{II}-U base pairs leads to significant enhancements in the overall thermal stability of the RNA duplexes. These results compliment the previous work done in our group signifying the strong effect of Hg^{II} ion coordination with the mismatched U-U base pairs.[3] Furthermore, the work also highlights the negligible effect of $[Ru(bpy)_2dppz]^{2+}$ on the melting temperature of the Hg^{II}-modified RNA duplexes. Compared to DNA, the overall melting temperature of RNA duplexes is much higher thanks to the inherent structural differences between RNA and DNA. The presence of metal-modified base pairs enhances this even further to 88° C as reported by our studies. These results are promising considering that such metal-modified base pairs can be used for applications in manufacturing nano-scale wires and magnets. Furthermore, melting studies of mismatched

duplexes could be studied in presence of $[Ru(bpy)_2dppz]^{2+}$. These studies will provide clues if intercalative binding is taking place or not, as the higher melting temperature in presence of metallointercalator will be direct proof of intercalation. These studies will also clear the speculation that lowered emission is caused due to incomplete shielding of the phenazine nitrogens due to the structural conformation such as the inherent hole in the A-form RNA helix. Probing the photophysical and electronic properties of such metal modified duplexes using metal complexes is an interesting opportunity to understand the structural complexities of RNA duplexes. Unlike in the case of DNA, we observe no luminescence enhancements upon interaction of rac-$[Ru(bpy)_2dppz]^{2+}$. It would be interesting to study the intercalative binding of separated enantiomers as we did with DNA to elucidate further the subtle differences with intercalative binding of metallointercalators. These findings would be useful to develop specific metal complexes that are more suitable for intercalating into RNA duplexes.

7 EXPERIMENTAL SECTION

7.1(A) MATERIALS & CHEMICALS

DNA oligonucleotides were purchased directly from Microsynth AG, Balgach (Switzerland) and the RNA oligonucleotides were either obtained HPLC-purified from IBA GmBH, Göttingen (Germany) or in vitro transcribed with homemade T7 polymerase.[184] Nucleotides for transcription were from Microsynth, Balgach (Switzerland).

For separation of enantiomers, the CHIRALPAK® IC00CJ-PK001 / Semi-Prep and IC00CE-QH045 / Analytical separation columns were obtained from Chiral Technologies Europe.

Deuterated reagents: D2O (100 %), D2O (99.999 % D), D2O (99.98 % D), NaOD (40 % in D2O; 99.9 % D), and DNO3 (65 % in D2O; 99.5 % D) were bought from Armar Chemicals, Doettlingen (Switzerland).

All other chemicals used to prepare sample solutions were at least puriss p.a. and were purchased either from Sigma-Aldrich, Buchs (Switzerland), Acros Organics, Belgium and Merck, Darmstadt (Germany).

7.1(B) BUFFERS

Transcription buffer: 40 mM Tris-HCl (pH 7.5), 40 mM DTT, 2 mM spermidine. Storage conditions: -20°C

TBE buffer for denaturing PAGE and electroelution: 90 mM Tris-HCl (pH 8.3), 90 mM boric acid, 0.2 mM EDTA.

Urea loading buffer for denaturing PAGE: 11.8 M urea, 8.3 % sucrose, 4.2 mM Tris-HCl (pH 7.5), 0.8 mM EDTA (pH 8), 0.08 % XC, 0.08 % BB. Storage conditions: 4 °C

Formamide loading buffer for denaturing PAGE: 82 % formamide, 0.16 % xylene cyanol (XC), 0.16 % bromophenol blue (BB), 10 mM EDTA (pH 8). Storage conditions: 4 °C

Native PAGE buffer: 66 mM HEPES, 34 mM Tris-HCl, 50 mM KCl, 5 mM MOPS, 100 mM $NaClO_4$, (pH 7.4).

Gel solution: 7M urea, TBE and 18-20% acrylamide/bisacrylamide (AccuGel).

Titration buffer: 5 mM MOPS, 10 mM $NaNO_3$ (pH 7.5) unless mentioned otherwise.

7.1(c) Instrumentation

The H_2O used for all experiments was treated with a Thermo Scientific™ Barnstead™ GenPure™ water purification system from Thermo Fischer Scientific Inc., USA.

The electroelution apparatus BIOTRAP and the Elutrap membranes BT1 and BT2 were purchased from Whatman, London (UK). For desalting either, Vivaspin 2 mL ultrafiltration tubes with a MWCO of 2000 Da, purchased from Sartorius Stedim Biotech GmBH, Göttingen (Germany) were used or NAP-10 columns from GE Healthcare Life Sciences, Glattbrugg (Switzerland) were used.

Centrifuges used were RC5C+ from Sorvall, Langenselbod (Germany) or a Sorvall RC6+ from Thermo Fischer Scientific, Osterode (Germany) with a SA-600, SH-3000 and a SLA-3000 rotor; Eppendorf Centrifuge 5804 R with a A-4-44 rotor.

pH values were measured using a Hamilton Spintrode glass electrode purchased from Hamilton AG, Bonaduz (Switzerland) connected to a Metrohm 605 digital pH-meter.

UV spectroscopic measurements were carried out on either a Cary 100 UV/Vis, Cary 500 UV/Vis-NIR (both: Varian Inc. (now Agilent), Palo Alto, USA) and Lambda 25 UV/Vis spectrophotometer from PerkinElmer (USA).

Fluorescence emission measurements were conducted on a Cary Eclipse fluorescence spectrometer from Varian Inc. (now Agilent, Palo Alto, USA) with a multicell holder.

CD measurements were carried out on a Jasco J-810 spectropolarimeter (Jasco Inc., Japan) with continuous flow of N_2 with a rate of 5 L/min. The temperature was maintained using a Peltier accessory from Jasco Inc., Japan. Data evaluation was done using the supplied software: Spectra Manager and Spectra Analysis.

NMR spectra were recorded on a Bruker Avance 700 MHz spectrometer with a 5 mm CRYO TXI inverse triple-resonance probehead with z-axis pulse-field gradient coil from Bruker BioSpin AG, (Switzerland). The measurements were carried out at the NMR facility of the Department of Chemistry at the University of Zurich.

Emission lifetimes were recorded on a Fluorolog FL3-222 spectrometer from Horiba Jobin Yvon GmBH, Unterhaching (Germany) with a laser diode of pulse width 65 ps (DeltaDiode DD-470L -peak wavelength 469 nm) as the excitation source, mounted on Fluorolog cell chamber. The photon detection module used was a PPD-900 photomultiplier module. The temperature was maintained at all times using a PCB-150 Peltier water bath from Varian (Agilent).

7.2 Preparation of DNA and RNA samples

All DNA oligonucleotides were purchased whereas the RNA oligonucleotides were either bought or transcribed. Below a list of all DNA and RNA sequences is given:

2T	a strand: 5′ – GGA GCG CG**T T**GT CCC TC – 3′ b strand: 3′ – CCT CGC GC**T T**CA GGG AG – 5′	Mismatch DNA
2TN	a strand: 5′ – GGA GCG CG**T T**GT CCC TC – 3′ b strand: 3′ – CCT CGC GC**A A**CA GGG AG – 5′	Natural DNA
2TGC	a strand: 5′ – GGA GCG CG**C G**GT CCC TC – 3′ b strand: 3′ – CCT CGC GC**G C**CA GGG AG – 5′	GC-modified Natural DNA

The calculated extinction coefficients for the DNA duplexes are 286.36 $mM^{-1}cm^{-1}$ (mismatch DNA 2T), 291.73 $mM^{-1}cm^{-1}$ (natural DNA 2TN) and 278.5 $mM^{-1}cm^{-1}$ (GC-modified natural DNA 2TGC).

Below is the list of RNA duplexes used.

2U	a strand: 5′ – GGA GCG CG**U U**GU CCC UC – 3′ b strand: 3′ – CCU CGC GC**U U**CA GGG AG – 5′	Mismatch RNA
2UN	a strand: 5′ – GGA GCG CG**U U**GU CCC UC – 3′ b strand: 3′ – CCU CGC GC**A A**CA GGG AG – 5′	Natural RNA
3U	a strand: 5′ – GGA GCG CG**U UU**G UCC CUC – 3′ b strand: 3′ – CCU CGC GC**U UU**C AGG GAG – 5′	Mismatch RNA with 3 U-U
6U	a strand: 5′ – GGA GCG CG**U UUU UU**G UCC CUC – 3′ b strand: 3′ – CCU CGC GC**U UUU UU**C AGG GAG – 5′	Mismatch DNA with 6 U-U
A2UNA	a strand: 5′ – GGA GCG CG**U U**GU CCC UCA – 3′ b strand: 3′ – ACC UCG CGC **AA**C AGG GAG – 5′	Natural RNA with overhangs
A2UA	a strand: 5′ – GGA GCG CG**U U**GU CCC UCA – 3′ b strand: 3′ – ACC UCG CGC **UU**C AGG GAG – 5′	Mismatch RNA with overhangs

The calculated extinction coefficients for the RNA duplexes are 310 $mM^{-1}cm^{-1}$ (mismatch RNA 2U), 298.16 $mM^{-1}cm^{-1}$ (natural RNA 2UN), 314.5 $mM^{-1}cm^{-1}$ (natural RNA with overhangs A2UNA) and 338 $mM^{-1}cm^{-1}$ (mismatch RNA with overhangs A2UA).

7.2.1 Transcription of small RNAs

In vitro transcription was accomplished as described previously using home-made T7 polymerase.[184] Reaction mixtures contained 5 mM each of ATP, GTP and CTP, 1-1.2 µM of

each strand of the synthetic (page-purified) double-stranded DNA. The concentration of UTP used for all strands was 5 mM except for 6Ub where it was 7.5 mM, and the concentration of $MgCl_2$ used was 45 mM except for 2Ua where 20 mM was used. The NTPs, Mg^{2+} and the strands were mixed in 1x transcription buffer with 0.01% triton X-100. Finally, the T7 RNA polymerase was added and according to the activity of each batch, the amounts used for transcription were adjusted. The reaction was run for 4-10 hours in a Thermomixer at 37°C and 400 rpm. Afterwards, the RNA was precipitated and PAGE-purified, the bands were visualized by UV shadowing, and the appropriate bands were cut from the gel, and the RNA strands were recovered by electroelution using Whatman elutrap system (Whatman, UK).

The RNA samples were then desalted and concentrated by ultrafiltration using Vivaspin® devices (Sartorius Stedim Biotech GmBH, Germany; 2000 Da MWCO) by washing 5 times with 1 M KCl, pH 8, and 5-7 times with water.

7.2.2 Formation of the DNA and RNA duplexes

All DNA and RNA oligonucleotide duplexes were prepared by combining equal concentrations of the single strand 'a' with 'b'. The 1:1 mixture of the oligonucleotides was dissolved in water, and after mixing gently with pipette, heated to 90 °C for 4 minutes and finally transferred on ice to allow re-annealing of the complementary strands. The duplexes were then subjected to NAP-10 column for desalting. Finally, the solutions were freeze dried for storage and reconstituted in sterile water for use.

The Hg^{II} modified DNA and RNA samples were prepared using the mismatched DNA or RNA duplexes containing 2 T-T or 2, 4, or 6 U-U base pairs, respectively, and adding the appropriate equivalents of $Hg(NO_3)_2$. One equivalent is defined as the amount of Hg^{II} needed to form and complete the set of T-Hg^{II}-T / U-Hg^{II}-U in a given duplex, respectively (Figure 3.4). For control experiments with natural DNA the same amount of $Hg(NO_3)_2$ as used for the mismatched DNA (equivalents) was added.

7.3 Synthesis of $[Ru(bpy)_2(dppz)]^{2+}$ and Separation of its enantiomers

The $[Ru(bpy)_2(dppz)]^{2+}$ was synthesized as a BF_4^- salt following established protocols[134] within an Advanced Practical course at the Department of Chemistry and was later converted to NO_3^- salt using Dowex cation resin. The separated enantiomers were checked for purity via mass spectrometry and were found to be sufficiently pure with $[M-NO_3]^+$ peak at 758.2 m/z. corresponding to $[Ru(bpy)_2(dppz)]NO_3^+$ mass of 758.12. The chirality of the enantiomers was further confirmed by comparing their CD signals with literature data (Appendix S9-C).

Enantiomers of $[Ru(bpy)_2(dppz)]^{2+}$ (Figure 3.5) were obtained by subjecting the racemic mixture of metal complex to HPLC separation using CHIRALPAK® IC00CJ-PK001 / Semi-Prep separation columns, in a MeOH:TFA:TEA=100:0.5:0.3 mobile phase solvent. To check the purity after the HPLC the enantiomers were tested on IC00CE-QH045 / Analytical column in a MeOH:TFA:TEA=100:0.5:0.3 mobile phase solvent (see Appendix S9).

7.4 UV MELTING STUDIES

Temperature dependent absorption spectra were measured for the RNA duplexes 2U, 3U and 6U using a concentration of 0.5 μM and 2 μM at pH 6.8 and pH7.5 each. The absorption at 260 nm was measured in the absence and presence of 1 equivalent of Hg^{II}, were the $Hg(ClO_4)_2$ solution was added just before the acquisition. In a second series of experiments, the temperature dependent absorption spectra at 260 nm were recorded for the RNA duplex 2UHg using concentration of 2 μM, in absence and presence of 2 μM and 34 μM $[Ru(bpy)_2(dppz)]^{2+}$. This led to achievement of duplex / Ru ratio of 1: 1 and base pair / Ru ratio of 1: 1. All the experiments were performed in 5 mM MOPS buffer with 100 mM $NaClO_4$. The samples were degassed for 30 seconds prior to measurement. The cuvette used for measurement was a 1cm path-length quartz cuvette with total volume capacity of 1 mL. All the samples were covered with paraffin oil to avoid sample evaporation and furthermore the cuvettes were shut with appropriate caps. The heating and cooling cycles were performed at a rate of 0.5 °C/min steps for a temperature range of 25 °C to 95 °C. The data from at least two repeated heating and cooling cycles were gathered to check for consistent and reproducible results. The melting temperature were obtained by calculating the first derivative of the individual melting curves.

7.5 SPECTROSCOPIC TITRATIONS

7.5.1 UV-VIS ABSORPTION TITRATIONS

All UV- Visible titrations were performed in a 1 cm path length quartz cuvette (also suitable for fluorescence measurements) from Starna scientific (England). Two different kinds of titration were carried out in which either the $[Ru(bpy)_2(dppz)]^{2+}$ concentration or the oligonucleotide concentration was kept constant.

In the first case the DNA or RNA duplexes were added stepwise to a 17 μM solution of $[Ru(bpy)_2(dppz)]^{2+}$ to achieve bp/Ru ratio from 1:1, 2:1, 3:1 and so on until 20:1 (ratio in format bp: Ru). After each addition the absorption was recorded from 600 nm to 200 nm. Each titration experiment was repeated in triplicates. The absorption values at 370 nm which corresponds to the dppz π- π* absorption band was then used to plot the data. The % hypochromism values were calculated according to the following formula:

$$\% \text{ hypochromism} = \left(\frac{\text{Abs}_{370}\text{at } 1:0 - \text{Abs}_{370}\text{at } 1:20}{\text{Abs}_{370}\text{at } 1:0}\right) * 100$$

Where, the ratio depicts Ru: DNA and the absorption at 370 nm relates to that of the metal complex.

In the second case, the $[Ru(bpy)_2(dppz)]^{2+}$ was added stepwise to a 1 μM solution of duplex DNA 2T to achieve Ru/duplex ratios from 1:1, 2:1, 3:1 and so on until 20:1. After each addition, the absorption was recorded from 600 nm to 200 nm. Each titration was repeated at least twice. Here since the DNA duplex was kept constant, the results were only used to cross-validate the fluorescence readings (see below) as the absorption from increasing ruthenium complex followed a linear increase with each stepwise addition.

7. 5.2 Fluorescence Emission titrations

Steady-state emission measurements were recorded on a Cary Eclipse fluorescence spectrometer from Varian (Agilent). The measurements were acquired with an excitation wavelength (λ_{ex}) of 444nm and a scan acquisition range from 470 nm to 850 nm. The slit size used was 10 nm and the scan rate and instrument sensitivity were kept at default (medium) settings in all cases except for measurements of RNA duplex titrations (Chapter 6). Both the absorption and emission experiments were performed simultaneously using the same sample and cuvette to be able to correct the emission intensities with the absorption of the complex only concentration. Hence, as described above in the absorption titration section, both series of experiments were performed and after acquiring each absorption reading, fluorescence emission readings were also acquired. The measurements were recorded at ambient temperatures in aerated solutions. Upon addition of increasing amounts of DNA, the emission from the metal complex was observed to increase at around 620 nm (depending on the enantiomer). The emission intensity from 500 nm to 850 nm was used in integrated form. All the titrations were performed at least three times.

7.5.3 Emission Lifetimes

The excited state lifetime of a luminescent molecule is the average time the molecule spends in the excited state before emitting a photon. The photoluminescence lifetimes were determined by the time-correlated single photon counting method on a Fluorolog FL3-222 spectrometer from Horiba Jobin Yvon GmBH, Unterhaching (Germany) with a laser diode of pulse width 65 ps (DeltaDiode DD-470L -peak wavelength 469 nm) as the excitation source, mounted on Fluorolog cell chamber. The measurement range of 3.2 μs was used with a total of 4096 channels. Furthermore, a double grating emission monochromator set at 620 nm (maximum emission wavelength of metal complex) was also used. A photomultiplier module PPD-900 was used as the detector. At all times during the experiment, the sample chamber was maintained at 25°C by a PCB-150 Peltier water bath from Varian Cary (Agilent). The

metal complex of 5 μM concentration was used in a quart fluorescence cuvette of 1 cm path length. The titrations were performed similar to the Fluorescence emission experiments, where increasing amounts of duplex DNA was added to a 5 μM metal complex (constant) before each measurement to achieve Ru/duplex ratios of 0.12: 1, 0.24: 1, 0.35: 1, 0.47: 1 and 1.06: 1 (ratio in the format- Ru: duplex). Each measurement was carried out at least twice. The time resolved data was fit by iterative re-convolution of IRF with the biexponential fitting model:

$$I(t) = \alpha_1 \exp\left(-\frac{t}{\tau_1}\right) + \alpha_2 \exp\left(-\frac{t}{\tau_2}\right)$$

The lifetimes were thereafter calculated by fitting the convoluted model with the emission decay obtained for each sample.

The concentration of the complex used was kept low (5 μM) to avoid any inner filter effects.

7.5.4 CD TITRATIONS

CD Spectra were recorded at 25°C on a Jasco J-810 spectrometer using a 1 cm path length quartz cuvette with volume capacity of 1 mL (Hellma Analytics, Germany). The buffer used was a 5mM MOPS buffer (pH 7.5) with 10mM $NaNO_3$ salt. The titration experiments were conducted by adding the Ru complex to a duplex concentration of 1 μM (constant) to achieve Ru/duplex ratios from 1: 0, 1: 2, 1: 4, 1: 6, 1: 8, until 1: 20. Each measurement was repeated 4 times at the rate of 100nm/min from 600nm to 200nm.

7.6 JOB-PLOT ANALYSIS

Binding stoichiometries were obtained for the two enantiomers using the method of continuous variation.[187] The concentration of metal complex and DNA duplex was varied (molar ratios of complex per DNA), while the sum of the concentrations of both was kept constant at 2 μM. For each DNA and complex, solutions were made in 5 mM MOPS and 10 mM $NaNO_3$ buffer, were mixed in separate tubes to achieve ratios of 2.03: 1, 3: 1, 4: 1, 5.06: 1, 9: 1 and 19: 1 Ru/duplex (final volume was 100 μL). The fluorescence emission intensities of the mixtures were measured at ambient temperatures (approx. 25 °C) using an excitation wavelength (λ_{ex}) of 444 nm. The scans were recorded from 480 nm to 800 nm. The readings at the emission-maximum wavelength (620 nm) were used to plot against the varying mole fraction ratios of Ru/duplex.

7.7 NMR SPECTROSCOPY

All samples contained 0.4 mM of duplex DNA, 10 mM $NaNO_3$ and the pH was adjusted to 6.8 in case of samples with 90 % H_2O + 10 % D_2O as solvent or to pD 6.8 in case of 100 %

D_2O as solvent. The final volume of the samples was around 275 µL. All NMR measurements were conducted in 5 mm Shigemi NMR tubes from Shigemi Co., LTD. Tokyo (Japan)

The DNA duplexes were prepared in a similar manner as previously described for UV-Vis and fluorescence titrations. [^{1}H]-NMR spectra were measured in D_2O with presaturation water suppression. [^{1}H,^{1}H]-NOESY spectra were acquired in 10 % D_2O, 90 % H_2O with a mixing time of 250 ms.

Non-exchangeable resonances of all the DNA duplexes were assigned from [^{1}H, ^{1}H]-TOCSY (50 ms mixing time) and [^{1}H,^{1}H]-NOESY (250 ms mixing time, 303 K) spectra at pD 6.8 in 100 % D_2O.

All NMR data were processed with TopSpin 2.0 or 3.2 (Bruker). The analysis of the data was done using Sparky (http://www.cgl.uscf.edu/home/sparky/).

The graphs depicted throughout the thesis were plotted using OriginPro software version 9.1.0 developed by OriginLab Corporation, Northampton, MA (USA).

8 APPENDICES

S1

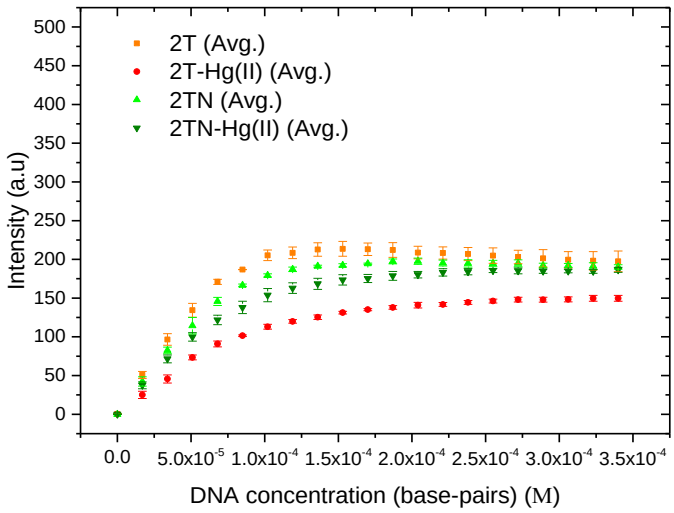

Figure S1: Emission titrations of rac-$[Ru(bpy)_2(dppz)]^{2+}$ with 2T, 2THg, 2TN and 2TNHg DNA duplexes. The buffer used was 5mM MOPS 100mM $NaNO_3$. The emission is mapped at 620nm against increasing DNA concentration. The scale on y-axis is given in DNA concentration (unlike in ratio from other figure in Chapter 4, but the same scale applies also here).

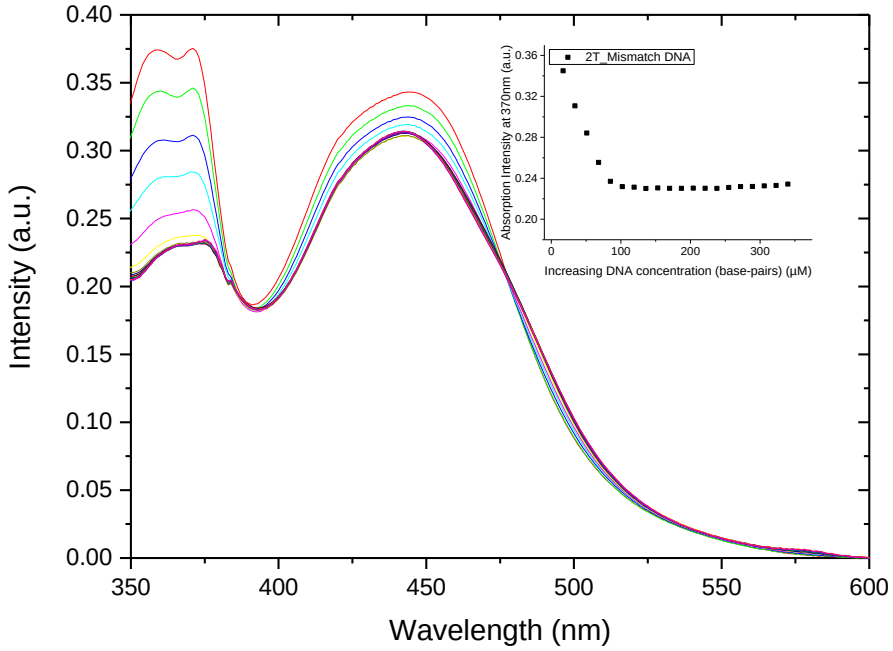

Figure S2-A: Typical absorption spectra for racemic-$[Ru(bpy)_2(dppz)]^{2+}$ complex titrated against increasing 2T DNA duplex. The buffer used was 5mM MOPS 10mM $NaNO_3$. The inset shows the absorption plot of racemic-$[Ru(bpy)_2(dppz)]^{2+}$ at its MLCT wavelength 370nm.

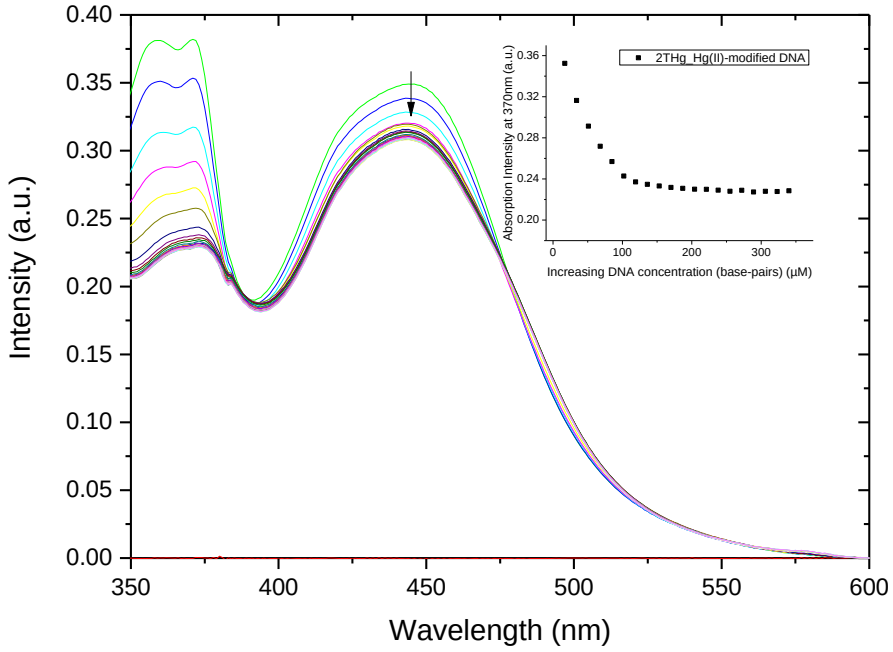

Figure S2-B: Typical absorption spectra for racemic-$[Ru(bpy)_2(dppz)]^{2+}$ complex titrated against increasing 2THg DNA duplex. The buffer used was 5mM MOPS 10mM $NaNO_3$. The inset shows the absorption plot of racemic-$[Ru(bpy)_2(dppz)]^{2+}$ at its MLCT wavelength 370nm.

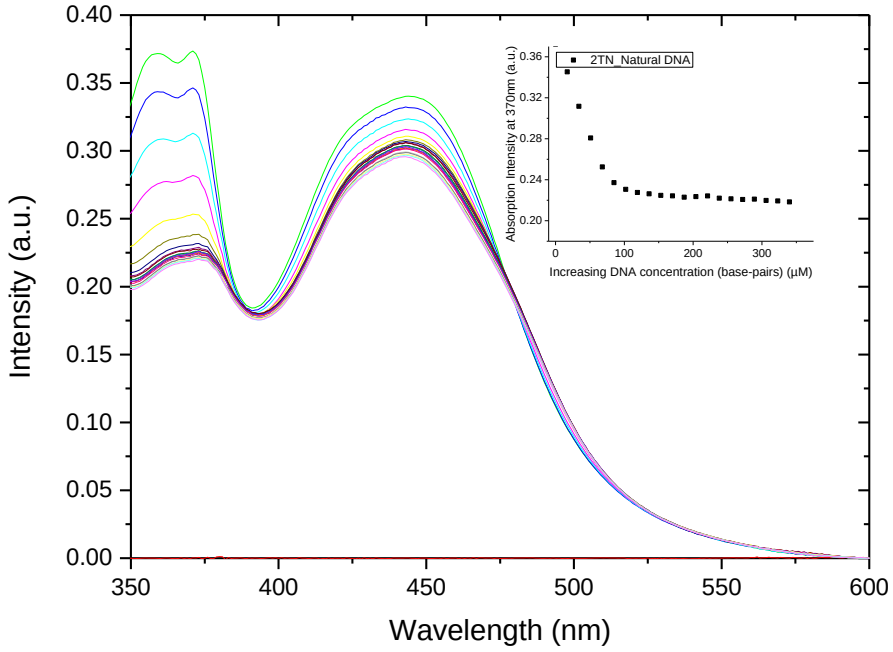

Figure S2-C: Typical absorption spectra for racemic-$[Ru(bpy)_2(dppz)]^{2+}$ complex titrated against increasing 2TN DNA duplex. The buffer used was 5mM MOPS 10mM $NaNO_3$. The inset shows the absorption plot of racemic-$[Ru(bpy)_2(dppz)]^{2+}$ at its MLCT wavelength 370nm.

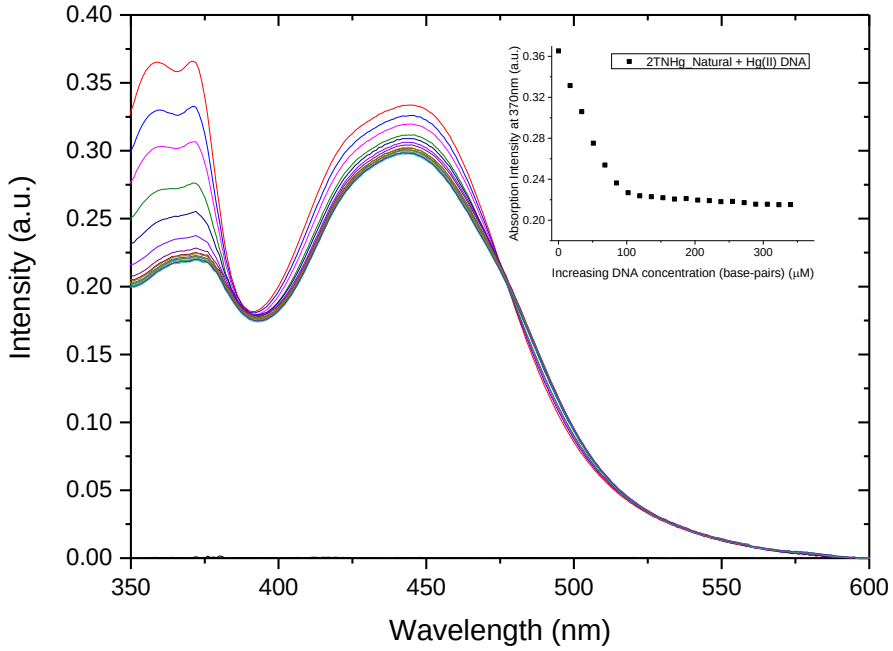

Figure S2-D: Typical absorption spectra for racemic-$[Ru(bpy)_2(dppz)]^{2+}$ complex titrated against increasing 2TNHg DNA duplex. The buffer used was 5mM MOPS 10mM $NaNO_3$. The inset shows the absorption plot of racemic-$[Ru(bpy)_2(dppz)]^{2+}$ at its MLCT wavelength 370nm.

S3: Typical emission spectra for racemic-$[Ru(bpy)_2(dppz)]^{2+}$ complex with each DNA duplex recorded during titration experiments described in Section 4.2.2. The inset depicts emission intensity plot at 620 nm:

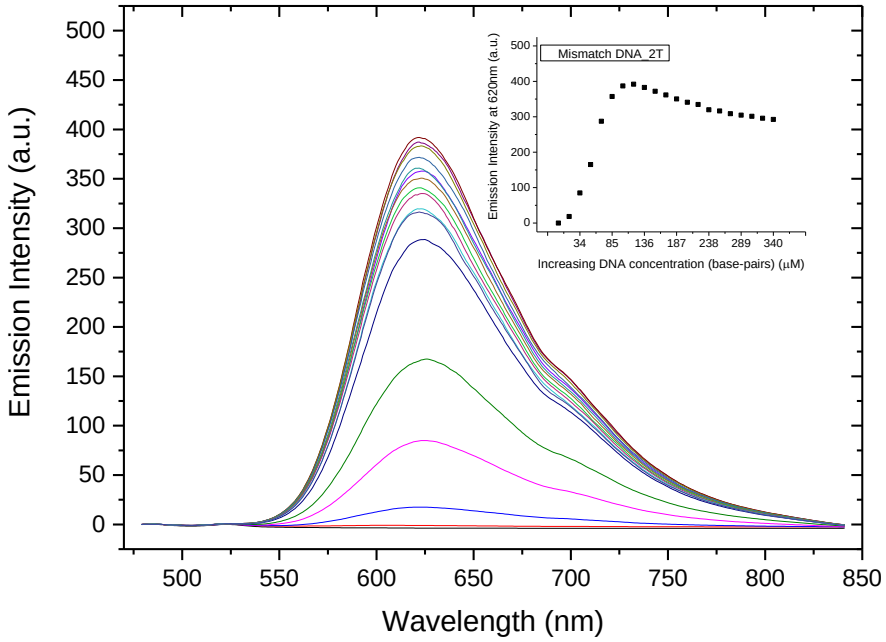

Figure S3-A: Typical emission spectra for racemic-$[Ru(bpy)_2(dppz)]^{2+}$ complex titrated against increasing 2T DNA duplex. Recorded during titration experiments as described in Section 4.2.2. The inset depicts emission intensity plot at 620 nm.

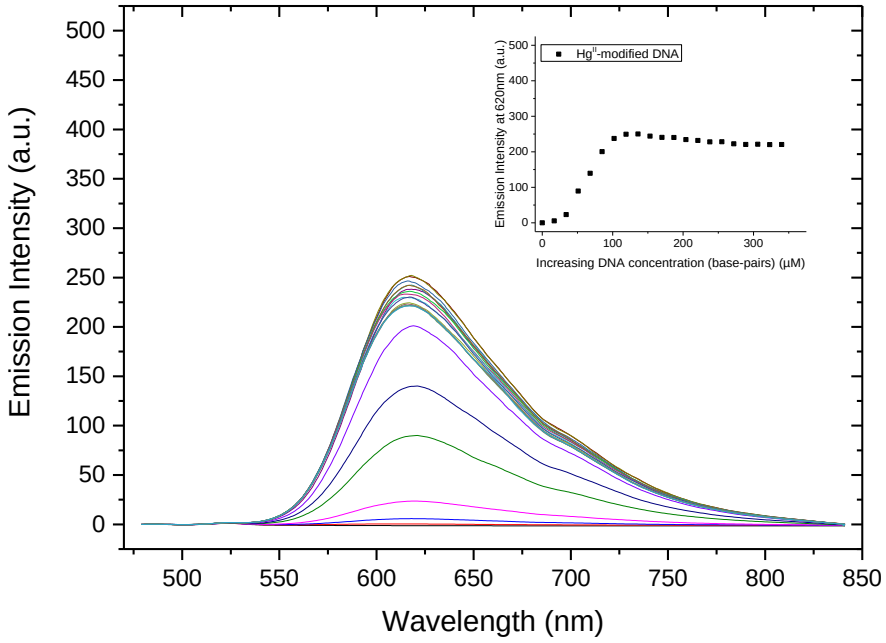

Figure S3-B: Typical emission spectra for racemic-$[Ru(bpy)_2(dppz)]^{2+}$ complex titrated against increasing 2THg DNA duplex. Recorded during titration experiments as described in Section 4.2.2. The inset depicts emission intensity plot at 620 nm

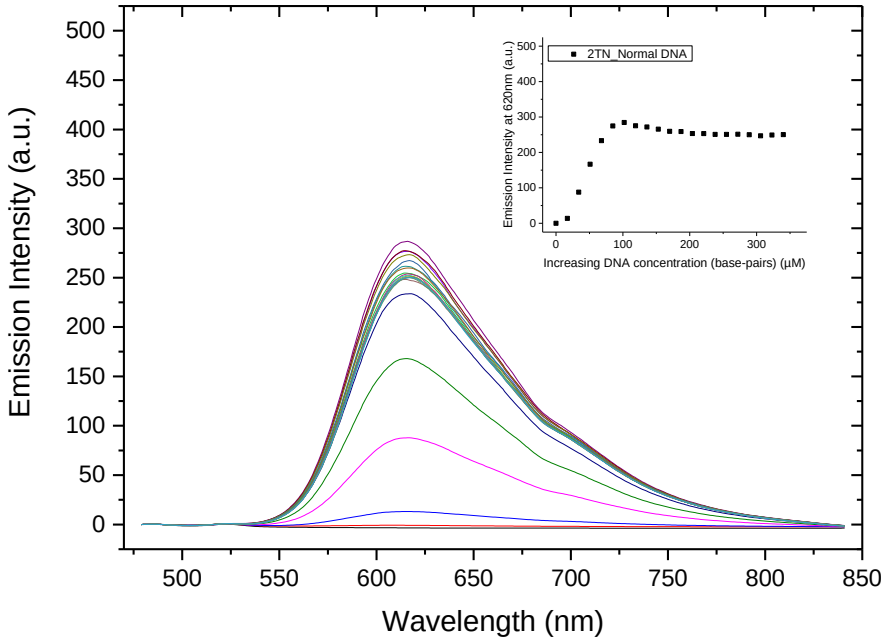

Figure S3-C: Typical emission spectra for racemic-$[Ru(bpy)_2(dppz)]^{2+}$ complex titrated against increasing 2TN DNA duplex. Recorded during titration experiments as described in Section 4.2.2. The inset depicts emission intensity plot at 620 nm.

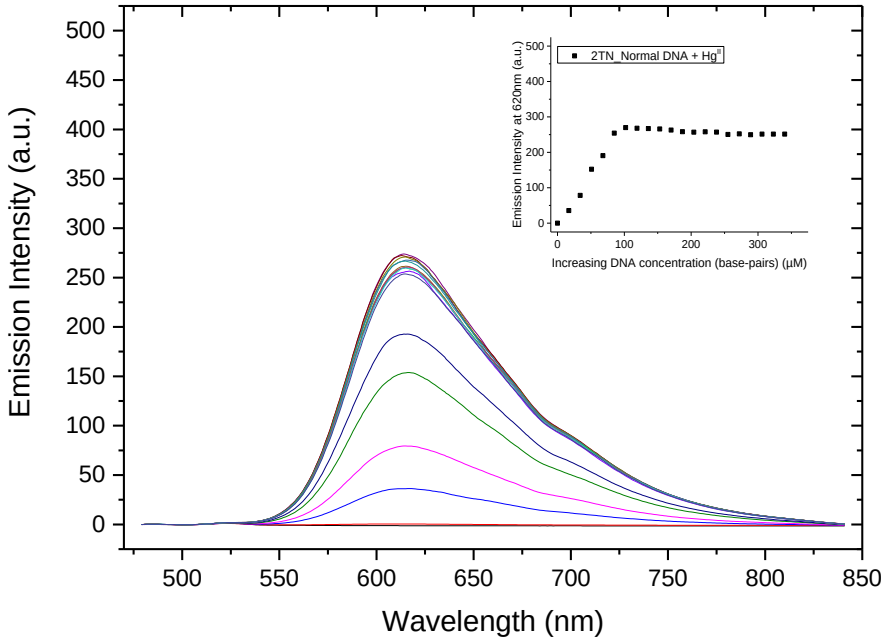

Figure S3-D: Typical emission spectra for racemic-$[Ru(bpy)_2(dppz)]^{2+}$ complex titrated against increasing 2TNHg DNA duplex. Recorded during titration experiments as described in Section 4.2.2. The inset depicts emission intensity plot at 620 nm.

S4: Fitted UV absorption data recorded for individual enantiomers bound to 2T, 2THg, 2TN and 2TNHg. See Section 4.2.1.

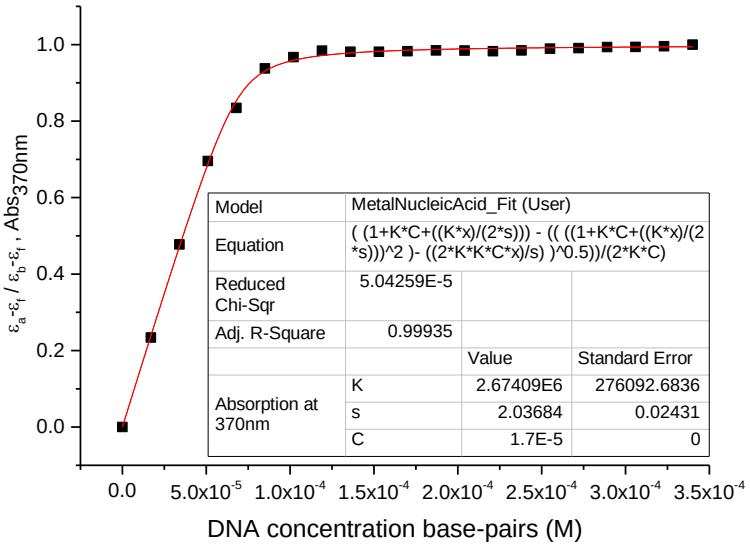

Figure S4-1A: Fitted UV absorption titration data (see Section 4.2.1) for calculating binding constants for the interaction of Δ-$[Ru(bpy)_2(dppz)]^{2+}$ with 2T DNA. Increasing amounts of DNA were titrated against constant metal-complex concentration in 5mM MOPS 10mM $NaNO_3$ buffer at pH 7.5.

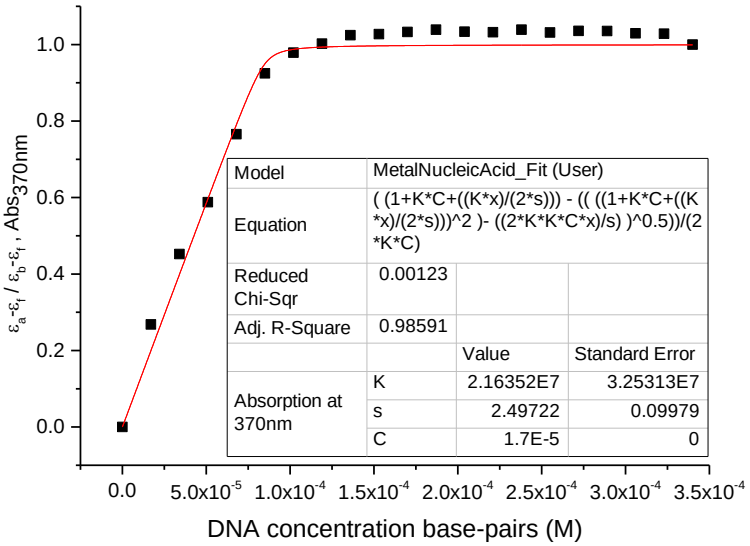

Figure S4-1B: Fitted UV absorption titration data (see Section 4.2.1) for calculating binding constants for the interaction of Δ-$[Ru(bpy)_2(dppz)]^{2+}$ with 2THg DNA. Increasing amounts of

DNA were titrated against constant metal-complex concentration in 5mM MOPS 10mM $NaNO_3$ buffer at pH 7.5.

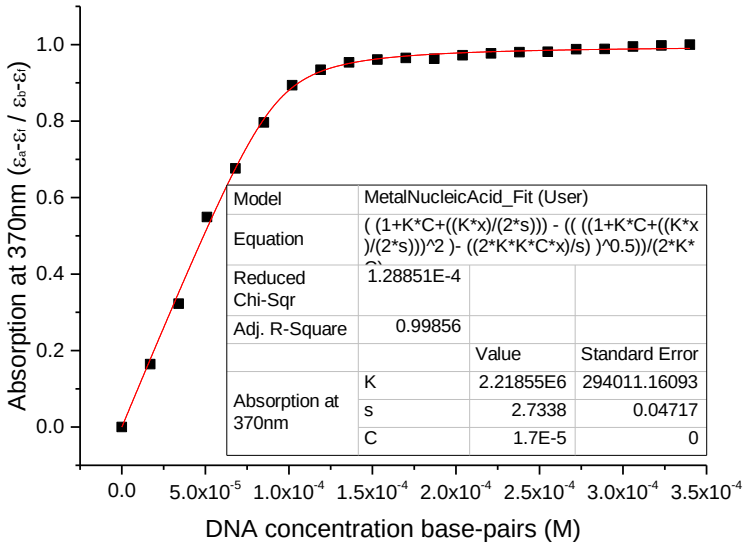

Figure S4-1C: Fitted UV absorption titration data (see Section 4.2.1) for calculating binding constants for the interaction of Δ-$[Ru(bpy)_2(dppz)]^{2+}$ with 2TN DNA. Increasing amounts of DNA were titrated against constant metal-complex concentration in 5mM MOPS 10mM $NaNO_3$ buffer at pH 7.5.

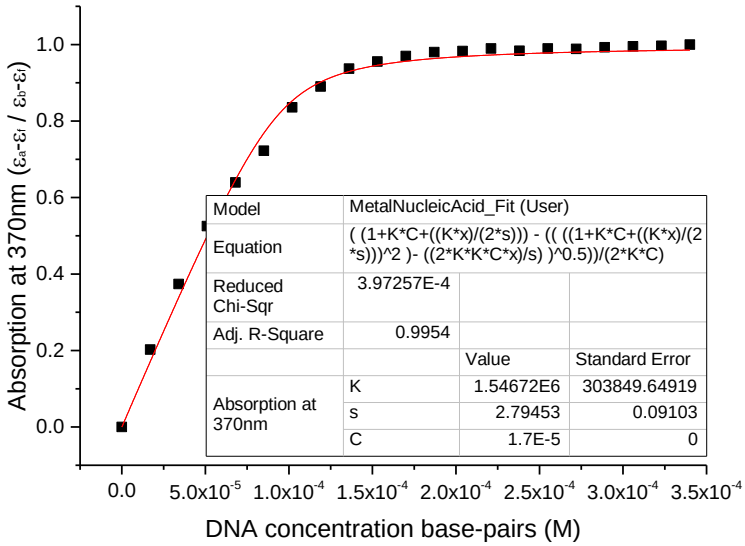

Figure S4-1D: Fitted UV absorption titration data (see Section 4.2.1) for calculating binding constants for the interaction of Δ-$[Ru(bpy)_2(dppz)]^{2+}$ with 2TNHg DNA. Increasing amounts

of DNA were titrated against constant metal-complex concentration in 5mM MOPS 10mM $NaNO_3$ buffer at pH 7.5.

S4-2:

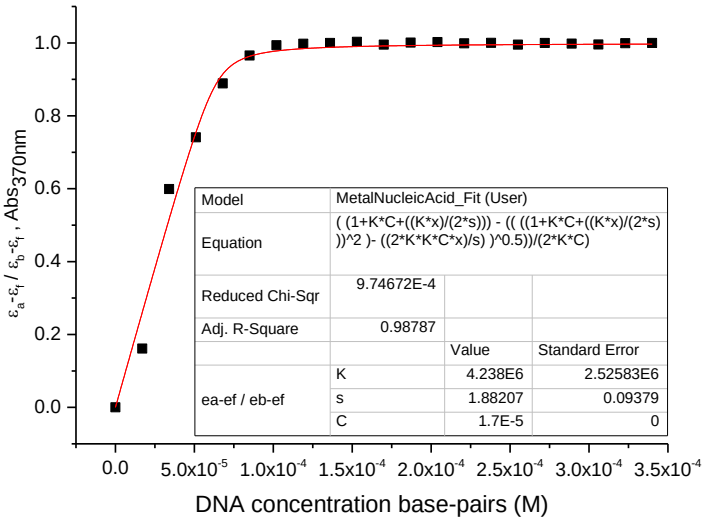

Figure S4-2A: Fitted UV absorption titration data (see Section 4.2.1) for calculating binding constants for the interaction of Λ-$[Ru(bpy)_2(dppz)]^{2+}$ with 2T DNA. Increasing amounts of 2T DNA were titrated against constant metal-complex concentration in 5mM MOPS 10mM $NaNO_3$ buffer at pH 7.5.

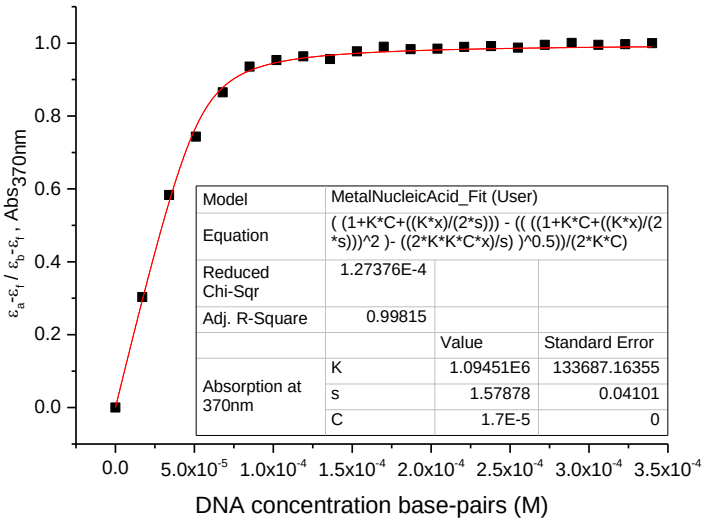

Figure S4-2B: Fitted UV absorption titration data (see Section 4.2.1) for calculating binding constants for the interaction of Λ-$[Ru(bpy)_2(dppz)]^{2+}$ with 2THg DNA. Increasing amounts of

2THg DNA were titrated against constant metal-complex concentration in 5mM MOPS 10mM $NaNO_3$ buffer at pH 7.5.

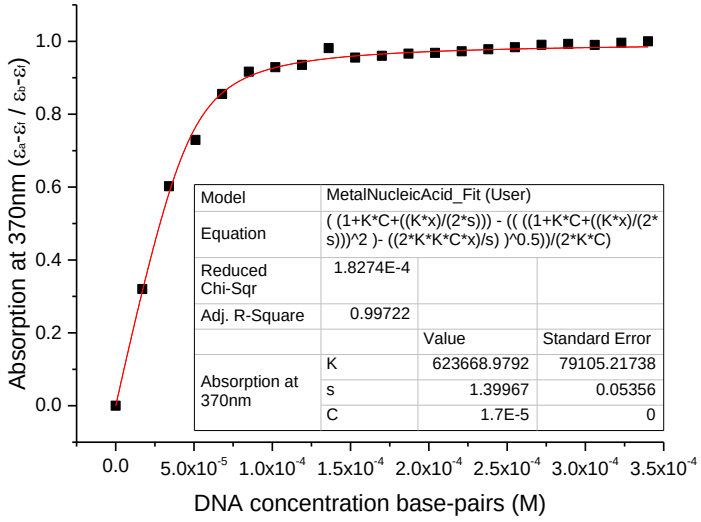

Figure S4-2C: Fitted UV absorption titration data (see Section 4.2.1) for calculating binding constants for the interaction of Λ-$[Ru(bpy)_2(dppz)]^{2+}$ with 2TN DNA. Increasing amounts of DNA were titrated against constant metal-complex concentration in 5mM MOPS 10mM $NaNO_3$ buffer at pH 7.5.

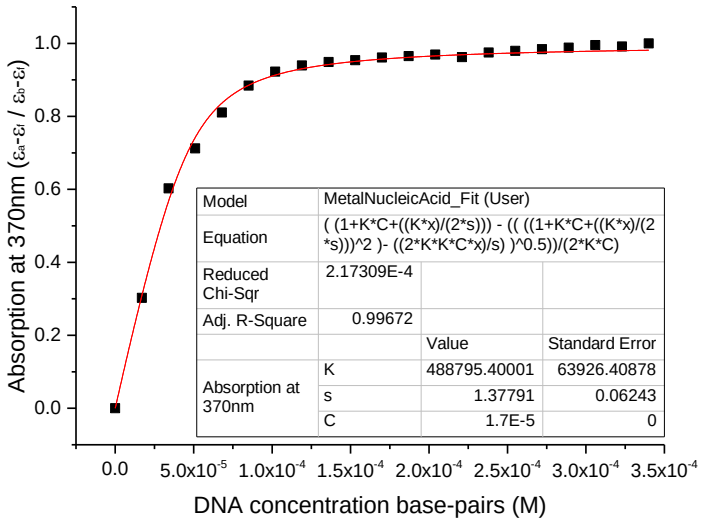

Figure S4-2D: Fitted UV absorption titration data (see Section 4.2.1) for calculating binding constants for the interaction of Λ-$[Ru(bpy)_2(dppz)]^{2+}$ with 2TNHg DNA. Increasing amounts of DNA were titrated against constant metal-complex concentration in 5mM MOPS 10mM $NaNO_3$ buffer at pH 7.5.

Table S1-A: Pre-exponential factors α_S and α_L recorded for Δ-$[Ru(bpy)_2(dppz)]^{2+}$ titrated against increasing concentration of various DNA duplexes (Section 7.5.3).

	Base-pair/Ru(II)	τ_S		α_S		τ_L		α_L	
2T	2	111	12.3	40	1.2	393	1.5	60	1.2
	4	114	0	40	0.52	406	0.5	60	0.52
	6	116	4.11	40	1.12	414	11	60	1.12
	8	118	2.62	40	1.19	424	8	60	1.19
	18	112	6.02	40	1.62	401	13	60	1.62
2THg	2	98	0.5	44	2.32	322	12	56	2.32
	4	98	2	43	1.29	324	13	57	1.29
	6	101	0.5	45	2.42	334	7	55	2.42
	8	98	2.5	44	2.51	324	0.5	56	2.51
	18	90	2.45	42	1.34	308	0.5	58	1.34
2TN	2	129	2.25	34	1.5	519	8.5	66	1.5
	4	130	0.2	34	1.36	524	2	66	1.36
	6	132	0	36	0.81	528	2	64	0.8
	8	131	0.85	37	2.57	525	6.5	63	2.57
	18	115	3	55	4.53	422	34	45	4.52
2TGC	2	106	1	42	0.55	320	0.5	58	0.55
	4	113	0	45	0.18	336	4.5	55	0.18
	6	113	5	44	1.87	334	7	56	1.87
	8	117	1	46	0.38	341	4.5	54	0.38
	18	117	1.5	43	1.31	330	3.5	57	1.31
2TNHg	2	126	0	35	0.68	510	4	65	0.67
	4	128	0	35	1.02	512	11.5	65	1.02
	6	129	1	35	0.6	510	9.5	65	0.6
	8	131	1	39	0.41	505	9.5	61	0.41
	18	122	0.5	52	0.22	427	24.5	48	0.22

Table S1-B: Pre-exponential factors α_S and α_L recorded for Λ-$[Ru(bpy)_2(dppz)]^{2+}$ titrated against increasing concentration of various DNA duplexes (Section 7.5.3).

	Base-pair/Ru(II)	τS		αS		τL		αL	
2T	2	71	3	31	3.68	382	21.5	69	3.68
	4	74	4.5	29	2.705	397	20.5	71	2.705
	6	76	6.5	29	3.105	394	22.5	71	3.105
	8	76	5.25	28	3.11	390	23.5	72	3.11
	18	75	1.5	41	0.26	347	19	59	0.26
2THg	2	67	0.15	60	1.65	297	3	40	1.65
	4	67	1	61	2.745	313	1.5	39	2.745
	6	66	2	60	3.325	309	5.5	40	3.325
	8	63	2	58	4.675	305	5	42	4.675
	18	58	0.6	53	6.37	285	3	47	6.37
2TN	2	65	0	57	2.545	246	3	43	2.545
	4	66	1	63	0.725	261	1.5	37	0.725
	6	66	1.5	63	0.37	261	0.5	37	0.37
	8	64	1.5	63	0.135	263	3	37	0.135
	18	54	0.5	58	0.435	257	0	42	0.435
2TGC	2	62	0.5	62	1.73	197	6.5	38	1.73
	4	63	0.5	64	0.395	202	1	36	0.395
	6	62	0.2	67	0.225	219	4	33	0.225
	8	61	1.15	68	0.185	232	4.5	32	0.185
	18	58	0	63	0.3	255	7	37	0.3
2TNHg	2	64	0.5	52	0.485	243	0.5	48	0.485
	4	68	0.5	61	1.67	268	7.5	39	1.67
	6	68	1	62	1.165	271	3.5	38	1.165
	8	65	0.1	62	0.87	262	8.5	38	0.87
	18	59	0.5	61	1.04	258	7	39	1.04

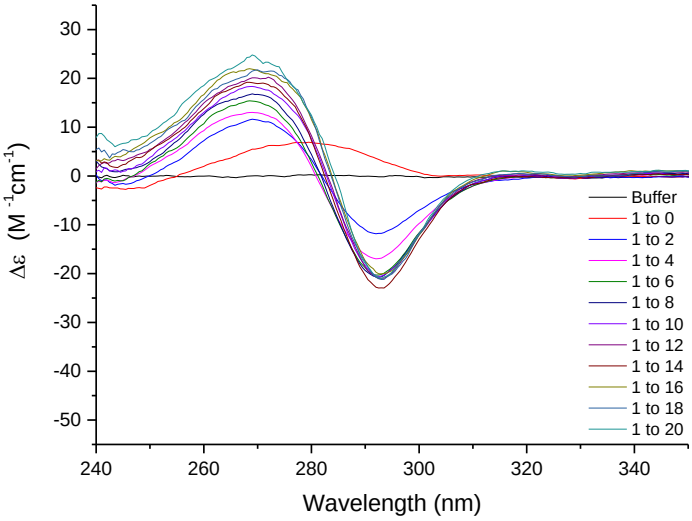

Figure S5: Changes in the CD spectra of 2TNHg titrated against increasing rac-$[Ru(bpy)_2(dppz)]^{2+}$ metal complex. See Section 7.5.4.

S6: Fitted data for method of continuous variations to determine binding stoichiometry

a. Job plot for 2T (with Δ and Λ enantiomers). From Figure 4.9

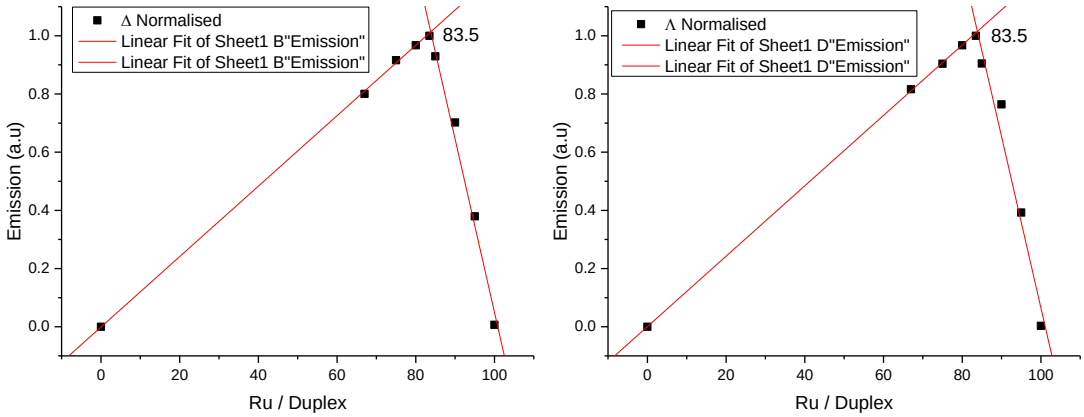

b. Job plot for 2THg (with Δ and Λ enantiomers)

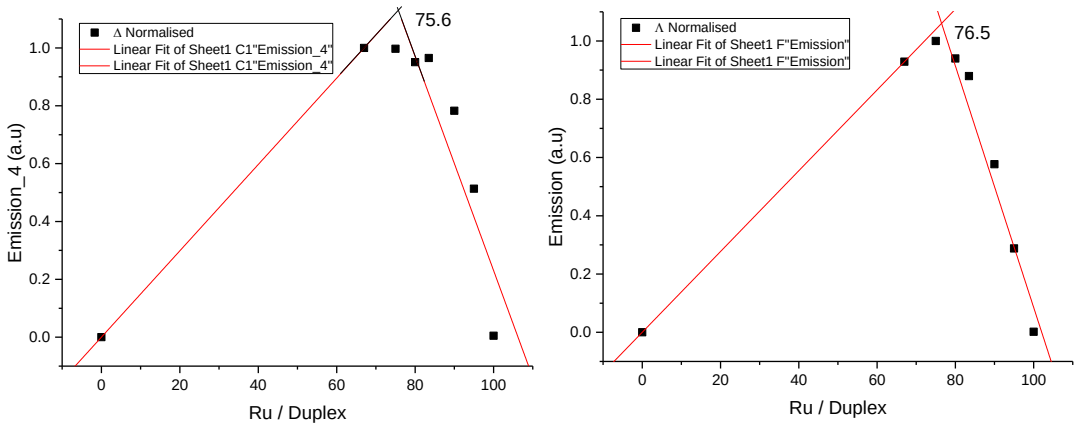

c. Job plot for 2TN (with Δ and Λ enantiomers)

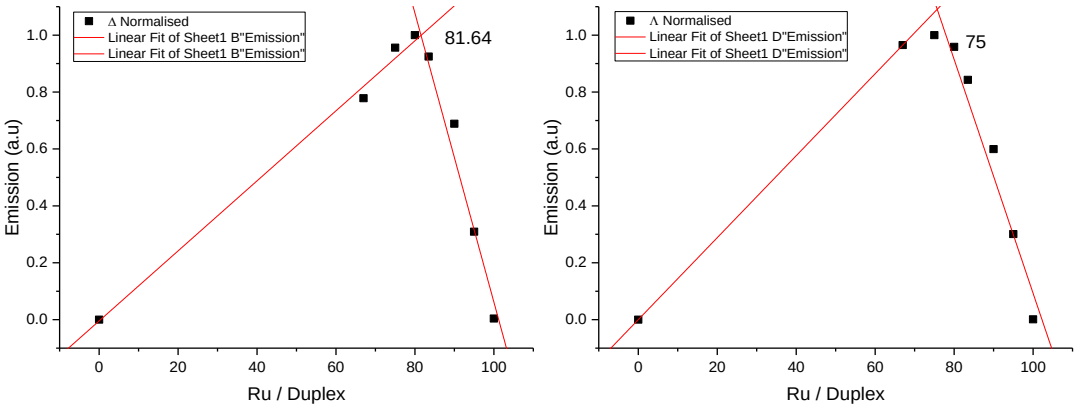

d. Job plot for 2TGC (with Δ and Λ enantiomers)

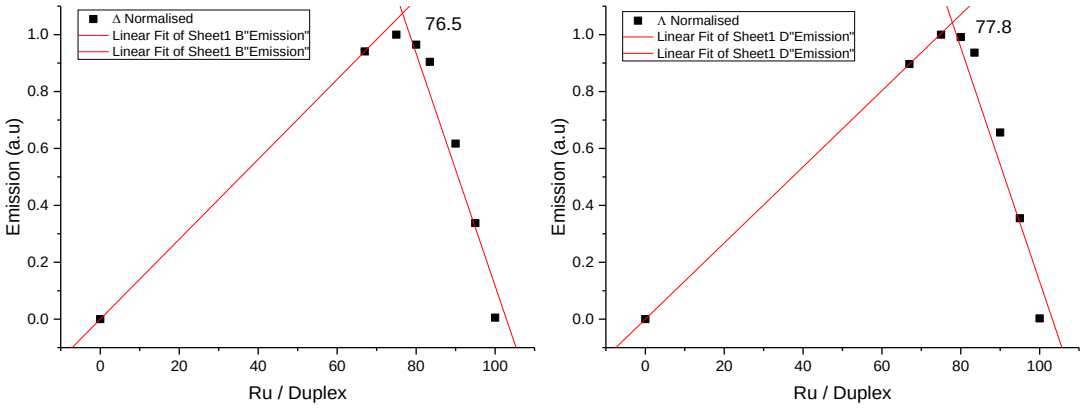

e. Job plot for 2TNHg (with Δ and Λ enantiomers)

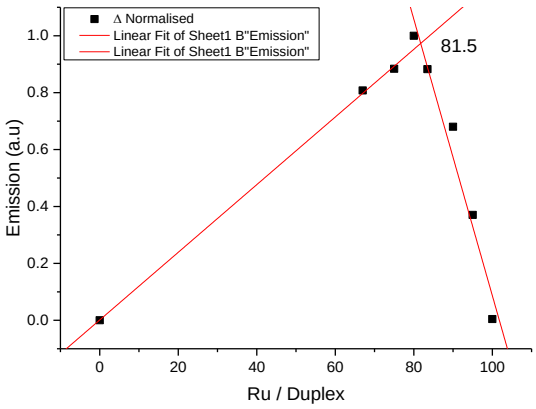
Δ Normalised
Linear Fit of Sheet1 B"Emission"
Linear Fit of Sheet1 B"Emission"
81.5
Emission (a.u)
Ru / Duplex
0.0
0.2
0.4
0.6
0.8
1.0
0
20
40
60
80
100

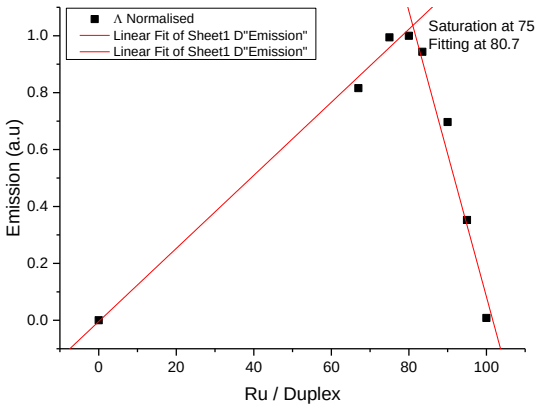
Λ Normalised
Linear Fit of Sheet1 D"Emission"
Linear Fit of Sheet1 D"Emission"
Saturation at 75
Fitting at 80.7
Emission (a.u)
Ru / Duplex
0.0
0.2
0.4
0.6
0.8
1.0
0
20
40
60
80
100

Table S2-A. Chemical shift difference (Δδ) between 2T and 2TN (Chemical shifts of 2TN considered standard). From 2D [^{1}H, ^{1}H]-NOESY spectra assignments.

	ppm_H1'	ppm_H2'	ppm_H2''	ppm_H5	ppm_H6	ppm_H8	ppm_H2
G6	-0.01	-0.006	-0.003	0	0	-0.011	0
C7	-0.037	0.153	0.04	-0.018	0.055	0	0
G8	-0.042	0	0.062	0	0	0.02	0
T9	0.174	0.091	0.106	-0.148	0.106	0	0
T10	0.063	0.196	0.128	0.116	0.068	0	0
G11	0.001	-0.019	-0.02	0	0	-0.056	0
T12	-0.106	-0.05	-0.041	0.014	-0.031	0	0
C13	-0.066	-0.031	-0.03	-0.024	-0.033	0	0
G22	-0.031	0.001	0.008	0	0	0.008	0
A23	-0.014	-0.024	0.032	0	0	0.028	-0.152
C24	-0.484	-0.326	-0.21	0.079	-0.072	0	0
T25	-0.038	0.776	0.435	-1.574	-7.255	0	7.113
T26	0.087	0.6	0.398	-1.502	-7.383	0	7.587
C27	0.168	-0.447	-0.139	-0.616	-0.472	0	0
G28	-0.095	-0.045	-0.045	0	0	-0.088	0
C29	-0.066	-0.055	-0.037	-0.059	-0.06	0	0

Table S2-B. Chemical shift difference (Δδ) between 2THg and 2TN (Chemical shifts of 2TN considered standard).

	ppm_H1'	ppm_H2'	ppm_H2''	ppm_H5	ppm_H6	ppm_H8	ppm_H2
G6	0.034	-0.006	0.024	0	0	-0.011	0
C7	-0.062	0.071	-0.044	-0.053	-0.003	0	0
G8	-0.02	0.065	-0.005	0	0	-0.087	0
T9	0.122	0.154	0.02	-0.14	0.156	0	0
T10	0.101	-0.099	-0.001	-0.162	-0.08	0	0
G11	-0.094	-0.021	-0.053	0	0	-0.017	0
T12	-0.127	-0.059	-0.041	0.089	-0.03	0	0
C13	-0.054	-0.026	-0.021	-0.023	-0.018	0	0
G22	0.004	0.019	0.026	0	0	0.001	0
A23	-0.004	-0.014	0.034	0	0	0.012	-0.168
C24	-0.476	-0.423	-0.266	0.016	-0.16	0	0
T25	0.086	0.97	0.579	-1.692	-7.176	0	7.113
T26	0.037	0.34	0.303	-1.63	-7.515	0	7.587
C27	-0.145	-0.32	-0.116	-0.543	-0.396	0	0
G28	-0.086	-0.043	-0.057	0	0	-0.079	0
C29	-0.023	-0.041	-0.027	-0.042	-0.033	0	0

S7

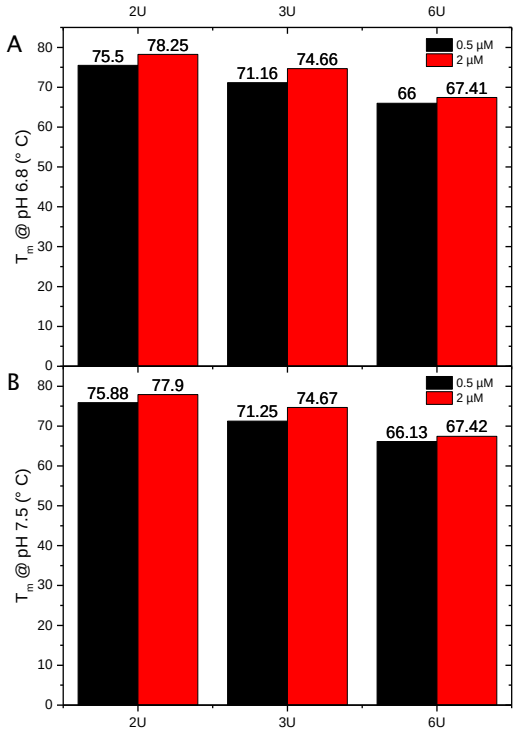

Figure S7: Melting temperature (T_m) of 0.5 µM (black) and 2 µM (red) 2U, 3U and 6U duplexes at pH 6.8 and pH 7.5

S8: Average (3 titrations) Fluorescence emission for racemic-$[Ru(bpy)_2(dppz)]^{2+}$ metal complex with various RNA duplexes 2U, 2UHg, 2UN and 2UNHg. See Section 6.2.2.

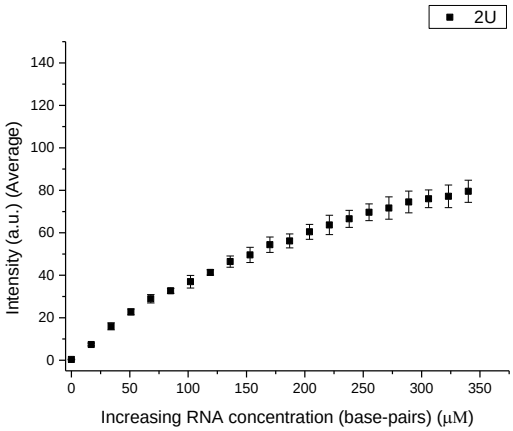

Figure S8-A: Against increasing 2U (Average of 3 titrations)

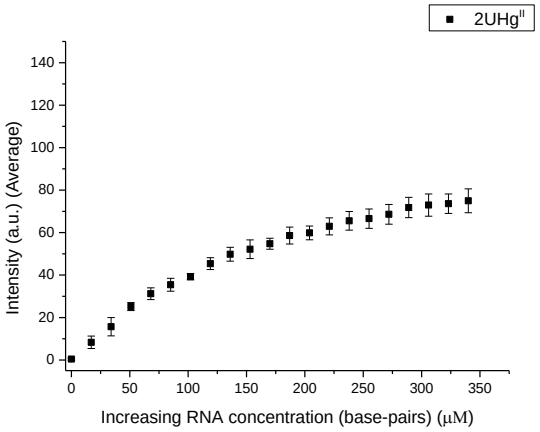

Figure S8-B: Against increasing 2U-Hg^{II} (Average of 3 titrations)

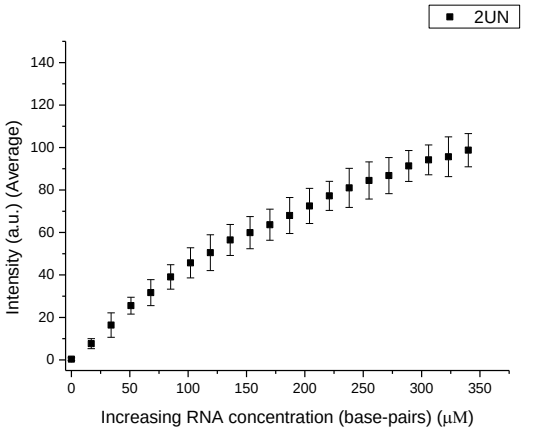

Figure S8-C: Against increasing 2UN (Average of 3 titrations)

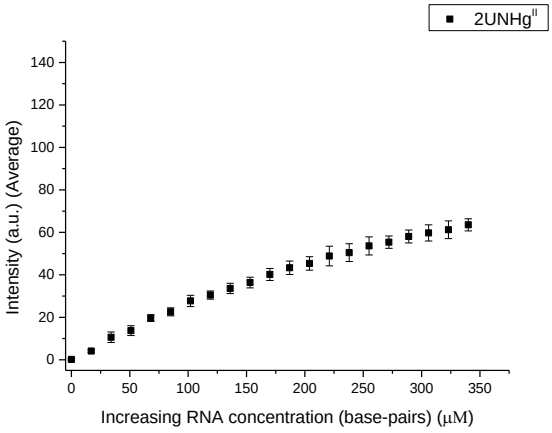

Figure S8-D: Against increasing 2UN-Hg^{II} (Average of 3 titrations)

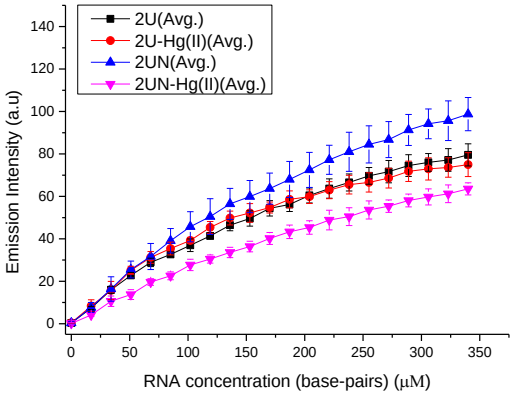

Figure S8-E: Fluorescence emission of racemic-$[Ru(bpy)_2(dppz)]^{2+}$ (Average of 3 titrations) against increasing concentration of 2U, 2UHg, 2UN and 2UNHg RNA duplexes.

S9: Separation of enantiomers using column chromatography. See Section 7.3.

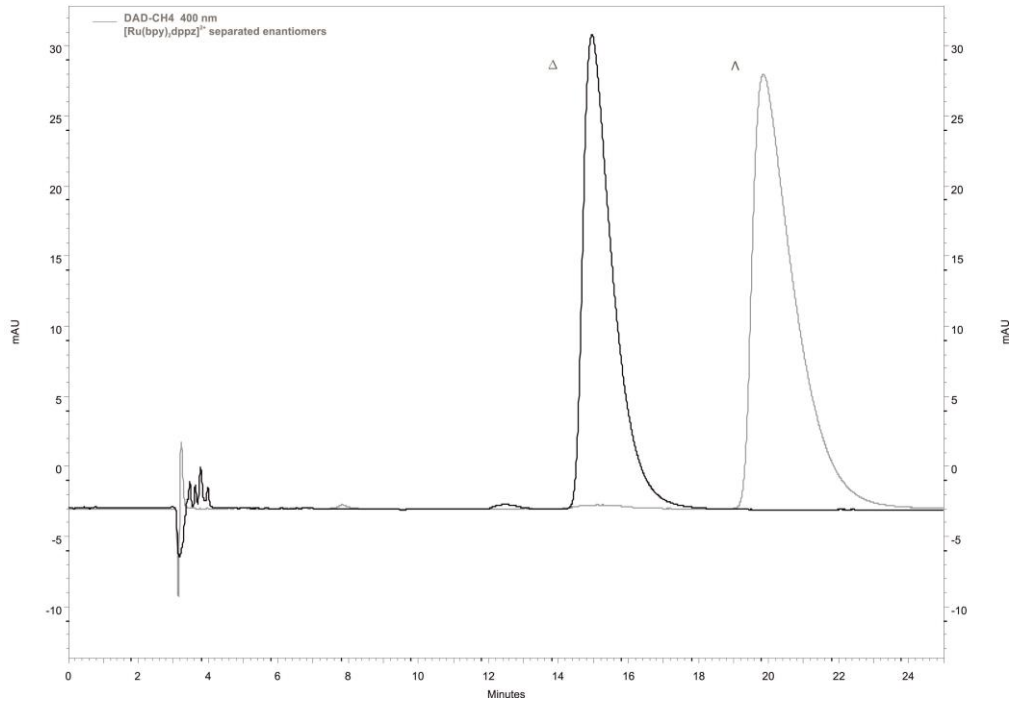

Figure S9-A: The separated enantiomers were run through analytical column to confirm for purity. The output (overlapped) for each enantiomer is depicted.

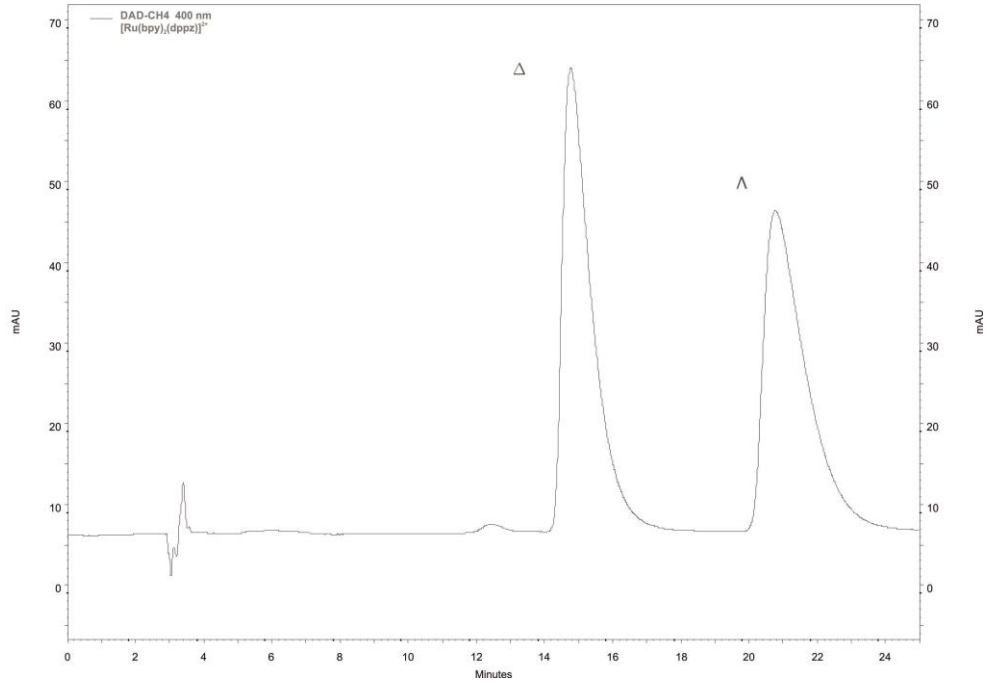

Figure S9-B: The reference (racemic mixture) under analytical column.

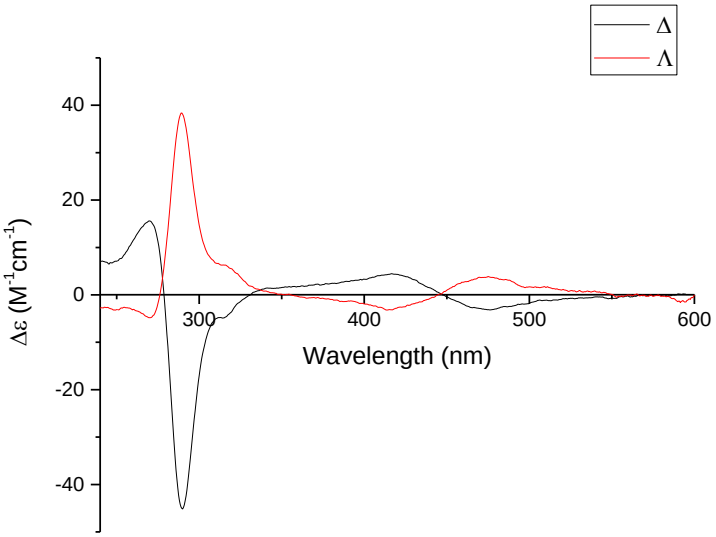

Figure S9-C: CD spectra recorded for individual enantiomers of $[Ru(bpy)_2(dppz)]^{2+}$. The enantiomer CD signals were cross-checked with literature data.

9 BIBLIOGRAPHY

(1) Wagenknecht, H.-A. *Angew. Chem. Int. Ed.* **2003**, *42* (28), 3204.

(2) Tanaka, K.; Tengeiji, A.; Kato, T.; Toyama, N.; Shionoya, M. *Science* **2003**, *299* (5610), 1212.

(3) Johannsen, S.; Paulus, S.; Düpre, N.; Müller, J.; Sigel, R. K. O. *J. Inorg. Biochem.* **2008**, *102* (5–6), 1141.

(4) Johannsen, S.; Megger, N.; Böhme, D.; Sigel, R. K. O.; Müller, J. *Nat. Chem.* **2010**, *2* (3), 229.

(5) Liu, S.; Clever, G. H.; Takezawa, Y.; Kaneko, M.; Tanaka, K.; Guo, X.; Shionoya, M. *Angew. Chem. Int. Ed.* **2011**, *50* (38), 8886.

(6) Barton, J. K.; Olmon, E. D.; Sontz, P. A. *Coord. Chem. Rev.* **2011**, *255* (7–8), 619.

(7) Murphy, C. J.; Arkin, M. R.; Jenkins, Y.; Ghatlia, N. D.; Bossmann, S. H.; Turro, N. J.; Barton, J. K. *Science* **1993**, *262* (5136), 1025.

(8) Andersson, J.; Fornander, L. H.; Abrahamsson, M.; Tuite, E.; Nordell, P.; Lincoln, P. *Inorg. Chem.* **2013**, *52* (2), 1151.

(9) McKinley, A. W.; Lincoln, P.; Tuite, E. M. *Dalton Trans.* **2013**, *42* (11), 4081.

(10) Andrew W McKinley, J. A. *Chem. Weinh. Bergstr. Ger.* **2012**, *27* (18), 15142.

(11) Liu, J.-G.; Zhang, Q.-L.; Shi, X.-F.; Ji, L.-N. *Inorg Chem* **2001**, *40* (19), 5045.

(12) Carter, M. T.; Rodriguez, M.; Bard, A. J. *J. Am. Chem. Soc.* **1989**, *111* (24), 8901.

(13) McGhee, J. D.; von Hippel, P. H. *J. Mol. Biol.* **1974**, *86* (2), 469.

(14) Song, H.; Kaiser, J. T.; Barton, J. K. *Nat. Chem.* **2012**.

(15) Lim, M. H.; Lau, I. H.; Barton, J. K. *Inorg. Chem.* **2007**, *46* (23), 9528.

(16) Lim, M. H.; Song, H.; Olmon, E. D.; Dervan, E. E.; Barton, J. K. *Inorg Chem* **2009**, *48* (12), 5392.

(17) Dahm, R. *Hum. Genet.* **2007**, *122* (6), 565.

(18) Watson, J. D.; Crick, F. H. C. *Nature* **1953**, *171* (4356), 737.

(19) Chargaff, E.; Lipshitz, R.; Green, C. *J. Biol. Chem.* **1952**, *195* (1), 155.

(20) Hou, Y.-M. In *eLS*; John Wiley & Sons, Ltd, 2001.

(21) Nikolova, E. N.; Zhou, H.; Gottardo, F. L.; Alvey, H. S.; Kimsey, I. J.; Al-Hashimi, H. M. *Biopolymers* **2013**, *99* (12), 955.

(22) Chastain, M.; Tinoco, I. *Prog. Nucleic Acid Res. Mol. Biol.* **1991**, *41*, 131.

(23) Saenger, W. *Principles of Nucleic Acid Structure*; Cantor, C. R., Series Ed.; Springer Advanced Texts in Chemistry; Springer New York: New York, NY, 1984.
(24) Peter B. Moore. *Cold Spring Harb. Monogr. Arch. Vol. 37 1999 RNA World 2nd Ed Nat. Mod. RNA Suggests Prebiotic RNA World* **1999**.
(25) Schrodinger. The PyMOL Molecular Graphics System, Version 1.3r1, 2010.
(26) Wang, A. H.; Quigley, G. J.; Kolpak, F. J.; Crawford, J. L.; van Boom, J. H.; van der Marel, G.; Rich, A. *Nature* **1979**, *282* (5740), 680.
(27) Dock-Bregeon, A. C.; Chevrier, B.; Podjarny, A.; Johnson, J.; de Bear, J. S.; Gough, G. R.; Gilham, P. T.; Moras, D. *J. Mol. Biol.* **1989**, *209* (3), 459.
(28) Grodick, M. A.; Muren, N. B.; Barton, J. K. *Biochemistry (Mosc.)* **2015**, *54* (4), 962.
(29) Beaucage, S. L.; Caruthers, M. H. *Tetrahedron Lett.* **1981**, *22* (20), 1859.
(30) Reese, C. B. *Org. Biomol. Chem.* **2005**, *3* (21), 3851.
(31) Keren, K.; Berman, R. S.; Braun, E. *Nano Lett.* **2004**, *4* (2), 323.
(32) Jäger, S.; Rasched, G.; Kornreich-Leshem, H.; Engeser, M.; Thum, O.; Famulok, M. *J. Am. Chem. Soc.* **2005**, *127* (43), 15071.
(33) Gierlich, J.; Burley, G. A.; Gramlich, P. M. E.; Hammond, D. M.; Carell, T. *Org. Lett.* **2006**, *8* (17), 3639.
(34) Kuwahara, M.; Obika, S.; Nagashima, J.; Ohta, Y.; Suto, Y.; Ozaki, H.; Sawai, H.; Imanishi, T. *Nucleic Acids Res.* **2008**, *36* (13), 4257.
(35) Hirao, I. *Curr. Opin. Chem. Biol.* **2006**, *10* (6), 622.
(36) Kool, E. T. *Acc. Chem. Res.* **2002**, *35* (11), 936.
(37) Buchini, S.; Leumann, C. J. *Curr. Opin. Chem. Biol.* **2003**, *7* (6), 717.
(38) Micklefield, J. *Curr. Med. Chem.* **2001**, *8* (10), 1157.
(39) Ray, A.; Nordén, B. *FASEB J.* **2000**, *14* (9), 1041.
(40) Eschenmoser, A. *Science* **1999**, *284* (5423), 2118.
(41) Piccirilli, J. A.; Benner, S. A.; Krauch, T.; Moroney, S. E. *Nature* **1990**, *343* (6253), 33.
(42) Switzer, C.; Moroney, S. E.; Benner, S. A. *J. Am. Chem. Soc.* **1989**, *111* (21), 8322.
(43) Lutz, M. J.; Horlacher, J.; Benner, S. A. *Bioorg. Med. Chem. Lett.* **1998**, *8* (10), 1149.

(44) Bain, J. D.; Switzer, C.; Chamberlin, R.; Bennert, S. A. *Nature* **1992**, *356* (6369), 537.
(45) Tanaka, K.; Shionoya, M. *J. Org. Chem.* **1999**, *64* (14), 5002.
(46) Clever, G. H.; Kaul, C.; Carell, T. *Angew. Chem. Int. Ed.* **2007**, *46* (33), 6226.
(47) He, W.; Franzini, R. M.; Achim, C. In *Progress in Inorganic Chemistry*; Karlin, K. D., Ed.; John Wiley & Sons, Inc., 2007; pp 545–612.
(48) Müller, J. *Eur. J. Inorg. Chem.* **2008**, *2008* (24), 3749.
(49) Shionoya, M.; Tanaka, K. *Curr. Opin. Chem. Biol.* **2004**, *8* (6), 592.
(50) Tanaka, K.; Shionoya, M. *Coord. Chem. Rev.* **2007**, *251* (21–24), 2732.
(51) Meggers, E.; Holland, P. L.; Tolman, W. B.; Romesberg, F. E.; Schultz, P. G. *J. Am. Chem. Soc.* **2000**, *122* (43), 10714.
(52) Atwell, S.; Meggers, E.; Spraggon, G.; Schultz, P. G. *J Am Chem Soc* **2001**, *123* (49), 12364.
(53) Böhme, D.; Düpre, N.; Megger, D. A.; Müller, J. *Inorg. Chem.* **2007**, *46* (24), 10114.
(54) Clever, G. H.; Polborn, K.; Carell, T. *Angew. Chem. Int. Ed.* **2005**, *44* (44), 7204.
(55) Clever, G. H.; Söltl, Y.; Burks, H.; Spahl, W.; Carell, T. *Chem. – Eur. J.* **2006**, *12* (34), 8708.
(56) Heuberger, B. D.; Shin, D.; Switzer, C. *Org. Lett.* **2008**, *10* (6), 1091.
(57) Ono, A.; Cao, S.; Togashi, H.; Tashiro, M.; Fujimoto, T.; Machinami, T.; Oda, S.; Miyake, Y.; Okamoto, I.; Tanaka, Y. *Chem. Commun.* **2008**, No. 39, 4825.
(58) Polonius, F.-A.; Müller, J. *Angew. Chem. Int. Ed.* **2007**, *46* (29), 5602.
(59) Switzer, C.; Shin, D. *Chem. Commun.* **2005**, No. 10, 1342.
(60) Switzer, C.; Sinha, S.; Kim, P. H.; Heuberger, B. D. *Angew. Chem. Int. Ed.* **2005**, *44* (10), 1529.
(61) Tanaka, K.; Clever, G. H.; Takezawa, Y.; Yamada, Y.; Kaul, C.; Shionoya, M.; Carell, T. *Nat. Nanotechnol.* **2006**, *1* (3), 190.
(62) Tanaka, K.; Yamada, Y.; Shionoya, M. *J. Am. Chem. Soc.* **2002**, *124* (30), 8802.
(63) Tanaka, Y.; Oda, S.; Yamaguchi, H.; Kondo, Y.; Kojima, C.; Ono, A. *J. Am. Chem. Soc.* **2007**, *129* (2), 244.
(64) Weizman, H.; Tor, Y. *J. Am. Chem. Soc.* **2001**, *123* (14), 3375.
(65) Wettig, S. D.; Wood, D. O.; Aich, P.; Lee, J. S. *J. Inorg. Biochem.* **2005**, *99* (11), 2093.

(66) Zhang, L.; Meggers, E. *J. Am. Chem. Soc.* **2005**, *127* (1), 74.
(67) Zimmermann, N.; Meggers, E.; Schultz, P. G. *J. Am. Chem. Soc.* **2002**, *124* (46), 13684.
(68) Zimmermann, N.; Meggers, E.; Schultz, P. G. *Bioorganic Chem.* **2004**, *32* (1), 13.
(69) Schlegel, M. K.; Essen, L.-O.; Meggers, E. *Chem. Commun.* **2010**, *46* (7), 1094.
(70) Franzini, R. M.; Watson, R. M.; Patra, G. K.; Breece, R. M.; Tierney, D. L.; Hendrich, M. P.; Achim, C. *Inorg. Chem.* **2006**, *45* (24), 9798.
(71) Gilmartin, B. P.; Ohr, K.; McLaughlin, R. L.; Koerner, R.; Williams, M. E. *J. Am. Chem. Soc.* **2005**, *127* (26), 9546.
(72) Küsel, A.; Zhang, J.; Alvariño Gil, M.; Stückl, A. C.; Meyer-Klaucke, W.; Meyer, F.; Diederichsen, U. *Eur. J. Inorg. Chem.* **2005**, *2005* (21), 4317.
(73) Ohr, K.; McLaughlin, R. L.; Williams, M. E. *Inorg. Chem.* **2007**, *46* (3), 965.
(74) Popescu, D.-L.; Parolin, T. J.; Achim, C. *J. Am. Chem. Soc.* **2003**, *125* (21), 6354.
(75) Watson, R. M.; Skorik, Y. A.; Patra, G. K.; Achim, C. *J. Am. Chem. Soc.* **2005**, *127* (42), 14628.
(76) Katz, S. *J. Am. Chem. Soc.* **1952**, *74* (9), 2238.
(77) Katz, S. *Biochim. Biophys. Acta BBA - Spec. Sect. Nucleic Acids Relat. Subj.* **1963**, *68*, 240.
(78) Kosturko, L. D.; Folzer, C.; Stewart, R. F. *Biochemistry (Mosc.)* **1974**, *13* (19), 3949.
(79) Miyake, Y.; Togashi, H.; Tashiro, M.; Yamaguchi, H.; Oda, S.; Kudo, M.; Tanaka, Y.; Kondo, Y.; Sawa, R.; Fujimoto, T.; Machinami, T.; Ono, A. *J. Am. Chem. Soc.* **2006**, *128* (7), 2172.
(80) Torigoe, H.; Ono, A.; Kozasa, T. *Chem. – Eur. J.* **2010**, *16* (44), 13218.
(81) Urata, H.; Yamaguchi, E.; Funai, T.; Matsumura, Y.; Wada, S. *Angew. Chem.* **2010**, *122* (37), 6666.
(82) Park, K. S.; Jung, C.; Park, H. G. *Angew. Chem.* **2010**, *122* (50), 9951.
(83) Wiley: Nanobiotechnology: Concepts, Applications and Perspectives - Christof M. Niemeyer, Chad A. Mirkin http://eu.wiley.com/WileyCDA/WileyTitle/productCd-3527306587.html (accessed Aug 15, 2015).
(84) Okamoto, I.; Iwamoto, K.; Watanabe, Y.; Miyake, Y.; Ono, A. *Angew. Chem. Int. Ed.* **2009**, *48* (9), 1648.

(85) Keene, F. R.; Smith, J. A.; Collins, J. G. *Coord. Chem. Rev.* **2009**, *253* (15–16), 2021.
(86) Erkkila, K. E.; Odom, D. T.; Barton, J. K. *Chem. Rev.* **1999**, *99* (9), 2777.
(87) Hannon, M. J. *Chem. Soc. Rev.* **2007**, *36* (2), 280.
(88) Zeglis, B. M.; Pierre, V. C.; Barton, J. K. *Chem. Commun.* **2007**, No. 44, 4565.
(89) Pinto, A. L.; Lippard, S. J. *Biochim. Biophys. Acta BBA - Rev. Cancer* **1985**, *780* (3), 167.
(90) Takahara, P. M.; Rosenzweig, A. C.; Frederick, C. A.; Lippard, S. J. *Nature* **1995**, *377* (6550), 649.
(91) Luger, K.; Mäder, A. W.; Richmond, R. K.; Sargent, D. F.; Richmond, T. J. *Nature* **1997**, *389* (6648), 251.
(92) Bostock-Smith, C. E.; Searle, M. S. *Nucleic Acids Res.* **1999**, *27* (7), 1619.
(93) Gavathiotis, E.; Sharman, G. J.; Searle, M. S. *Nucleic Acids Res.* **2000**, *28* (3), 728.
(94) Suh, D.; Chaires, J. B. *Bioorg. Med. Chem.* **1995**, *3* (6), 723.
(95) Metcalfe, C.; Thomas, J. A. *Chem. Soc. Rev.* **2003**, *32* (4), 215.
(96) Bond, P. J.; Langridge, R.; Jennette, K. W.; Lippard, S. J. *Proc. Natl. Acad. Sci. U. S. A.* **1975**, *72* (12), 4825.
(97) Bloomfield, V. A.; Crothers, D. M.; Tinoco, I. *Nucleic Acids: Structures, Properties, and Functions*; University Science Books, 2000.
(98) Sitlani, A.; Long, E. C.; Pyle, A. M.; Barton, J. K. *J. Am. Chem. Soc.* **1992**, *114* (7), 2303.
(99) Rajendiran, V.; Murali, M.; Suresh, E.; Palaniandavar, M.; Periasamy, V. S.; Akbarsha, M. A. *Dalton Trans.* **2008**, No. 16, 2157.
(100) Friedman, A. E.; Chambron, J. C.; Sauvage, J. P.; Turro, N. J.; Barton, J. K. *J Am Chem Soc* **1990**, *112* (12), 4960.
(101) Dupureur, C. M.; Barton, J. K. *J. Am. Chem. Soc.* **1994**, *116* (22), 10286.
(102) Kielkopf, C. L.; Erkkila, K. E.; Hudson, B. P.; Barton, J. K.; Rees, D. C. *Nat. Struct. Mol. Biol.* **2000**, *7* (2), 117.
(103) Haq, I.; Lincoln, P.; Suh, D.; Norden, B.; Chowdhry, B. Z.; Chaires, J. B. *J. Am. Chem. Soc.* **1995**, *117* (17), 4788.
(104) Jenkins, Y.; Friedman, A. E.; Turro, N. J.; Barton, J. K. *Biochemistry (Mosc.)* **1992**, *31* (44), 10809.

(105) Turro, C.; Bossmann, S. H.; Jenkins, Y.; Barton, J. K.; Turro, N. J. *J. Am. Chem. Soc.* **1995**, *117* (35), 9026.
(106) Gill, M. R.; Thomas, J. A. *Chem. Soc. Rev.* **2012**, *41* (8), 3179.
(107) Mari, C.; Pierroz, V.; Ferrari, S.; Gasser, G. *Chem. Sci.* **2015**, *6* (5), 2660.
(108) KLAJNER, M. J. ORGANOMETALLIC COMPOUNDS AS ANTI-CANCER AGENTS: INTERACTION WITH DNA AND MIGRATION IN CELLS.
(109) Kasha, M. *Discuss. Faraday Soc.* **1950**, *9* (0), 14.
(110) *Principles of Fluorescence Spectroscopy*; Lakowicz, J. R., Ed.; Springer US: Boston, MA, 2006.
(111) Stokes, G. G. *Philos. Trans. R. Soc. Lond.* **1852**, *142*, 463.
(112) Garbett, N. C.; Ragazzon, P. A.; Chaires, J. B. *Nat. Protoc.* **2007**, *2* (12), 3166.
(113) Rodger, A.; Blagbrough, I. S.; Adlam, G.; Carpenter, M. L. *Biopolymers* **1994**, *34* (12), 1583.
(114) Pagni, R. M. *J. Chem. Educ.* **1998**, *75* (9), 1095.
(115) Lying, R.; Rodger, A.; Nordén, B. *Biopolymers* **1991**, *31* (14), 1709.
(116) Lyng, R.; Rodger, A.; Nordén, B. *Biopolymers* **1992**, *32* (9), 1201.
(117) O'Neill, M. A.; Barton, J. K. In *Longe-Range Charge Transfer in DNA I*; Schuster, G. B., Ed.; Topics in Current Chemistry; Springer Berlin Heidelberg, 2004; pp 67–115.
(118) Karp, G. *Cell and molecular biology: concepts and experiments*; John Wiley, 2008.
(119) Murray, R. K.; Granner, D. K.; Mayes, P. A.; Rodwell, V. W. *Harper's Illustrated Biochemistry*; Mcgraw-hill, 2003.
(120) Marcus, R. A.; Sutin, N. *Biochim. Biophys. Acta BBA - Rev. Bioenerg.* **1985**, *811* (3), 265.
(121) Winkler, J. R.; Gray, H. B. *Chem. Rev.* **1992**, *92* (3), 369.
(122) Arkin, M. R.; Stemp, E. D. A.; Holmlin, R. E.; Barton, J. K.; Hörmann, A.; Olson, E. J. C.; Barbara, P. F. *Science* **1996**, *273* (5274), 475.
(123) Niemeyer, C. M. *Angew. Chem. Int. Ed.* **2001**, *40* (22), 4128.
(124) Seeman, N. C. *Nature* **2003**, *421* (6921), 427.
(125) Dietz, H.; Douglas, S. M.; Shih, W. M. *Science* **2009**, *325* (5941), 725.
(126) Douglas, S. M.; Dietz, H.; Liedl, T.; Högberg, B.; Graf, F.; Shih, W. M. *Nature* **2009**, *459* (7245), 414.
(127) Rothemund, P. W. K. *Nature* **2006**, *440* (7082), 297.
(128) Bax, A.; Grzesiek, S. *Acc. Chem. Res.* **1993**, *26* (4), 131.

(129) Pervushin, K.; Riek, R.; Wider, G.; Wüthrich, K. *J. Am. Chem. Soc.* **1998**, *120* (25), 6394.
(130) Pervushin, K. *Q. Rev. Biophys.* **2000**, *33* (02), 161.
(131) Riek, R. In *BioNMR in Drug Research*; Zerbe, O., Ed.; Wiley-VCH Verlag GmbH & Co. KGaA, 2002; pp 227–241.
(132) Prestegard, J. H.; Al-Hashimi, H. M.; Tolman, J. R. *Q. Rev. Biophys.* **2000**, *33* (04), 371.
(133) Fürtig, B.; Richter, C.; Wöhnert, J.; Schwalbe, H. *ChemBioChem* **2003**, *4* (10), 936.
(134) Amouyal, E.; Homsi, A.; Chambron, J.-C.; Sauvage, J.-P. *J. Chem. Soc. Dalton Trans.* **1990**, No. 6, 1841.
(135) Hartshorn, R. M.; Barton, J. K. *J. Am. Chem. Soc.* **1992**, *114* (15), 5919.
(136) Lehn, J.-M. *Science* **2002**, *295* (5564), 2400.
(137) *Supramolecular Chemistry: Concepts and Perspectives*, 1 edition.; Wiley-VCH: Weinheim ; New York, 1995.
(138) Rau, S.; Walther, D.; Vos, J. G. *Dalton Trans.* **2007**, No. 9, 915.
(139) Dupureur, C. M.; Barton, J. K. *Inorg Chem* **1997**, *36* (1), 33.
(140) Barton, J. K. *Science* **1986**, *233* (4765), 727.
(141) Zeglis, B. M.; Barton, J. K. *Inorg. Chem.* **2008**, *47* (14), 6452.
(142) Zeglis, B. M.; Barton, J. K. *J. Am. Chem. Soc.* **2006**, *128* (17), 5654.
(143) Marnett, L. J. *Carcinogenesis* **2000**, *21* (3), 361.
(144) Hoeijmakers, J. H. J. *Nature* **2001**, *411* (6835), 366.
(145) Kunkel, T. A. *Cancer Cell* **2003**, *3* (2), 105.
(146) Liu, J. G.; Ye, B. H.; Zhang, Q. L.; Zou, X. H.; Zhen, Q. X.; Tian, X.; Ji, L. N. *J. Biol. Inorg. Chem. JBIC Publ. Soc. Biol. Inorg. Chem.* **2000**, *5* (1), 119.
(147) Gazit, E. *FEBS J.* **2007**, *274* (2), 317.
(148) Bloomfield, V. A.; Crothers, D. M.; Tinoco, I. *Physical chemistry of nucleic acids*; Harper & Row, 1974.
(149) Carlson, D. L.; Huchital, D. H.; Mantilla, E. J.; Sheardy, R. D.; Murphy, W. R. *J. Am. Chem. Soc.* **1993**, *115* (14), 6424.
(150) Kondo, J.; Yamada, T.; Hirose, C.; Okamoto, I.; Tanaka, Y.; Ono, A. *Angew. Chem.* **2014**, *126* (9), 2417.
(151) Clever, G. H.; Shionoya, M. *Coord. Chem. Rev.* **2010**, *254* (19–20), 2391.
(152) Murphy, C. J.; Arkin, M. R.; Ghatlia, N. D.; Bossmann, S.; Turro, N. J.; Barton, J. K. *Proc. Natl. Acad. Sci. U. S. A.* **1994**, *91* (12), 5315.

(153) Holmlin, R. E.; Stemp, E. D. A.; Barton, J. K. *Inorg Chem* **1998**, *37* (1), 29.
(154) Hiort, C.; Lincoln, P.; Norden, B. *J Am Chem Soc* **1993**, *115* (9), 3448.
(155) Berova, N.; Nakanishi, K. *Circular Dichroism: Principles and Applications*; John Wiley & Sons, 2000.
(156) Allenmark, S. *Chirality* **2003**, *15* (5), 409.
(157) Maj, M.; Jeon, J.; Góra, R. W.; Cho, M. *J. Phys. Chem. A* **2013**, *117* (29), 5909.
(158) Choi, S.-D.; Kim, M.-S.; Kim, S. K.; Lincoln, P.; Tuite, E.; Nordén, B. *Biochemistry (Mosc.)* **1997**, *36* (1), 214.
(159) McConnell, A. J.; Song, H.; Barton, J. K. *Inorg. Chem.* **2013**, *52* (17), 10131.
(160) SantaLucia, J.; Hicks, D. *Annu. Rev. Biophys. Biomol. Struct.* **2004**, *33* (1), 415.
(161) Tanaka, Y.; Yamaguchi, H.; Oda, S.; Kondo, Y.; Nomura, M.; Kojima, C.; Ono, A. *Nucleosides Nucleotides Nucleic Acids* **2006**, *25* (4-6), 613.
(162) Kuklenyik, Z.; Marzilli, L. G. *Inorg. Chem.* **1996**, *35* (19), 5654.
(163) Rossetti, G.; Dans, P. D.; Gomez-Pinto, I.; Ivani, I.; Gonzalez, C.; Orozco, M. *Nucleic Acids Res.* **2015**, gkv254.
(164) Yamaguchi, H.; Šebera, J.; Kondo, J.; Oda, S.; Komuro, T.; Kawamura, T.; Dairaku, T.; Kondo, Y.; Okamoto, I.; Ono, A.; Burda, J. V.; Kojima, C.; Sychrovský, V.; Tanaka, Y. *Nucleic Acids Res.* **2013**, gkt1344.
(165) Crick, F. H. *Symp. Soc. Exp. Biol.* **1958**, *12*, 138.
(166) Hoagland, M. B.; Stephenson, M. L.; Scott, J. F.; Hecht, L. I.; Zamecnik, P. C. *J. Biol. Chem.* **1958**, *231* (1), 241.
(167) Guerrier-Takada, C.; Gardiner, K.; Marsh, T.; Pace, N.; Altman, S. *Cell* **1983**, *35* (3, Part 2), 849.
(168) Cech, T. R.; Zaug, A. J.; Grabowski, P. J. *Cell* **1981**, *27* (3, Part 2), 487.
(169) Crick, F. *Nature* **1970**, *227* (5258), 561.
(170) Stark, B. C.; Kole, R.; Bowman, E. J.; Altman, S. *Proc. Natl. Acad. Sci. U. S. A.* **1978**, *75* (8), 3717.
(171) Zaug, A. J.; Cech, T. R. *Nucleic Acids Res.* **1982**, *10* (9), 2823.
(172) Paige, J. S.; Wu, K. Y.; Jaffrey, S. R. *Science* **2011**, *333* (6042), 642.
(173) Daigle, N.; Ellenberg, J. *Nat. Methods* **2007**, *4* (8), 633.
(174) In *Encyclopedia of Genetics, Genomics, Proteomics and Informatics*; Springer Netherlands, 2008; pp 1731-1731.
(175) Srisawat, C.; Engelke, D. R. *Methods* **2002**, *26* (2), 156.

(176) Chakalova, L.; Carter, D.; Fraser, P. Enzymology, B.-M. in, Ed.; Chromatin and Chromatin Remodeling Enzymes, Part A; Academic Press, 2003; Vol. 375, pp 479–493.
(177) Wiley: Biochemistry, 4th Edition - Donald Voet, Judith G. Voet http://eu.wiley.com/WileyCDA/WileyTitle/productCd-EHEP001782.html (accessed Sep 9, 2015).
(178) Hud, N. V. *Nucleic Acid–Metal Ion Interactions*; RSC Biomolecular Sciences; The Royal Society of Chemistry, 2008.
(179) Freisinger, E.; Sigel, R. K. O. *Coord. Chem. Rev.* **2007**, *251* (13–14), 1834.
(180) Schnabl, J.; Sigel, R. K. *Curr. Opin. Chem. Biol.* **2010**, *14* (2), 269.
(181) Sigel, R. K. O.; Freisinger, E.; Lippert, B. *J. Biol. Inorg. Chem.* **2000**, *5* (3), 287.
(182) Sigel, R. K. O.; Pyle, A. M. *Met. Ions Biol. Syst.* **2003**, *40*, 477.
(183) Yang, H.; Metera, K. L.; Sleiman, H. F. *Coord. Chem. Rev.* **2010**, *254* (19–20), 2403.
(184) Gallo, S.; Furler, M.; Sigel, R. K. O. *Chim. Int. J. Chem.* **2005**, *59* (11), 812.
(185) Milligan, J. F.; Groebe, D. R.; Witherell, G. W.; Uhlenbeck, O. C. *Nucleic Acids Res.* **1987**, *15* (21), 8783.
(186) Pierre, V. C.; Kaiser, J. T.; Barton, J. K. *Proc. Natl. Acad. Sci.* **2007**, *104* (2), 429.
(187) Job, P. *Ann Chim* **1928**, *9*, 113.